STATUS REPORTS

to the

PAPER PHYSICS

PROJECT ADVISORY COMMITTEE

March 26, 1997

INSTITUTE OF PAPER SCIENCE AND TECHNOLOGY

Atlanta, Georgia

ANNUAL RESEARCH REVIEW

PAPER PHYSICS

March 26, 1997

February 13, 1997

TO: MEMBERS OF THE PAPER PHYSICS PROJECT ADVISORY COMMITTEE

Attached for your review are the Status Reports for the projects to be discussed at the Paper Physics Project Advisory Committee meeting. The Program Review is scheduled for Wednesday, March 26, 1997, at 8:00 a.m.- 12:00 p.m. and the PAC Committee Meeting will be held from 1:00 p.m. to 5:00 p.m.

Please note that the meeting is being held at the Institute of Paper Science and Technology.

We look forward to seeing you at this time.

Sincerely,

David I. Orloff, Ph.D.
Professor of Engineering & Director
Engineering and Paper Materials Division

DIO/map

Attachment

Institute of Paper Science and Technology, Inc.

500 10th Street, N.W.
Atlanta, GA 30318-5794

Telephone 404-894-5700
FAX# 404-894-IPST (4778)

PAPER PHYSICS
PROJECT ADVISORY COMMITTEE

IPST Liaison: Dr. David Orloff (404) 894-6649; FAX (404) 894-1496
RAC Liaison: Dr. Walter Freeman (302) 995-3249; FAX (302) 995-3794

Dr. Thomas E. Altman *(1997) (Chairman)
Research Scientist
Union Camp Corporation
Post Office Box 3301
Princeton, NJ 08543-3301
(609) 844-7428
(609) 844-7323 FAX

Dr. George L. Batten, Jr. *(1997)
Manager, Research & Development
Georgia-Pacific Corporation
2883 Miller Road
Decatur, GA 30035-4036
(770) 593-6837
(770) 322-9973 FAX

Dr. Keith A. Bennett *(1994)
Senior Research Scientist
Weyerhaeuser Company
WTC 2B22
Tacoma, WA 98477-0001
(206) 924-6714
(206) 924-6324 FAX

Dr. William Boyd *(1997)
Research Physicist
Buckeye Cellulose Corporation
1001 Tillman Street
Post Office Box 8407
Memphis, TN 38108
(901) 320-8100
(901) 320-8394 FAX

Dr. Michael F. Forbes *(1998)
Director, Printing Technology
Repap Technologies, Inc.
2650 Eisenhower Avenue
Valley Forge, PA 19482
(610) 630-9630
(610) 630-0966 FAX

Dr. John Goss *(1997)
Director, Sensor Products
Measurex Corporation
One Results Way
Cupertino, CA 95014
(408) 255-1500 x4446
(408) 864-7551 FAX

Mr. Timothy Hess *(1998)
Chemist/Engineer
P.H. Glatfelter Co.
228 South Main Street
Spring Grove, PA 17362-1000
(717) 225-4711 x2626
(717) 225-7394 FAX

Dr. Leslie L. Martin *(1998)
Manager, Papermaking R&D
Potlatch Corporation
Fiber R&D - Post Office Box 503
East End Avenue E
Cloquet, MN 55720-0503
(218) 879-2387
(218) 879-2375 FAX

Mr. William W. Maslanka *(1997)
Research Associate
Hercules Incorporated
Research Center
500 Hercules Road
Wilmington, DE 19808-1599
(302) 995-3115
(302) 995-4565 FAX

Dr. William J. McNown *(1996)
Research Engineer
Westvaco Corporation
Research Center - Mill Road
Covington, VA 24426-0950
(540) 969-5152
(540) 969-5148 FAX

Dr. Robert J. Niebauer *(1997)
Manager, R&D, Raw Materials, and ISO Department
Crane & Co., Inc.
30 South Street
Dalton, MA 01226-1751
(413) 684-2600
(413) 684-1789 FAX

Mr. James W. Replogle *(1999)
Senior Project Manager
Stone Container Corporation
1979 Lakeside Parkway
Suite 300
Tucker, GA 30084
(770) 621-6716
(770) 621-6733

Paper Physics PAC (cont.)

Mr. Arvind Sahuy *(1999)
Asten, Inc.
213 Boulevard Du Harve
Valleyfield, Quebec CANADA J6S 1R9
(514) 373-2424
(514) 373-4745 FAX

Dr. Jack Schulz *(1998)
Portfolio Manager - Product Development
Champion International Corporation
West Nyack Road
West Nyack, NY 10994
(914) 578-7000
(914) 578-7175 FAX

Mr. Dirk E. Swinehart *(1998)
Fellow, Paper Physics
Mead Central Research
The Mead Corporation
Eighth & Hickory Streets
Chillicothe, OH 45601-5700
(614) 772-3570
(614) 772-3595 FAX

Mr. Dan H. Sze *(1997)
Manager, Paper Technology
Beloit Corporation
Rockton Research Center
1165 Prairie Hill Road
Rockton, IL 61072-1595
(608) 364-8525
(608) 364-8600 FAX

Dr. Gary L. Worry *(1998)
Manager, Core Technology
James River Corporation
1915 Marathon Avenue
Post Office Box 899
Neenah, WI 54957-0899
(414) 729-8470
(414) 729-8144 FAX

PAPER PHYSICS
PROJECT ADVISORY COMMITTEE MEETING

March 26, 1997

Institute of Paper Science and Technology
Atlanta, Georgia

PROGRAM REVIEW AGENDA

Seminar Room

8:00 a.m. - 8:05 a.m.	Opening Remarks and Antitrust Statement	Ted Altman
8:05 a.m. - 8:10 a.m.	Welcome from Vice President of Research	Gary Baum
8:10 a.m. - 8:20 a.m.	Overview of IPST Paper Physics Research	Derek Page
8:20 a.m. - 8:55 a.m.	Project F008 Fundamentals of Acoustic Radiation Pressure on Fiber Suspensions	Pierre Brodeur
8:55 a.m. - 9:30 a.m.	Project F020 Fundamentals of Dimensional Stability	Doug Coffin
9:30 a.m. - 10:05 a.m.	Project F023 Applications of Micromechanics in Paper Physics	Martin Ostoja
10:05 a.m. - 10:20 a.m.	Break	
10:20 a.m. - 11:05 a.m.	Project F024 - Fundamentals of Fiber Properties	John Waterhouse
11:05 a.m. - 11:40 a.m.	Project F007 On-Line Measurement of Paper Properties	Mac Hall
11:40 a.m. - 12:00 p.m.	Student Projects in Paper Physics	Pierre Brodeur

Room 177

5:00 p.m. - 6:00 p.m.	Paper Physics Committee Discussions	Derek Page

PAPER PHYSICS
PROJECT ADVISORY COMMITTEE MEETING

March 26, 1997

Institute of Paper Science and Technology
Atlanta, Georgia

COMMITTEE DISCUSSIONS AGENDA

Room 177

1:00 p.m. - 1:15 p.m.
- Antitrust Statement
- New Members
- Review of RAC - PAC Meeting & Paper Physics Strategic Plan
- Review of Agenda

1:15 p.m. - 2:30 p.m. Subcommittee Discussions
- Applications of Micromechanics in Paper Physics
  Worry, Batten, Replogle
- Fundamentals of Acoustic Radiation Pressure
  Schulz, Altman
- Fundamentals of Dimensional Stability
  Bennett, Hess, Sze
- Fundamentals of Fiber Properties
  Maslanka, Niebauer, Swinehart
- On-Line Measurement of Paper Properties
  McNown, Martin, Goss
- Microscopy
  Altman, Orloff, Page, Sze

Full Committee Discussion
- 2:30 - 2:50 Micromechanics
- 2:50 - 3:10 Acoustic Radiation Pressure

  3:10 - 3:25 Break
- 3:25 - 3:45 Dimensional Stability
- 3:45 - 4:05 Fiber Properties
- 4:05 - 4:25 On-Line Measurement
- 4:25 - 4:40 Microscopy
- 4:40 - 5:00 Other Project Work

TABLE OF CONTENTS

FUNDAMENTALS OF ACOUSTIC RADIATION PRESSURE

STATUS REPORT

FOR

PROJECT F008

Pierre Brodeur
Joe Gerhardstein

March 26, 1997

Institute of Paper Science and Technology
500 10th Street, N.W.
Atlanta, Georgia 30318

TECHNICAL PROGRAM REVIEW

Project Title:	FUNDAMENTALS OF ACOUSTIC RADIATION PRESSURE
Project Code:	FARPE
Project Number:	F008
Division:	Engineering and Paper Materials Division
Project Staff:	Pierre Brodeur, Joe Gerhardstein
Students:	Michelle Oakland, John Blanz
Project Budget:	$89,832 (FY96-97)

OBJECTIVES

- Investigate fundamentals of acoustic radiation pressure (ARP) effects on fiber suspensions;
- Investigate mechanisms of acoustic fiber agglomeration and reorientation;
- Demonstrate the concept of acoustic wet fiber flexibility/compactibility;
- Demonstrate the concept of acoustic fiber separation/fractionation;
- Explore other process-related applications of acoustic radiation pressure; and
- Determine the economic viability of acoustically based industrial processes.

GOAL THIS PERIOD (MARCH 96 - FEBRUARY 97)

- Develop a laboratory prototype acoustic separation system.

GOAL NEXT PERIOD (MARCH 97 - FEBRUARY 98)

- Demonstrate the concept of acoustic separation/fractionation/removal.

SUMMARY

During the past year, the main accomplishment was the design and fabrication of a laboratory prototype acoustic separation system. The experimental setup was fully integrated in January 97 and performance tests are currently underway. Its intended use is to demonstrate, in a realistic manner, various separation, fractionation, and removal concepts using acoustic radiation pressure principles. In a related student project carried out by M. Oakland, preliminary work was accomplished toward the preparation of a series of experiments to demonstrate the removal of vessel elements from eucalyptus fibers using acoustic radiation pressure. Exploratory experiments are scheduled to begin in February 1997 using the new separation system.

Significant progress was made in another student project (J. Blanz) regarding the development of an experimental methodology to investigate the concept of ultrasonic refining of pulp suspensions. A final series of experiments using unbleached Kraft softwood fibers and a dedicated test apparatus is scheduled to begin in March 1997.

A proposal, titled "Acoustic Separation Technology," was recommended for funding in 1997 through the AF&PA-DOE Agenda 2020 program for the Pulp and Paper Industry (Recycling area). It is anticipated that funding for this proposal will significantly increase the level of research activities on the fundamentals of acoustic separation, fractionation, and removal. A second proposal, titled "Closed Water Treatment in Pulp Mills Using a Dual Flocculation/Ultrasonic Clarification Method" (in collaboration with Y. Deng, Surface and Colloid Chemistry), was recommended for funding in July 1997 by the Georgia Consortium for the Technological Competitiveness in Pulp and Paper.

Finally, a research paper reporting the demonstration of acoustic wet fiber compactibility was published in the August 1996 issue of the *Journal of Pulp and Paper Science* ["Compactibility of a Wet Fiber Mat Using Acoustic Radiation Pressure", P.H. Brodeur and T.M. Runge, *J. Pulp & Paper Sc.* 22(8) J278-J282 (1996)]. Our research program on the development of a new laboratory/on-line sensor technology to determine wet fiber compactibility and predict the apparent density of paper was not pursued this past year due to lack of resources.

1. Background

Project F008 was initiated in July 1992 to study the fundamentals of acoustic radiation pressure effects on fiber suspensions. In essence, when water-suspended fibers interact with acoustic radiation pressure, they are subjected to an acoustic force which results in fiber migration [1-4]. There is also an acoustic torque which reorients fibers. Both acoustic force and torque are nonlinear effects.

Very early in the project, a basic experimental setup was built to investigate the acoustic force on stationary and moving fiber suspensions. A special acoustic cell mounted in a vertical pipe flow was devised to deflect an input stream of fibers interacting with a progressive ultrasonic wave field (unidirectional acoustic force) normal to the flow direction. The cell was composed of a 2 x 10 cm^2 active area piezoelectric ceramic transducer operating at 150 kHz and a sound absorber of equivalent area. The separation distance between these components was 2 cm.

Since experimentation indicated that the acoustic force could be used to separate/fractionate fibers based on fiber width [5], fiber collection was achieved by installing an in-flow divider blade above the acoustic cell in such a way as to separate highly deflected fibers (coarse fibers)

from weakly deflected or undeflected fibers (slender fibers and/or fines). Literature/patent searches since 1987 did not reveal evidence of past work in the use of an ultrasonic field to manipulate fiber suspensions. A patent application was filed by IPST in 1996.

In a particular series of experiments using the basic experimental setup, rayon fibers of constant width/variable length and constant length/variable width were tested as a function of acoustic intensity and flow rate at 0.05% consistency. Separation efficiency was indirectly determined by measuring the cleanliness efficiency of the weakly deflected fiber output stream. Results supporting the fiber width hypothesis are shown in Figure 1a and 1b. While the cleanliness efficiency increases as a function of intensity for all test samples (at constant flow rate), indicating an increased fiber migration rate from the transducer to the absorber, the cleanliness efficiency is not significantly affected by fiber length in Figure 1a and increases as a function of fiber width in Figure 1b.

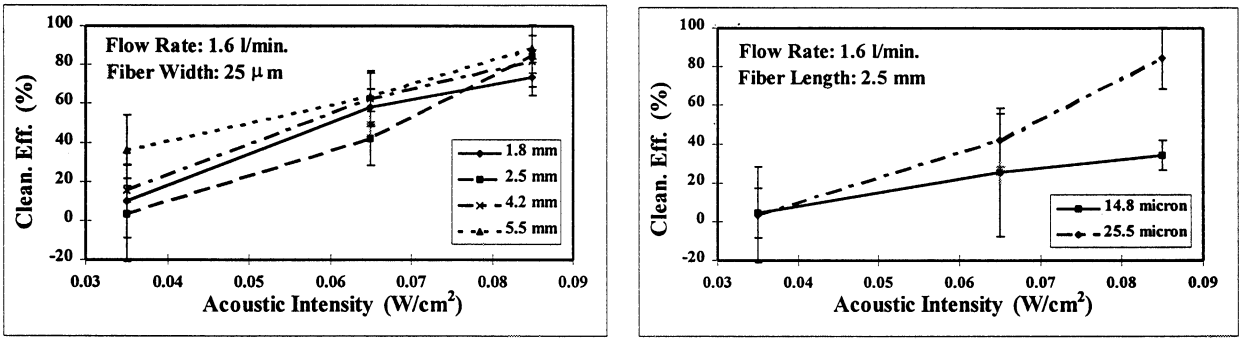

Figure 1a and 1b. Cleanliness efficiency as a function of acoustic intensity for a) constant width/variable length rayon fibers and b) constant length/variable width rayon fibers.

In a similar set of experiments, a Bauer-McNett classifier was used to separate two fractions of never-dried hardwood fibers (sample A, average fiber length: 0.78 mm; sample B, average fiber

length: 1.10 mm). The cleanliness efficiency was determined for samples A and B and a mixture labeled M (25% A - 75% B; predicted fiber length: 1.02 mm). Results are presented in Figure 2. Clearly, the efficiency increases as a function of fiber length (related to fiber width in this case).

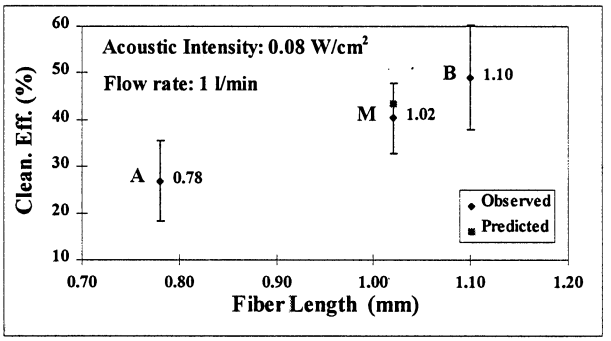

Figure 2. Cleanliness efficiency for samples of never-dried hardwood fibers.

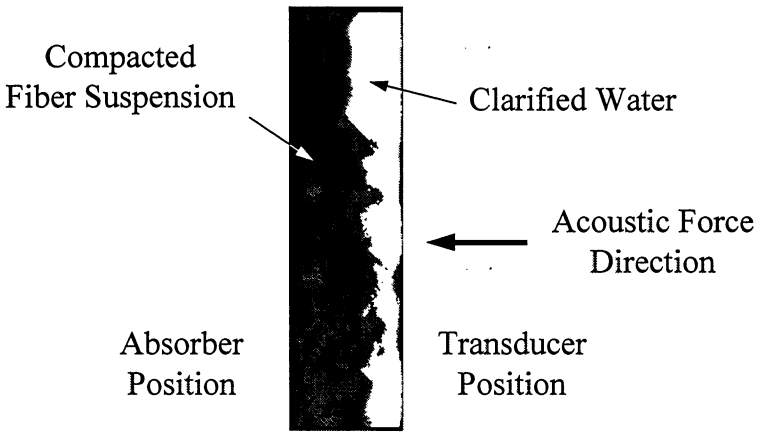

Figure 3. Pulp thickening effect [2 cm (horizontal) x 10 cm (vertical)].

Another series of observations was obtained using softwood fibers under zero-flow conditions to study the compactibility of fiber suspensions. Figure 3 shows a compacted fiber suspension for an initial pulp consistency of 1% (*white indicates water and black indicates fiber*). The acoustic intensity is 0.3 W/cm^2. One can easily see a pulp thickening effect. A new test method, acoustic

wet fiber compactibility, has been proposed to control the refining process and predict the apparent density of paper [6].

Using a more efficient transducer (> 90% power efficiency conversion from electrical to mechanical power), video recordings were obtained for different acoustic intensity levels at 70 l/min (18 gal/min) using never-dried softwood fibers (at max. pump capacity; Re ≈ 6000 - turbulent regime). Results are shown in Figure 4 (*black indicates fiber*). Pulp consistency is 0.1%. One can see that fiber deflection (toward the left) significantly increases as a function of intensity (shown as a thickening of the fiber mat (*black*) on the left side of the cell). At 4 W/cm^2, the intensity is already too large and deflected fibers bounce back.

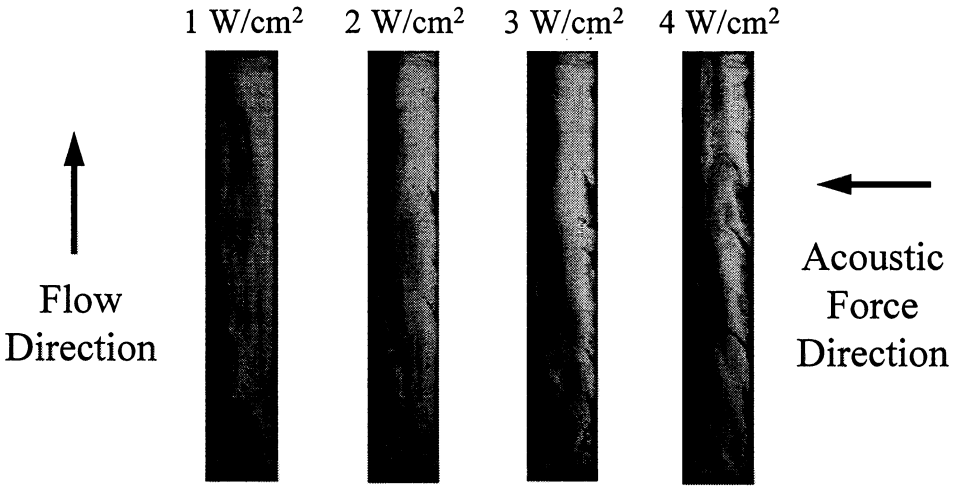

Figure 4. Video recordings under turbulent flow conditions. [2 cm (hor.) x 10 cm (vert.)].

Other test results can be summarized as follows:

(1) Migration rate for shives is significantly larger than that for fibers;

(2) Migration rate for earlywood fibers is larger than that for latewood fibers;

(3) Observations using OCC fibers show that the fiber fraction migrates but the fines do not; and

(4) Observations using mixtures of fibers and ink particles attached to air bubbles show that the air bubbles are not affected by the acoustic force, thus providing a means to enhance the removal of fibers in flotation deinking.

Experiments were also conducted using a standing ultrasonic wave field. This field is obtained by replacing the sound absorber by a reflector. Providing that the separation distance between the transducer and the reflector corresponds to n ($\lambda/2$), where λ is the acoustic wavelength (10 mm at f = 150 kHz in water), interference between the transmitted and reflected wavefronts produces a standing wave field pattern. Since the transducer-reflector separation distance was 2 cm, four nodal pressure planes were created. Observations in the presence of fiber suspensions showed that the fibers quickly migrated toward pressure planes when the sound field was turned on, thus leading to the formation of four parallel agglomeration planes. This is illustrated in Figure 5.

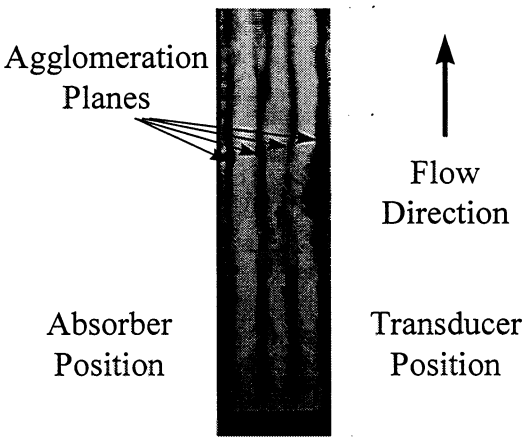

Figure 5. Agglomeration of 5.9 mm rayon fibers at 1% consistency in a standing wave field. Four layers are produced. The Reynold's number is approximately 500.

Technical limitations (small size of equipment, consistency and flow limitations) in the quest to perform realistic separation experiments using the basic experimental setup led to the decision to proceed with the design and fabrication of a laboratory-scale acoustic separator. Details of this apparatus are reported in the next Section.

2. Laboratory Acoustic Separator

The development of a laboratory-scale prototype acoustic separator was initiated in March 1996. System integration was completed in January 1997. Schematic diagrams of the separator and the accompanying flow system are shown in Figures 6 and 7, respectively.

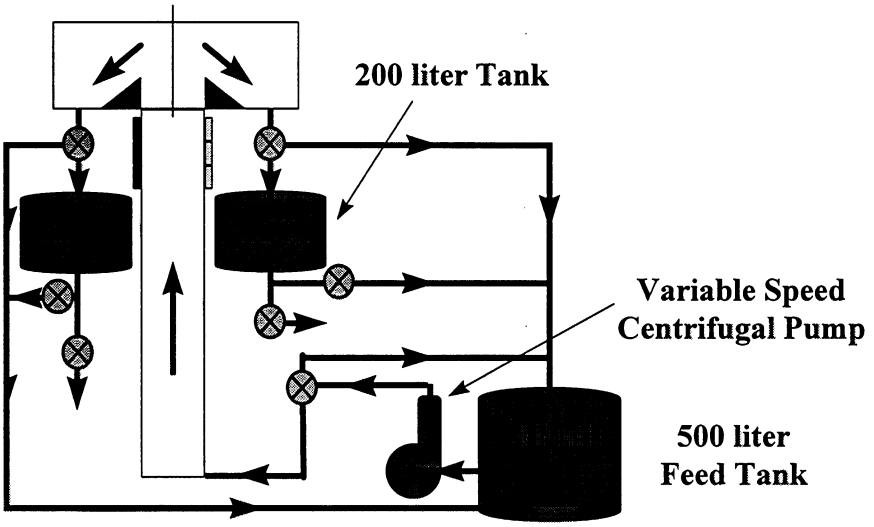

Figure 6. Flow system for the laboratory prototype acoustic separator (drawing not to scale).

As seen in Figure 6, the setup is composed of a 500-liter feed stream tank, a 20-to 450-l/min variable speed centrifugal pump, the acoustic separator, and two 200-liter output stream tanks. Not seen in the drawing are a magnetic flow meter located at the exit of the centrifugal pump and a mixer for the feed tank. The flow system is capable of feed consistencies up to 2-3%. It is unpressurized. Separation and recirculation modes are possible.

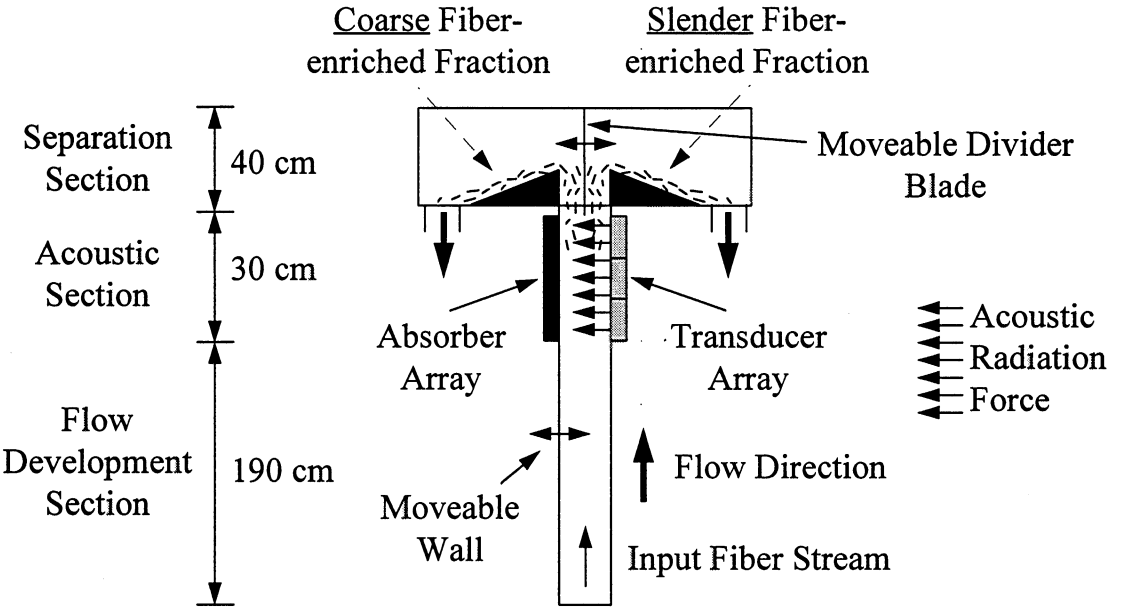

Figure 7. Schematic diagram of the laboratory prototype acoustic separation system (drawing not to scale). Separation using a progressive wave field (unidirectional) is shown.

As best described in Figure 7, the separator itself is composed of three consecutive sections mounted vertically: 1) flow development section; 2) acoustic section; 3) separation section. The overall height of the separation column is 2.6 m. The separation distance between the transducer and absorber positions can be modified by using different transverse walls; available widths are 5, 10, and 15 cm.

The inlet into the flow development section is a 5-cm diameter pipe which is angled up at 60 degrees. This, in combination with the 1.5 m height of the flow development section allows flows up to 2.4 m/s (360 l/min for 5-cm transverse walls, 1080 l/min for 15-cm transverse walls) to completely develop before entering the acoustic section. Reynolds numbers available will range from 400-140,000 (turbulent transition for pipe flows is between 2100 and 4000).

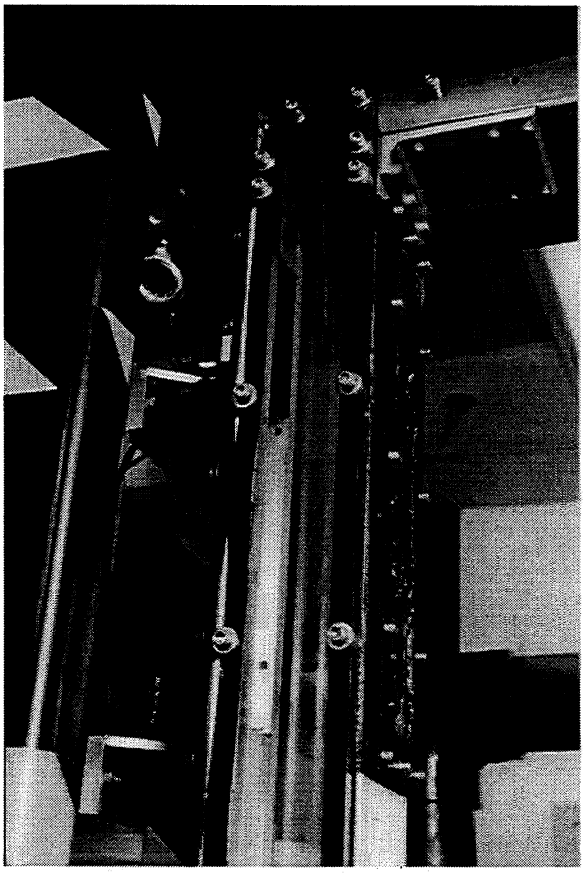

Figure 8. Photograph of the separation section as seen from the absorber side. One can see a miniature hydrophone used to determine the acoustic power delivered by the transducers.

The acoustic section is 30 cm in length. Figure 8 displays a photograph of the acoustic section. It was designed to accommodate up to three transducer/absorber sets mounted in series, each 10 cm in length and 5 cm wide. Transducers and absorbers are easily replaceable and can be mounted on either side of the cell. By having three separate transducer/absorber sets, the effect of acoustic dwell length can be studied by varying the number of transducers used. The transducers may also be staggered on either side of the cell, or even mounted across from each other. This leads to significant flexibility in the acoustic section which was not present in the

original system. Also, reflectors can be used for more advanced standing wave field separation studies.

Transducers are custom-designed and made of piezoelectric ceramic material. Their active area is 50 cm^2 and the frequency is 150 kHz. Different impedance matching networks are available to power one, two, or three transducers, and hence, control the acoustic dwell length. The transducer's electrical-to-mechanical conversion efficiency is around 95%.

The separation section, located above the acoustic section, is composed of an adjustable divider blade (Note: more than one blade can be installed for fractionation studies). The blade is used to separate highly deflected fibers from barely deflected or undeflected fibers. Since the consistency of the deflected stream may be larger than 2-3%, especially when considering pulp thickening observations, pipe diameter for the output streams is 100% larger than the pipe diameter for the input stream. The use of a mechanical blade is temporary as it is known that fibers tend to hang-up on the blade tip.

At the time of this writing, very early observations using one transducer and Kraft softwood fibers at 0.1% consistency looked very promising as far as the general functioning of the separator is concerned.

3. Removal of Vessel Elements from Hardwood Fibers (M. Oakland)

At the Fall 1996 Project Advisory Committee meeting, it was suggested by at least two Committee Members that an investigation of the use of acoustic radiation pressure principles to remove vessel elements from hardwood fibers be undertaken. It is well known that the presence of vessel elements

during offset printing can be detrimental because vessels do not bond very well to fibers, and consequently, can be picked by impression cylinders (vessel picking problem). Since there are currently no satisfactory methods to remove vessel elements, the industry addresses the problem by using pulp mixtures to reduce the concentration of vessel elements. Also, refining is practiced to reduce the size of these particles.

Michelle Oakland, second-year M.S. Student at IPST, refocused her M.S. project from the separation of softwood from hardwood fibers to the removal of vessel elements. Although the separation of softwood from hardwood fibers is worth pursuing (and it will be), it was considered easier from an experimental standpoint and of more economical value to the industry to explore the removal of vessel elements.

In addition to a review of the literature, preliminary work has been done to identify wood species for the purpose of experimentation. While red and white oak species contain a relatively large proportion of vessel elements compared to other hardwood species, pure commercial pulps made from these species are unavailable. Vessel elements are also problematic with eucalyptus pulp. Following discussion with Prof. H. Nanko and industry representatives familiar with vessel elements, two options were considered: a) pulping of a white oak log; b) use of eucalyptus pulp. The second option was selected. Eucalyptus pulp in dry lap form was received in January 1997.

One obstacle encountered during pulp characterization was determination of the percentage of vessel elements, and hence, a quantitative measurement to assess separation efficiency. Since a standard microscopy test method is unavailable to count vessel elements, a test method was developed based on industry practices. The method reports an average number of vessel elements per milligram of

oven-dried fibers. Measurements using the eucalyptus pulp at our disposal indicate that this pulp has 119 ± 8.3 vessel elements per mg of o.d. pulp.

Experiments are scheduled to begin in February 1997. Acoustic power, flow rate, and consistency will be considered to optimize separation efficiency. Preliminary work is expected to be completed in May 1997.

4. Ultrasonic Refining (J. Blanz)

Ultrasonic refining had been an active subject of research during the '50s and '60s, and then the field was somewhat abandoned. Research findings generally indicated that high-power ultrasonics (cavitation) can be used to increase fiber flexibility while avoiding fiber cutting and fines generation. However, this was obtained at the expense of a prohibitive use of electrical power.

Further analysis of the literature has shown that none of the above work was carried out in a systematic manner because different parameters were varied using different experimental setups. It is within the context of revisiting ultrasonic refining in a very controllable manner to gather more physical evidence about the process that an exploratory project was devised. This project was initiated in 1996 by John Blanz, now a second-year M.S. student at IPST.

Figure 9 depicts a schematic diagram of the experimental setup developed for refining studies. An ultrasonic horn operating at 20 kHz or circular piezoelectric ceramic transducers operating at 250, 500, or 1000 kHz (not shown in the figure) is used to induce cavitation in a temperature-controlled glass beaker. A calorimetric technique is used to quantify the level of acoustic power delivered in the pulp slurry.

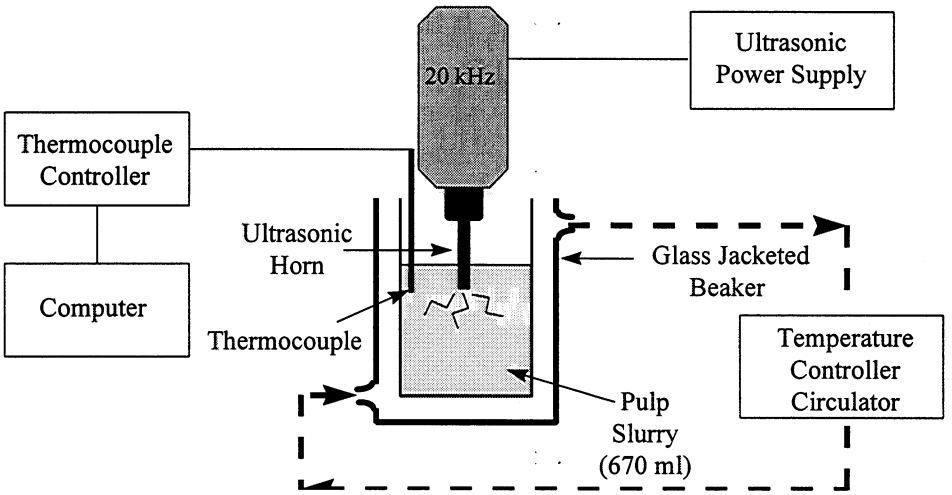

Figure 9. Schematic diagram of the exploratory experimental setup for pulp refining using high power ultrasonics. In addition to the 20 kHz ultrasonic probe shown in this figure, higher frequency transducers are used.

Experiments are performed using fines-free (~3%) unbleached softwood Kraft fibers. Each test consists in the processing of 670 ml of pulp slurry. The following parameters are considered: treatment time, temperature (20 and 65 °C), consistency (0.5 and 1%), frequency, acoustic power, and percentage of dissolved oxygen in water.

Several preliminary tests have been conducted so far to evaluate the effect of each of the above parameters. A typical test involves the measurement of the freeness level and average fiber length, and the preparation of three handsheets for paper properties testing. The following nondestructive paper measurements are obtained: apparent density, in-plane ultrasonic longitudinal and shear specific stiffnesses, and out-of-plane ultrasonic longitudinal specific stiffness. Results are compared to similar measurements obtained using a PFI mill. A final series of experiments is scheduled for

March-April. Additional fiber measurements such as fiber curl and fiber flexibility will be made during these experiments.

Figure 10 shows a graph of the in-plane and out-of-plane ultrasonic longitudinal stiffnesses as a function of treatment time at 20 °C, 20 kHz, 0.5% consistency, and 80 W_{rms} acoustic power. As expected, stiffness properties increase as a function of time.

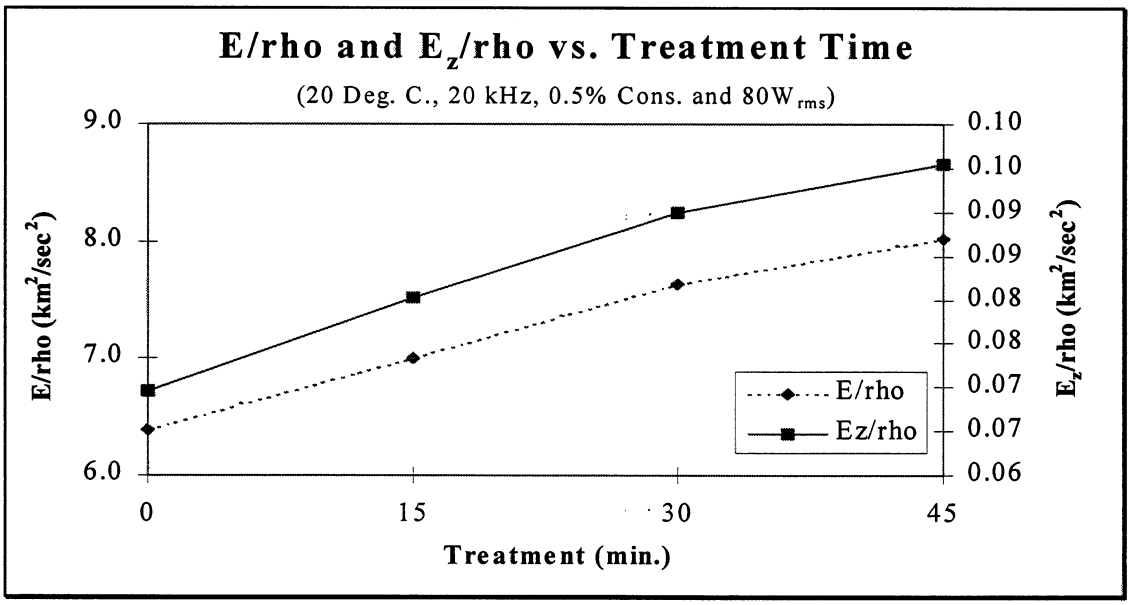

Figure 10. Graph of in-plane and out-of-plane ultrasonic longitudinal stiffnesses as a function of treatment time.

One major outcome of the research work will be to determine optimized conditions for ultrasonic refining. Also, a preliminary power consumption analysis will be performed. The study will be completed in May 1997.

5. Proposal Abstract: "Acoustic Separation Technology"

A proposal was submitted to the Agenda 2020 Recycling Task Group in October 1996 and this proposal was recommended to the Department of Energy for funding in early January. It is anticipated that the proposed work will begin late spring or during the summer. The proposal's abstract as well as the "Benefits to Industry" Section are reproduced below.

5.1 Abstract

A four-year R&D program is proposed to demonstrate a multi-use in-line acoustic separation technology from the laboratory-to-pilot-scale level. The electrically driven process is free of screens and moving parts. Separation is primarily based on fiber width. Several applications have been identified: fiber fractionation, separation of vessel elements from fibers, shives from fibers, earlywood from latewood, softwood from hardwood, fibers from fines, contaminants from fines, fibers from air bubbles (and attached ink particles) in flotation deinking, pulp thickening, clarification, dewatering of waste products, and removal of flocculated particles in closed water systems. The project has three phases. Phase I (first year) involves a laboratory demonstration and a preliminary economical assessment of the separation method. A newly developed 80 GPM acoustic separator will be used for that purpose. Various separation schemes will be tested to optimize separation efficiency, power consumption, and specific throughput. Phase II addresses the development of a 500 GPM pressurized pilot-scale acoustic separator. Also, it considers a computational analysis of fiber suspensions subjected to a progressive ultrasonic wave field

under laminar and turbulent flow conditions. The pilot-scale system will be tested during Phase III and a comprehensive economical assessment of the technology will be made.

5.2 Benefits to Industry

The proposed separation technology is free of screens and moving parts, and as such, clogging, fiber damage, and pulsation are unlikely. Since it is electrically driven, it has the potential for excellent controllability (e.g., in-line adaptation to varying recycled input streams). Versatility and applicability are key issues. The process has the potential to address several unfulfilled separation needs such as the separation of vessels or shives from fibers, and the separation of fiber species (e.g., earlywood from latewood, softwood from hardwood, Kraft pulp from NSSC, bleached chemical pulp from groundwood-rich newsprint). Anticipated superior separation efficiency when compared to pressure-screen systems and access to more than two fractions (if desired) would lead to better use of raw materials, less refining (energy savings), product quality enhancement, and reduction of water consumption. Other applications relate to enhanced deinking, pulp thickening, and removal of particles in closed water systems. Calculations based on experimental data and estimates of energy losses during power amplification and transduction show that the power consumption per ton of pulp for a hypothetical commercial acoustic separator would be competitive with that of a pressure screen fractionator of equivalent size.

6. Proposal Abstract: "Closed Water Treatment in Pulp Mills Using a Dual Flocculation/Ultrasonic Clarification Method"

In collaboration with Professor Yulin Deng (Surface and Colloid Chemistry), a proposal was submitted in July 1996 to the *Georgia Consortium for the Technological Competitiveness in*

Pulp and Paper. This proposal was recommended for funding, beginning in July 1997. The proposal's abstract is now reproduced.

6.1 Abstract

With increasingly restrictive environmental regulations and the need to optimize raw material usage, paper mills are required to totally close up their water system. Obviously, maintaining environmentally sound and technologically competitive pulp and paper mill operations is a key to the success of the State of Georgia because Georgia is one of the nation's leading producers of pulp and paper. When water systems are closed, the number of contaminates significantly increases. Unless efficient removal techniques are used, accumulating solid suspensions will be detrimental to the papermaking process and the quality of the final products.

It is proposed to demonstrate the feasibility of a novel dual method combining chemical flocculation and ultrasonic separation to remove contaminates from closed water streams. The research program, which is scheduled to last two years, will address the following issues for FY 98:

(1) Chemistry of flocculation of solid suspensions in closed paper mill water;

(2) Feasibility study of the flocculation/ultrasonic clarification method;

(3) Economic and energy assessment of the proposed technology.

It is anticipated that a large-volume, energy-efficient method for contaminates removal (clarification) can be developed, which can substantially enhance water closure operations of paper mills. Also, it is expected that the fundamental understanding obtained through the proposed work can be used in other relevant applications such as ultrasonic fiber

separation/fractionation and ultrasonically assisted flotation deinking. Funding for this program should provide the basic knowledge and justification to scale up the technology in collaboration with industry suppliers and then transfer the technology to Georgia mills.

7. Bibliography of Key Literature

[1] Brodeur, P.H., "Motion of Fluid Suspended Fibers in a Standing Wave Field," *Ultrasonics* 29 302-307 (1991).

[2] Brodeur, P., Dion, J.L., Garceau, J.J., Pelletier, G., and Massicotte, D., "Fiber Characterization in a Stationary Ultrasonic Field," *IEEE Trans. Ultrason. Ferroelec. Freq. Control.* 36 549-553 (1989).

[3] Garceau, J.J., Dion, J.L., Brodeur, P., and Luo, H., "Acousto-optical Fiber Characterization," *Tappi J.* 72 171-173 (1989).

[4] Dion, J.L., Brodeur, P., Garceau, J.J., and Chen, R., "Caractérisation des fibres par un nouveau procédé acousto-optique: nouveaux résultats." *J. Pulp & Paper Sci.* 14 J125-J128 (1988).

[5] Brodeur, P.H., "Acoustic Separation in a Laminar Flow," Proc. IEEE Ultrasonics Symp., Cannes, France Vol. 3 1359-1362 (1994).

[6] Brodeur, P.H. and Runge, T.M., "Compactibility of a Wet Fiber Mat Using Acoustic Radiation Pressure," *J. Pulp & Paper Sci.* 22(8) J278-J282 (1996).

FUNDAMENTALS OF DIMENSIONAL STABILITY

STATUS REPORT

FOR

PROJECT E00102/F020

Douglas W. Coffin
Barry Hojjatie
Kennisha Collins

March 26, 1997

Institute of Paper Science and Technology
500 10th Street, N.W.
Atlanta, Georgia 30318

TECHNICAL PROGRAM REVIEW

Project Title:	Dimensional Stability
Project Code:	DIMSTAB
Project Number:	E00102/F020
Division:	Engineering and Paper Materials
Project Staff:	Douglas Coffin, Barry Hojjatie, Kennisha Collins
Project Budget:	FY '96-97 $227,568

I. OBJECTIVE

To develop a science-based understanding of the dimensional stability of paper and paperboard, especially the phenomenon of cockle, and to apply these fundamental results to practical industrial problems.

The strategic objective of this project is to reduce the amount of paper rejected because of cockle through improved efficiency in identifying the causes of cockle and/or use of corrective measures to prevent cockle.

II. GOALS

The primary goals of this program are to (1) build a science-based understanding of cockle in paper; (2) develop tools to evaluate cockle of paper that occurs in the manufacture, conversion, and end-use of paper; and (3) transfer this technology to industry so that cockle problems can be controlled, eliminated, or avoided.

III. SUMMARY

Work during the past year has focused on the development of tools to evaluate cockle. These tools will be utilized in an experimental evaluation of cockle. Concurrently with the development of the cockle evaluation equipment, several other tasks were completed during 1996. The key accomplishments of this period are summarized below.

- New Tools Developed:

  - Constructed humidity generator - mixes dry air and saturated air in a controlled manner to produce a prescribed humidity in a given chamber.

  - Constructed cockle measurement device - frame and rail system for controlled movement of CCD camera and/or laser displacement system.

- New Tools Designed

  - Designed humidity chamber - chamber to allow specimen evaluation in controlled humidity environment. Includes balance for measurement of moisture in similar sample.

  - Designed hygroexpansive buckling tester - testing apparatus for producing buckling of paper strips subjected to increase in moisture. Compressive load, moisture content, and out-of-plane displacement recorded.

- Developed techniques to produce handsheets with nonuniform properties.

- Performed preliminary investigation of refining, drying, and nonuniformity on the cockle of handsheets.

- Developed analytic solution of the hygroexpansive buckling of a strip of paper.

- Published Member Company Report Number 1: *Cockle and the Hygroexpansive Buckling: A survey of Initial Buckling and Postbuckling of Thin Plates*

- Published Member Company Report Number 2: *A Literature Review of Cockle and a Proposed Mechanism*

BACKGROUND

This project was initiated and started in July of 1994. The scope of work for this project is to gain an understanding of cockle in paper and to develop the knowledge and tools required to eliminate its occurrence. Cockle is a manifestation of the dimensional instability of paper due to local variations in the physical state of the paper coupled with a change in moisture content. The phenomenon of cockle is directly related to the mechanical, hygroexpansive, and physical properties of paper. These properties will be a result of the constituent materials and the papermaking process used to produce the sheet. With an understanding of how cockle occurs, steps can be taken to eliminate it by modifying the constituent materials or papermaking process. Since cockle is inherently a complex problem and is influenced by many different factors, the advances made in this research program will benefit the scientific understanding in all areas of dimensional stability.

After completing a thorough review of the literature on cockle [1], it was found that little scientific results have been published that provide a basis for understanding cockle. The first task completed in this project was to develop a fundamental analysis that illustrated a plausible mechanism for cockle. The results of this analysis together with findings in the literature lead to the following mechanism for cockle.

> *Cockle results from an in-plane variation of the free hygroexpansive strains resulting from a change in moisture content of the sheet. The nonuniformity in the potential for free expansion creates compressive stresses in the sheet. If the compressive stresses are of sufficient magnitude, the sheet will buckle out-of-plane; thus, creating cockle. The free hygroexpansive strain is the stress free strain resulting from a change in dimensions of a material undergoing a change in moisture content. In addition to the nonuniformity in the free hygroexpansive strains, planar nonuniformities in mechanical or physical properties must be present to induce local buckling of the sheet.*

DISCUSSION

Buckling and Postbuckling Theory

As stated in the last section, it is proposed that cockle is the result of local buckling of the sheet. A clear understanding of buckling and postbuckling theory for plates will provide insight into cockle. The effect of parameters such as geometry, boundary support, loading conditions, constitutive behavior, material symmetry, and imperfections on the critical buckling loads, buckled shape, and postbuckling response can be obtained from the literature. This information can be used to help interpret, classify, and describe cockle. A review of the buckling and postbuckling behavior of thin plates was completed in 1996. A summary of these results was published as a member company report [2]. A full report will be completed in the Spring of 1997 and be available to member companies upon request. This report will serve as a reference and guide to understanding cockle in paper.

The literature review covers buckling due to an applied external loading, which creates a stress state possessing compressive components. For paper, the compressive stress develops because of constrained shrinkage/expansion due to moisture changes. Therefore, the change in moisture is the driving force leading to cockle or buckling, and the magnitude of the stresses should relate to the hygroexpansive properties of the sheet.

The review of the literature revealed that for an orthotropic material, such as paper, buckling theory predicts that the number of waves formed in the sheet increases as the ratio of directional properties, say E_{MD}/E_{CD}, increases. In addition, the buckled waves in a circular plate tend to orient themselves with the material properties rather than the direction of loading. Some cockle in machine-made papers tend to be elliptical showing a preference of one direction over the other. This could be related to the orthotropy of the material. The preceding examples illustrate how the literature review may lead to insight into the cockle problem.

The buckling and postbuckling theory reviewed in the report will be useful in interpreting experimental results of cockle. In 1996, Nam and Thorpe [3] presented some observations on the cockle behavior of copy paper in changing moisture conditions. Their observations fit well with what would be expected from buckling theory. For example, Nam and Thorpe found that hygroexpansivity of the sheet plays a major role. The change in moisture multiplied by the hygroexpansion of the sheet is the driving force leading to buckling. As the hygroexpansion increases, the critical buckling load is reached under a smaller change in moisture. Therefore, it is not surprising that hygroexpansion is a major factor. Nam and Thorpe [3] observed that as the moisture decreased, cockle height increased. This is typical of the postbuckling response of plates in which an increase in the applied force causes an increase in the deflection. Nam and Thorpe [3] observed a mobility of the cockles during changes in moisture. In other words, it appeared that the cockles moved from one location to another in the sheet. Nam and Thorpe [3] state that this appears counter to the accepted argument that local nonuniformity sets up local stresses that govern the deformation. This is probably not a correct argument. From buckling theory [2], we learn that the deformation can be strongly influenced by imperfections or heterogeneity. In addition, under large deformations, secondary buckling may occur in which the deformation moves from one state to another. This would then account for the "mobility" observed by Nam and Thorpe [3].

One specialized area of plate buckling research is thermal buckling or buckling due to restrained thermal expansion. The mathematics of this case is exactly analogous to the hygroexpansive buckling of paper where the potential for thermal expansion and hygrothermal expansion can be interchanged. The literature on thermal buckling is currently being reviewed and will be completed by Spring 1997.

Hygroexpansive Buckling

In the last section, an analogy between buckling due to compressive loads and restrained hygroexpansion was made. The direct analogy holds when the applied load gives the same stress state as the restrained expansion/shrinkage. To determine the critical buckling load, the analogy works well, but there are differences between the two cases that make methods of solution distinct for postbuckling analysis.

The first and obvious difference is that the driving force for hygroexpansive buckling is the change in moisture and not the applied force. For hygroexpansive buckling, the magnitude of the compressive stresses is a result of the amount of restraint and the degree of buckling. In classical load buckling, the stresses are a direct result of the applied load, which is known *a priori*. Therefore, the postbuckling response of stress magnitude versus out-of-plane deflection for hygroexpansive buckling may not be the same as it is with the case of load buckling. In fact, this is what was found for the problem described below.

The second difference between load buckling and hygroexpansive buckling pertains to the assumptions on the kinematic equations. In classical buckling, the plate is assumed to be inextensible in-the-plane of the plate, meaning that the prebuckled plate length is the same as the postbuckled plate length. This is an adequate assumption because most of the in-plane deformation is a result of movement at the boundaries where the load is applied due to the buckling. In hygroexpansive buckling, the distance between the boundary supports remains fixed, and therefore, the length of the plate must increase if buckling occurs. In other words, the cord length is the original length and is always smaller than the arc length of the buckled state. Therefore, the simplifying constraint of inextensibility cannot be applied to the postbuckling solution for hygroexpansive buckling.

If the hypothesis of hygroexpansive buckling for cockle is to be proven and buckling theory utilized to increase the understanding of cockle, hygroexpansive buckling of paper must be studied experimentally and the results compared to theory. The simplest problem in which the theory of hygroexpansive buckling can be tested is the buckling of a strip of paper fully restrained from expansion along the longitudinal axis and subjected to an increase in moisture content.

This simple problem is illustrated in Figure 1. During 1996, a testing apparatus was designed to perform these tests. The fixture is currently being built and should be complete by the end of March 1997. The paper sample will be clamped between two end supports. One end is adjustable so that the length of the specimen can be varied. The fixture can accept a width of 1.25 cm. The other end-support is attached to a load cell which will measure the compressive axial load exerted by the paper onto the clamps during expansion. The fixture will be placed in a humidity chamber. The out-of-plane displacement will be monitored with a laser displacement sensor. The laser displacement sensor is mounted to an x-y positioning rail so that the entire buckled mode shape can be measured.

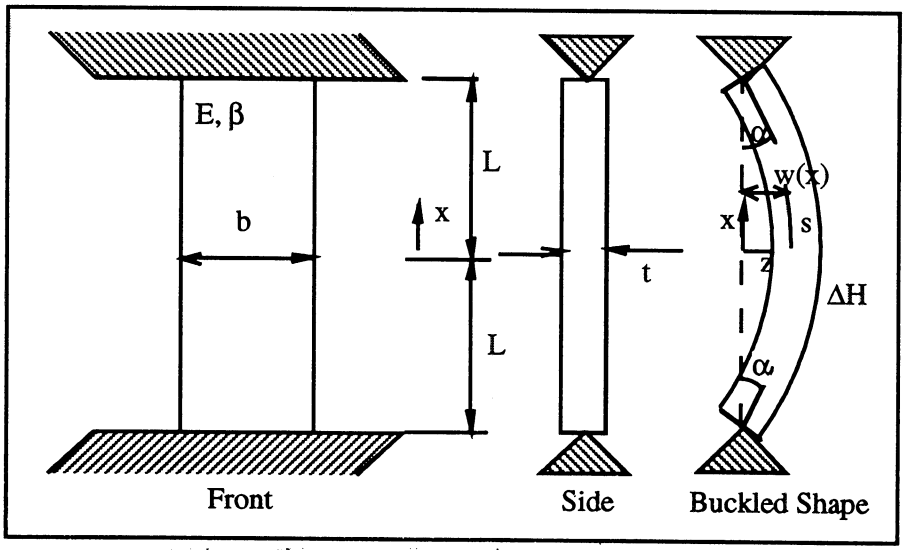

Figure 1. Hygroexpansive buckling of a strip of paper. (E is the elastic modulus, β is the coefficient of hygroexpansion, ΔH is the change in moisture content, α is the angle of rotation at end of beam)

The hygroexpansive buckling test consists of mounting a paper strip in the fixture. The humidity of the surrounding air is increased, and the moisture pick-up of a similar sample is recorded. The load cell will record the compressive load that results from the restrained axial expansion, and the laser will record the out-of-plane deflection of the sample. For each increase in humidity, data for load, moisture gain, and deflection will be recorded. As the moisture content increases, the sheet will buckle, and the postbuckling response of the sheet will be recorded.

This experimental postbuckling response can then be compared to analytical results. An analytic solution of the postbuckling solution for the problem shown in Figure 1 was derived. For the solution, the paper was assumed to be a linear elastic material with linear hygroexpansion. Dimensional changes in the cross-section were neglected. In order to obtain the postbuckling solution, large deformation and finite strain expressions were used. With these assumptions, an analytical solution for the postbuckling load was obtained. The solution is in the form of two coupled integrals of elliptic form which must be solved numerically. A member company report will be written describing the formulation and giving the solution of this problem.

The numerical solution of the problem showed that the axial load will reach a critical level. At this load level the onset of buckling will occur. After buckling, the compressive axial load will decrease in magnitude. This trend is shown in Figure 2 where the nondimensional axial force is shown as a function of the angle of rotation at the ends of the beam. This decrease in load is a result of the buckling which allows the strip to expand. This result differs from classical buckling where the applied axial load must be increased to increase the out-of-plane deflection. For the current problem, the change in moisture content must be increased to increase the out-of-plane deflection. This relationship depends on the slenderness ratio or length-to-thickness ratio of the strip. As the strip becomes more slender,

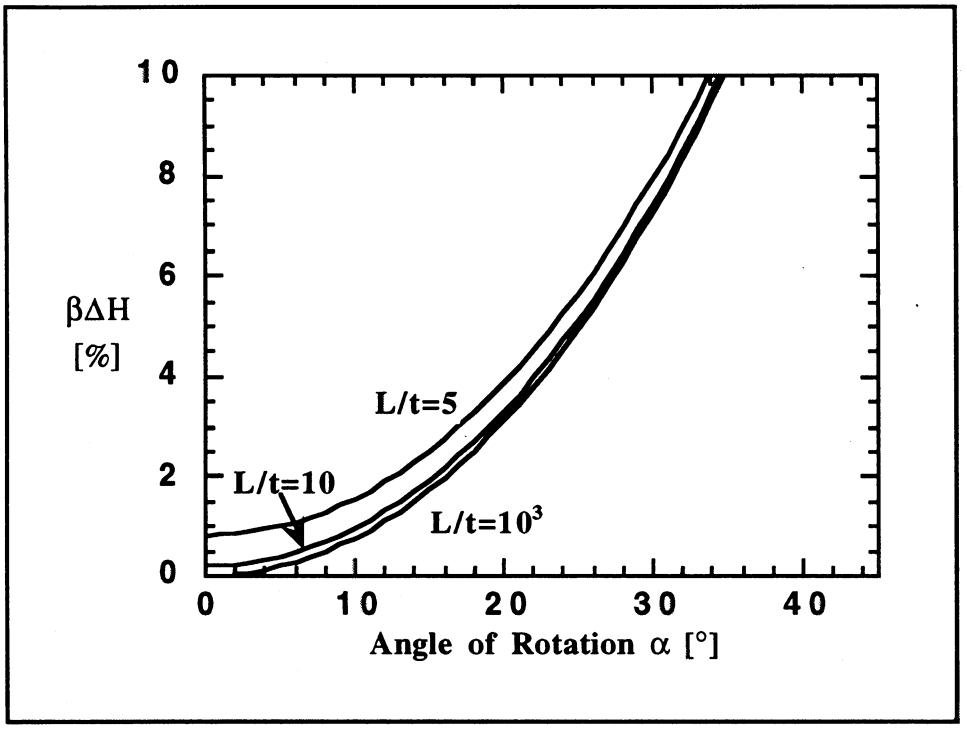

Figure 3. Hygroexpansive strain versus angle of rotation.

As needed, the model can be updated to reflect dependence of properties on moisture content and viscoelastic behavior.

Humidity Generator

During 1996, a humidity generator was built at IPST for use with the dimensional stability testing program. The generator combines dry air and saturated air to produce mixed air of the desired relative humidity. The dry air is obtained from IPST in-house supply of compressed air. The saturated air is produced by forcing dry air through a water column. Air bubbles traveling through the water column become saturated. The dry air and moist air are mixed at the inlet point of a chamber. The relative humidity of the air in the chamber is measured with an Rh sensor. The Rh signal is used as the process variable in a control scheme to regulate the flow rates of the dry and saturated air.

The amount of air flow is determined by the degree to which two solenoid valves are opened. The valves (BP2EV0014) are manufactured by Honeywell. A 4-20 mA signal controls the opening of the valves, allowing for a range of flow rates. The signal is sent to the solenoid valves from a dual-input, programmable process controller (CN003 by OMEGA). The controller can accept two 4-20 mA input signals and provide two 4-20 mA output signals. The relative humidity is being used to control the valve openings. A desired humidity profile is established, and then depending on whether the Rh signal is below or above the set point, the solenoid valves will open or close.

The relative humidity in the chamber is sensed with the Vaisala HMP 233 humidity sensor with capabilities of measuring the full range of Rh from 0 to 100%. The accuracy of the sensor is ±1% Rh in the range 0 to 90% and ±2% Rh in the range 90 to 100% Rh. The temperature is measured with a PT-100 sensor.

In trials, the humidity generator was able to maintain the desired humidity of a given chamber. The generator was also able to produce cyclic changes in relative humidity approximating a step change in Rh. In the present set-up the humidity generator controls the Rh of a closed chamber. The rate at which the Rh changes is dependent on the size of the chamber. A new chamber is being constructed in the Winter of 1997. When this chamber is ready, the humidity generator will be tested in a more complete manner. Figure 4 shows a example of a humidity profile produced by the generator.

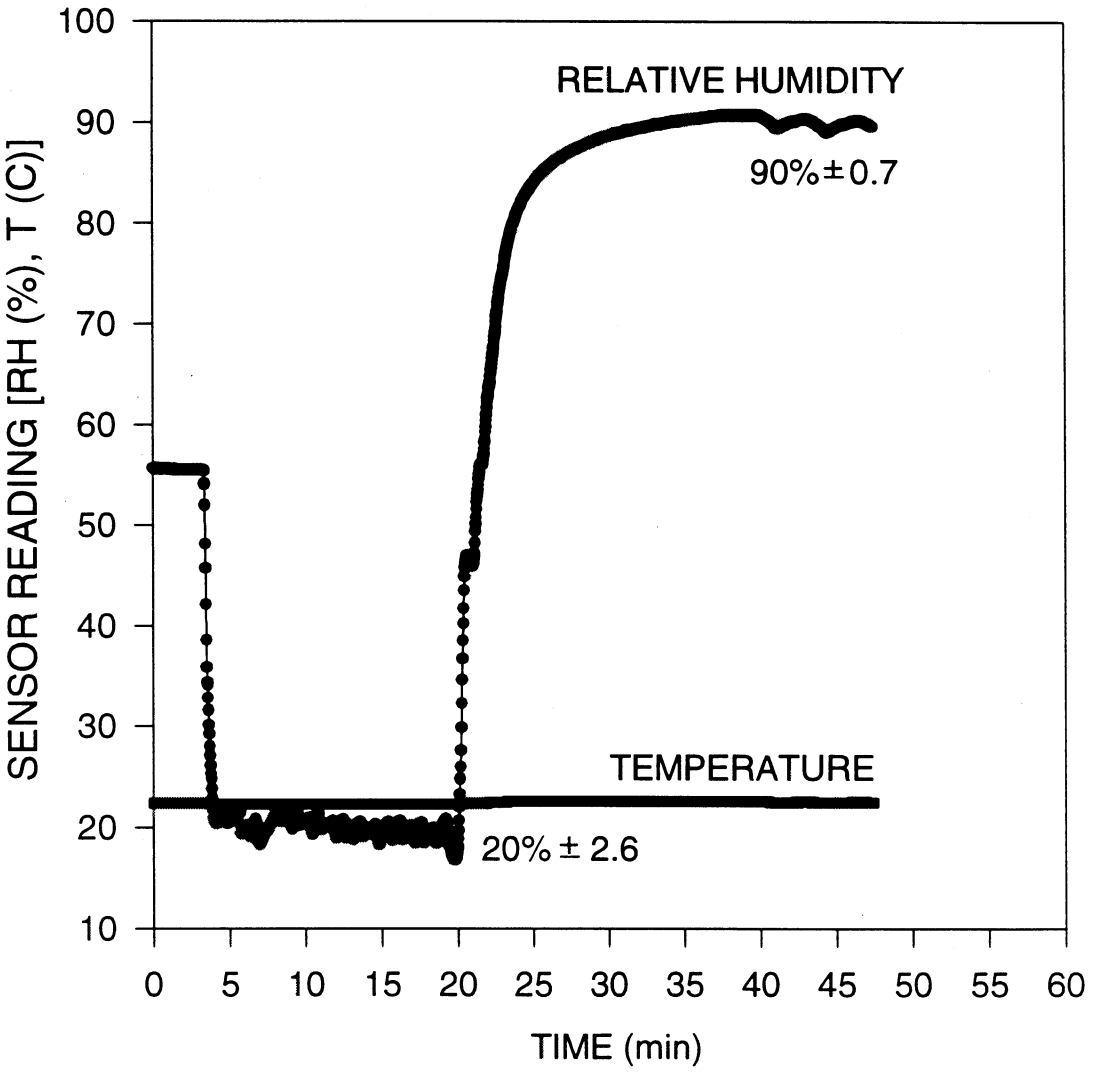

Figure 4. Example of humidity profile produced by humidity generator

Dimensional Stability Evaluation Test Stand

In order to evaluate cockle and dimensional stability, one needs to be able to measure the surface topography of paper at a given humditiy and the deformation of the paper under changes in moisture content. During 1996, a test stand and measurement device was designed and constructed at IPST. Currently, it is being used to measure cockle, and during 1997, it will be used to measure hygroexpansivity of paper and changes in displacements with changes in moisture content.

The test stand consists of an x-y-z linear positioning rail system mounted on a steel frame. The frame was designed to minimize deflection due to movement of the rails, and provide access to the testing area. Either a CCD camera or a laser displacement sensor is mounted on the rail system. The sensors can be moved to the proper position relative to the specimen being tested. The vertical (z) positioning is operated manually using a winch. It allows for 5 feet of vertical movement. The horizontal (x and y) positioning rails are motor driven and controlled with the use of a PC computer. The reason for mounting the camera and laser on the rail system is so that the paper sample remains stationary during testing.

The camera or laser is mounted from above the specimen. There is ample room to place an environmental chamber below the rail system so that the specimen can be tested in a controlled humidity environment. The z-direction rail allows for proper placement of the camera/laser so that the specimen is in focus. Then, the sample can be scanned using the x/y-direction rails. Scanning the sample with the laser will provide the topography or out-of-plane displacement of the sample. The camera can be used in a stationary position to determine the in-plane displacements of the sheets.

During the past year, work focused on setting up this equipment, writing software to control the motion of the rails, and verifying the accuracy of the laser displacement sensor. The laser

was found to have a linear response of voltage versus displacement in the range of 0 to 20 mm. The resolution of the laser set up is ±0.05 mm, and the error in measurements of known displacements was found to be ±0.1 mm.

During 1997, the laser will be used to measure cockle of sheets. The resulting sheet topography will then be used to characterize the cockle. Filtering and frequency content analysis will be completed on the data, and methodology will be developed to characterize the degree and type of cockle in sheets.

The laser system will also be used to measure the hygroexpansive buckling of sheets and the change in cockle with changes in moisture content. The camera system was set up in 1996, but, at present, testing has not been completed. In 1997, the camera system will be used to measure hygroexpansion of sheets.

During 1997, the capability for full-field measurement of surface topography will be added to the test stand. The limitation of the laser sensor is that only one point can be measured at a time and the sheet must be scanned. During changing humidity environments, the change in topography can occur faster than the time needed to scan the sheet. Therefore, a technique that measures the full field quickly would provide more insightful information. A shadow Moiré method will be employed for this purpose.

Nonuniform Handsheets and Preliminary Cockle Investigation

During 1996, a method to produce nonuniform handsheets was developed. The reasons for developing these procedures were to determine if specific nonuniformities lead to cockle through nonuniform shrinkage of the sheet, and develop an experiment that could be used to verify the fundamental cockle model.

The nonuniformity was introduced by placing a round tube into the British handsheet mold. Then, one pulp type was placed inside the tube and another pulp type was placed outside the tube. When most of the water drained from the mold, the tube was pulled out of the mold. Forming sheets in this manner allowed for the center of the sheet to be at a higher or lower basis weight, or to be formed with stock of higher or lower freeness.

With practice, a handsheet possessing a continuous boundary between the two regions can be produced. If the tube is pulled up too soon, the two pulps mix and the boundary is not clearly defined. If the tube is pulled up too late, the boundary region is too distinct and, in the extreme, two separate sheets are produced.

The deformation that was produced in the sheet was very dependent on the method of drying. Freely dried sheets developed extensive curl and wrinkling, while sheets dried under full restraint were very flat. When sheets were dried between blotters so as to give partial restraint, the sheet deformation was much less severe than the freely dried sheet.

In order to produce a sheet with a well-defined cockle in the center of the sheet, the sheet had to be dried nonuniformly. That is, the center of the sheet was dried first, then the outer region was dried. In these instances, the center of the sheet buckled out-of-the-plane during drying of the outside region.

Some of the sheets made during the development of the method for making nonuniform sheets, some of which were uniform sheets, were evaluated for degree of cockle. The degree of cockle was defined as severity of out-of-plane displacements. The scoring was qualitative. A score of 10 represents severe distortion and 0 represents no distortion of the sheet. Table 1 provides an example of this classification. For these samples, two levels of freeness are shown. Only one sample had a nonuniform basis weight. One sample was dried using a ring,

and one was dried on a drum. The results are as expected. The higher the restraint during drying, the lower the distortion. As the freeness is lowered, one would expect the shrinkage to increase and consequently, the distortion-upon-drying to increase. The example given in the table, shows that the sheet made in the nonuniform manner had slightly more distortion than the uniform sheet. But in some instances the uniform sheets dried in the same manner as the nonuniform sheets had slightly less distortion.

Table 1. Preliminary cockle evaluation of handsheets

Drying	drum	free	free	ring	free
Freeness	344	344	344	115	115
Nonuniform Handsheet	no	no	yes	no	no
Cockle Score	0	3	4	0	10

The information given above is only meant to show the potential for experimental work. Once the methods for evaluating cockle have been developed, a quantitative cockle number can be obtained. Then a study of the effect of process variables on the amount of cockle can be conducted. Such tests are planned for 1997.

REFERENCES

1. D. W. Coffin, *Literature Review of Cockle and a Proposed Mechanism*, Project E00102, Report 2 to the member companies of the Institute of Paper Science and Technology, September 1996.

2. D. W. Coffin, F. Bloom, *Cockle and Hygroexpansive Buckling: A Survey of Initial Buckling and Postbuckling of Thin Plates*, Project E00102, Report 1 to the member companies of the Institute of Paper Science and Technology, September 1996.

3. W-S. Nam and J. Thorpe, "Deformation of Copy Paper with Changing Moisture Conditions," *Proceedings of Progress in Paper Physics - A Seminar*, June 9-14, 1996, Stockholm, Sweden, pp. 65-68.

MICROMECHANICS OF CONVERTING OPERATIONS

STATUS REPORT

FOR

PROJECT F023

Martin Ostoja-Starzewski
Marco B. Quadrelli

March 26, 1997

Institute of Paper Science and Technology
500 10th Street, N.W.
Atlanta, Georgia 30318

TECHNICAL PROGRAM REVIEW

Project Title: MICROMECHANICS OF FIBER NETWORKS
Project Code: MICRO
Project Nmuber: F023
Division: Engineering and Paper Materials
Project Staff: Martin Ostoja-Starzewski (PI) and Marco B. Quadrelli (Asst. Scientist)
Project Budget: $168,700

OBJECTIVE

The objective of this project is to develop an understanding of the relation of the macroscopic (scales of centimeters to meters) to the microscopic (fiber scales) properties of paper. As the primary focus of this project is on mechanical properties, this goes under the name 'micromechanics of paper', with the main interest being in elasticity and strength in the MD-CD plane. The same framework also serves in the determination of macroscopic thermal conductivity, also in the MD-CD plane, in terms of single fiber properties.

SUMMARY

Several micromechanical models of paper have been developed. Within a quasi-single-fiber-layer setting, they cover a spectrum of materials: from those that are more suited for papers of high porosity (such as hygenic tissues), to the ones that are more adequate for highly compacted fibers. It is well-known that paper is a multiscale disordered material, yet what is typically desired in applications are simple formulas in terms of but very few microscopic parameters. Basic considerations of this subject are being made in Part I.

A basic model, which may grasp fiber-fiber interactions, is based on a periodic lattice - its advantage is a possibility of derivation of explicit continuum-type formulas in terms of fiber properties and fiber volume fraction (equivalently, paper porosity). In Part II, such formulas have been obtained for in-plane thermal conductivity, in-plane elasticity, and out-of-plane plate-bending paper sheet response - all within a framework of single layer fiber networks. In the second of

these models, effective elastic moduli have been analyzed as a function of fiber segment's aspect ratio displaying an augmenting effect of its bending and shear effects as a function of increasing fiber volume fraction; comparisons to the Cox model and perforated plate model have been drawn.

In Part III, a general framework for qualitatively and quantitatively analyzing paper as a spatially random network of elastic fibers, "welded" at their mutual contacts, has been drawn. Such a network is described by fiber elastic moduli, an angular distribution function as well as probability distributions of fiber lengths, thicknesses, and crossings. It is shown that spatial disorder prevents us from formulating an effective Hooke's law in a unique form. Indeed, a constitutive response law is dependent on the scale of resolution, that is chosen by an experimentalist or a theoretician: the larger this scale, the closer we are to a classical, deterministic continuum concept. Hierarchies of scale-dependent bounds are shown for thermal conductivities of several random fiber networks, while, in the case of elasticity, a specially developed finite element program simulates complex systems of fiber-beams.

As described in Part IV, the latter computer program is a basis for an ongoing development of a program for simulation of paper fracture, where two failure modes would be present: fiber segment failure and fiber-fiber debonding. In order to verify this model, tensile displacement and strength tests on small (2 *mm* x 2 *mm*) very thin paper specimens of Kozo fibers are being set up in a load cell under an optical microscope equipped with a video recording equipment. Such experiments in concert with the computer model will also permit a determination of microscale strength properties, as well as an investigation of larger paper specimens over a wide range of parameter space. Additionally, a set of two-meter-wide grips is being developed for strength tests to allow a study of size/scale effects in tensile strength of paper and the related statistics.

The report is divided into five parts (Part I, II, ..., V) and an Appendix. All the equations and figures are numbered according to a scheme (p, e), where p stands for a given part, while e stands for a given equation or figure.

GOALS

Project goals for the period beginning March 1996 (time of the preceding PAC review) involved:

1. Acquainting myself with the pulp and paper industry, while focusing attention on paper mechanics. This was accomplished through:

a) Study of the literature on paper mechanics and micromechanics.

b) Attending a TAPPI short course "Improving Converting Operations for Flexo Folder-Gluers & Soft Anvil Rotary Die Cutters."

c) Visits to several Japanese paper research institutes in September 1996:

- New Oji Paper Co., Tokyo
- Research Institute, Government Printing Bureau, Odawara
- Wood Science Department, Kyoto University, Kyoto

d) Presentation of a paper:

- M. Ostoja-Starzewski, "Random fiber networks: Bounds on effective elastic and transport moduli," *1996 Progress in Paper Physics - A Seminar*, Stockholm.

e) Writing of an Annual Technical Report.

Status: partially complete.

2. Development of experiments and theoretical models for determination of effective (macroscopic) elasticities, strengths, and conductivities of paper from the standpoint of a disordered (random) network of interacting fibers. Focus is on size/scale effects.

Status: partially complete.

TABLE OF CONTENTS

DISCUSSION: PART I

PASSAGE FROM THE FIBROUS NETWORK TO AN EFFECTIVE CONTINUUM MEDIUM (repeated from [1] for the sake of completeness of this report)

The challenge

The challenge in paper micromechanics is illustrated in Fig. 1.1 below. That is, we have a system of interconnected/interacting fibers, whose properties are known to some extent, and for which we want to determine effective properties at some scales L larger than the fiber length. For simplicity at this stage, fibers have a shape of ribbons of width w and thickness t. For the sake of clarity, only a single-layer mat of straight fibers is shown - in the sense of [2] - called a *quasi-single-fiber-layer*; hence, t is also the apparent mat thickness t_a. The effective properties are desired in a continuum mechanics sense (e.g., mass density, stress, strain, heat flux, temperature gradient, ...), so that L signifies the scale of a *Representative Volume Element* (RVE), dV. The tool for passage from a discrete fiber network encompassed by the window $L \times L$ is outlined in the next section.

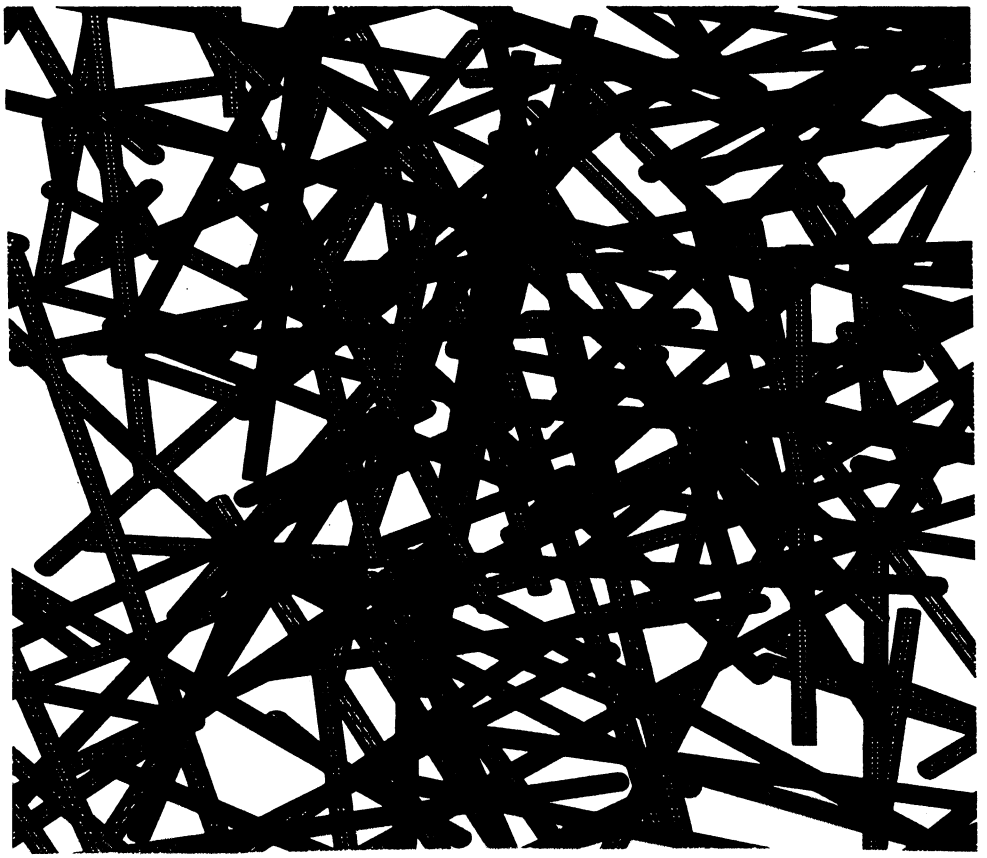

Fig. 1.1 A simple schematic diagram of a network of fibers in the MD-CD plane.

Basic geometric concepts:

Grammage is defined as

$$W \equiv \frac{m}{L \times L} \tag{1.1}$$

where m is the mass of the given window and is given as

$$m = V_f \rho_f = V \rho_a \tag{1.2}$$

where V_f is the total volume occupied by all the fibers, where ρ_f is the mass density of the fibers, $V = L^2$, and ρ_a is the apparent mass density.

Fiber volume fraction:

$$P_f \equiv \frac{V_f}{V} \tag{1.3}$$

where V_f is the total volume occupied by all the fibers.

Porosity, or the volume fraction of pores,

$$P_p \equiv \frac{V - V_f}{V} = 1 - P_f = 1 - \frac{\rho_a}{\rho_f} \tag{1.4}$$

Notation P_f and P_p reflects the fact that these are the probabilities of hitting the f-phase or the p-phase. Indeed, for experiments conducted on one sample versus another, all the four quantitites defined above display fluctuations dependent on the window size L. These are due to the flocculation, and therefore [3] defines grammage as a coefficient of variation of W

$$grammage \equiv \frac{\langle W \rangle}{\langle W^2 \rangle - \langle W \rangle^2} \tag{1.5}$$

in order to measure the statistics of those fluctuations; $\langle\ \rangle$ stands for a statistical ensemble average. At this stage, we work with the definition (1.1), unless specified otherwise.

Equivalence of the fiber network with the continuum model

Let us suppose that all the fibers inside the $L \times L$ window are elastic and contacts do not dissipate energy such as would be caused by friction. The basic idea in formulating an effective continuum of the window is based on the equivalence of strain (potential) energy stored in the window

B_L, of boundary ∂B_L, of volume V with strain energy of the network in the window

$$E_{network} = E_{continuum} \tag{1.6}$$

under specific boundary conditions on ∂B_L. The energy $E_{network}$ is given by

$$E_{network} = \sum_f E^{(f)} = \frac{1}{2}\sum_f^{|f|} (\vec{F} \cdot \vec{u})^{(f)} \tag{1.7}$$

The summation in (1.7) is carried out over all the fibers f (or fiber segments, depending on the model and interpretation), with a total of all the fibers being $|f|$. Thus, for example, $E^{(f)}$ in (1.7) stands for the energy stored in the f-th fiber; we place f in the superscript because the subscript will be reserved for the tensor indices.

The energy $E_{continuum}$ is

$$E_{continuum} = \frac{1}{2}\int_V \underline{\underline{\sigma}} \cdot \underline{\underline{\varepsilon}} dV \tag{1.8}$$

where $\underline{\underline{\sigma}}$ and $\underline{\underline{\varepsilon}}$ stand for the stress and strain fields, respectively. By the volume V in (1.8) we actually mean the projected area of the $L \times L$ window (a plate of thickness of one fiber), because we deal with planar fiber systems exclusively.

In the sequel, we will restrict ourselves to linear elastic fibers so that (1.2) will become

$$\begin{aligned} E_{network} &= \frac{1}{2}\sum_f^{|f|} (ku^2)^{(f)} \\ E_{continuum} &= \frac{V}{2}\bar{\varepsilon} \cdot \underline{\underline{C}}_L^{eff} \cdot \bar{\varepsilon} \end{aligned} \tag{1.9}$$

because the equivalent continuum medium will be linear elastic, too. In $(1.9)_1$, u is a generalized spring deformation and k its corresponding spring constant, both of which will depend on the actual fiber model used. Knowledge of both energies in (1.9) will allow, through the use of (1.6), the determination of an effective stiffness $\underline{\underline{C}}_L^{eff}$. The subscript L denotes here the explicit dependence of the effective (continuum-type) response on the chosen size of the window B_L - this will naturally grasp, say, the intrinsic scale-dependence of the statistics, even the averages, of effective stiffnesses. L-dependence will be an important tool in the future study of paper strength.

The challenge made transparent by $(1.9)_1$ is the need to know all the u's, i.e., the deformations of all the fibers. These will depend on the particular geometry of the fiber network in the window and on the particular model of fibers and their interactions. In the next sections, we introduce sev-

eral models of fiber networks - from the simplest to more complex - and systematically show how $\underline{C}_L^{eff}$ is to be determined. We begin with spatially periodic fiber networks, which do not offer much freedom for introducing the geometric and physical randomness, but have the advantage of allowing an explicit analytical derivation of $\underline{C}_L^{eff}$ for various fiber models: rod-type, beam-type, etc; here the unit volume element is that of one unit cell. Next, we go to spatially disordered network topologies - much closer to reality - where a resort has to be made to computer simulations. At this stage, the former periodic models serve as a guidance, while various types of microstructural disorder (such as the relative bonded area) can be investigated quantitatively. Also, these models will become essential in studying paper response beyond the linear elastic range: viscoelasticity, plastic-type hardening, crack formation and propagation, etc.

DISCUSSION: PART II
SINGLE-LAYER PERIODIC MODELS OF FIBER NETWORKS

Basic concepts (RBA, porosity, fiber aspect ratio)

It will be important, for the sake of reference, to have several basic relationships. First, after [12], grammage is defined as

$$W \equiv \frac{m}{L \times L} \tag{2.1}$$

where m is the total mass of fibers in the given $L \times L$ window and is given as $m = V_f \rho_f = V \rho_a$. Here V_f is the total volume occupied by all the fibers; ρ_f is the mass density of the fibers; $V = L^2 t_a$ is the total volume; and ρ_a is the apparent mass density; and t_a is the apparent thickness. Next, the fiber volume fraction and the porosity (or the volume fraction of pores) are

$$P_f \equiv \frac{V_f}{V} \qquad P_p \equiv \frac{V - V_f}{V} = 1 - P_f = 1 - \frac{\rho_a}{\rho_f} \tag{2.2}$$

Notations P_f and P_p reflect the fact that these are the probabilities of hitting the f-phase (fibers) or the p-phase (pores) in an image analysis.

There are, basically, three periodic nearest-neighbor lattices in two dimensions (2D): triangular, square, and honeycomb, see Fig. 2.1. Suppose we consider the triangular lattice (Fig. 2.1a) as

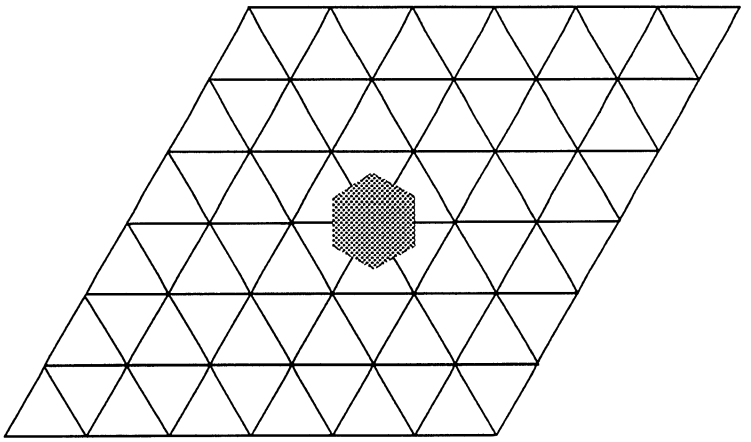

a)

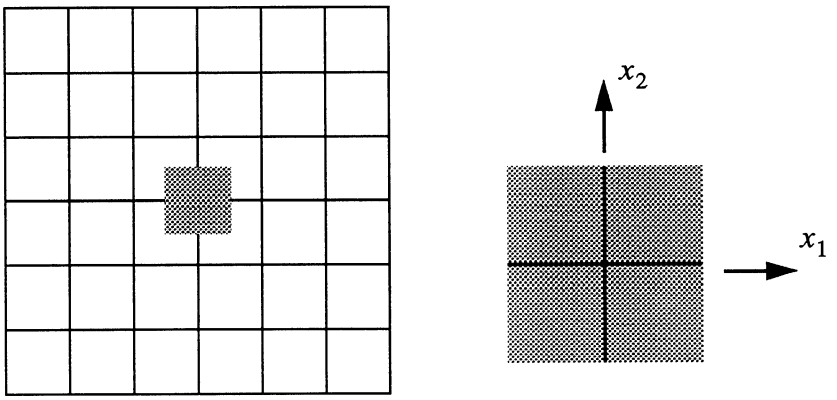

b)

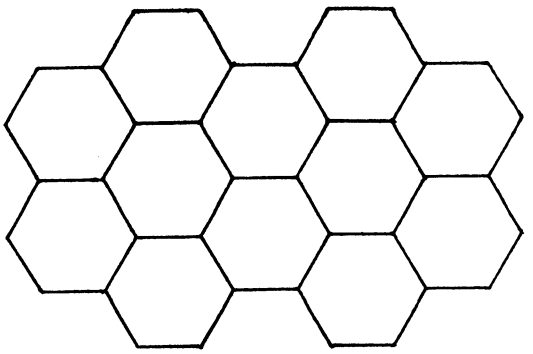

c)

Fig. 2.1a) A triangular lattice with a hexagonal unit cell shown;
b) a square lattice with a square unit cell shown; c) a honeycomb lattice.

an idealized model of a single-layer fiber network, which may be interpreted as a single-layer mat of intersecting long fibers. The internode elements play the role of free fiber segments [2]; their thickness, width, and length are denoted by t_a, w, and the internode spacing s, respectively. Pores are clearly defined in such a lattice (Fig. 2.2) so that porosity P_p and relative bonded area RBA are expressed in terms of the fiber aspect ratio w/s

$$P_f = 2\sqrt{3}\frac{w}{s} - 3\left(\frac{w}{s}\right)^2 \qquad RBA = \frac{2\frac{w}{s}}{2\sqrt{3} - 3\frac{w}{s}} \tag{2.3}$$

Note that in the hypothetical limiting case of $P_f = 1.0$, $w/s = 1/(\sqrt{3})$, and RBA becomes 2/3. On the other hand, in the case of $P_f = 0.0$, $w/s = 0$, and $RBA = 0$. In the following, a formula, inverse to (2.3), will be useful

$$\frac{w}{s} = \frac{1 - \sqrt{1 - P_f}}{\sqrt{3}} \tag{2.4}$$

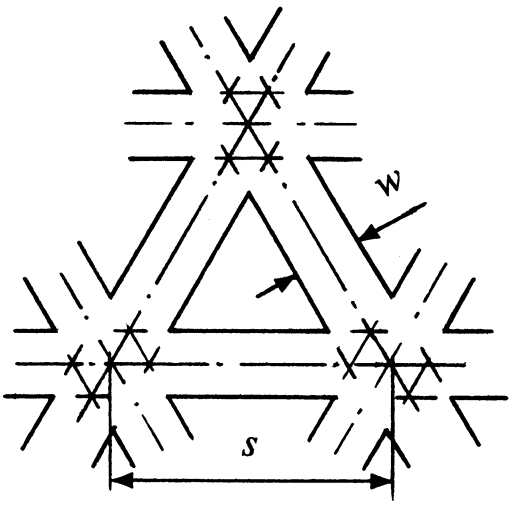

Fig. 2.2 Pore structure in a triangular lattice network showing the relationship between porosity, fiber volume fraction P_f, and aspect ratio w/s.

Considering the fiber overlap at the lattice nodes of either lattice, one could proceed here with a somewhat different interpretation for the apparent thickness of the fiber mat: namely, t_a to be effectively equal to three or two fiber thicknesses rather than just one. The ambiguity of t_a for 2D fiber mats is also noted in other models of fiber networks. For example, Kallmes & Corte [4] define a 2D sheet as one in which the area covered by more than two fibers is negligible, i.e., less than 1%.

In-plane thermal conductivity

In this section, we focus on the in-plane (MD-CD) thermal conductivity of a paper sheet. However, we note that (i) several other problems (e.g., electrical conductivity) are equivalent to it by virtue of mathematical analogies, and (ii) it provides a stepping-stone for studies of elasticity. In the continuum setting we thus have the constitutive law

$$q_i = K_{ij} T_{,j} \qquad i, j = 1, 2 \tag{2.5}$$

where $\underset{\sim}{q} \equiv (q_1, q_2)$ and $\nabla T = (T_{,1}, T_{,2})$. Upon substitution into the first law of thermodynamics (in the steady-state case)

$$q_{i,i} = 0 \tag{2.6}$$

we obtain

$$(K_{ij} T_{,j})_{,i} = 0 \tag{2.7}$$

Given the periodic lattice models of Fig. 2.1, we are interested in approximations of locally homogeneous media so that the governing equation becomes

$$K_{ij} T_{,ij} = 0 \tag{2.8}$$

In the special case of an isotropic medium, (2.8) simplifies to a Laplace equation

$$K T_{,ii} = 0 \tag{2.9}$$

Let us now consider the material to have a square lattice microstructure, Fig. 2.1b), whereby nearest neighbor nodes are connected by bonds (i.e., fiber segments) of conductivity k. It follows that the entropy production rate of a unit cell of such a lattice is

$$\dot{S} = \frac{1}{2} k \sum_{b=1}^{4} l_i^{(b)} l_j^{(b)} \overline{T}_{,i} \overline{T}_{,j} \tag{2.10}$$

where the summation is carried out over all the four bonds. In the above, we employed the uniform strain $\overline{\nabla T} = (\overline{T}_{,1}, \overline{T}_{,2})$. Also, $\underset{\sim}{l}^{(b)} = (l_1^{(b)}, l_2^{(b)})$ is the vector of half-length of bond b. In view of (1.6), the stiffness tensor is obtained as

$$K_{ij} = \frac{k}{V} \sum_{b=1}^{4} l_i^{(b)} l_j^{(b)} \qquad i, j = 1, 2 \tag{2.11}$$

where $V = 4$ if all the bonds are of unit length ($\left|\underset{\sim}{l}^{(b)}\right| = 1$). This leads to a relation between the bond conductivity k and the K_{ij} tensor

$$K_{11} = K_{22} = \frac{k}{2} \qquad K_{12} = K_{21} = 0 \tag{2.12}$$

In order to model an orthotropic medium, different bonds are applied in the x_1 and x_2 directions: $k^{(1)}$ and $k^{(2)}$. The strain energy of a unit cell is now

$$\dot{S} = \frac{1}{2} \sum_{b=1}^{4} k^{(b)} l_i^{(b)} l_j^{(b)} \overline{T}_{,i} \overline{T}_{,j} \tag{2.13}$$

with the conductivity tensor

$$K_{ij} = \frac{1}{V} \sum_{b=1}^{4} k^{(b)} l_i^{(b)} l_j^{(b)} \tag{2.14}$$

or, equivalently

$$K_{11} = \frac{k^{(1)}}{2} \qquad K_{22} = \frac{k^{(2)}}{2} \qquad K_{12} = K_{21} = 0 \tag{2.15}$$

If one wants to model an anisotropic medium (i.e., with $K_{12} \neq 0$), one may either choose to rotate its principal axes to coincide with those of the square lattice and use the network model just described, or introduce diagonal bonds.

The above simple derivation of (2.12) and (2.15) is a paradigm of passage from fiber segment properties to effective continuum properties in a periodic lattice setup. In contradistinction to the conductivity problem describable by a second rank tensor, the case of elasticity discussed below is more complex in that it needs a fourth rank tensor. We restrict ourselves, of course, to linear phenomena.

In-plane elasticity of fiber-beam networks

The fact that any two cellulosic fibers have a finite contact area of hydrogen bonding calls into question any fiber network model in which fiber segments are joined by pinned joints. This suggests that we now consider the regular triangular lattice of Fig. 2.2 to be made of fiber segments behaving as flexing beams and connected through 'welded contacts' at their mutual bonds. The concept of welded contacts is dictated by the presence of a region of hydrogen bonding having a

finite area at any fiber-fiber node. While it is difficult to assess experimentally whether this region is or is not deformable, a special case of our model will recover the situation of pin-type frictionless connections between fiber segments carrying axial forces only. A perspective view of such a single-fiber network of fiber-beams is given in Fig. 2.3a), where the lattice nodes are assumed to have the same thickness as the single fiber.

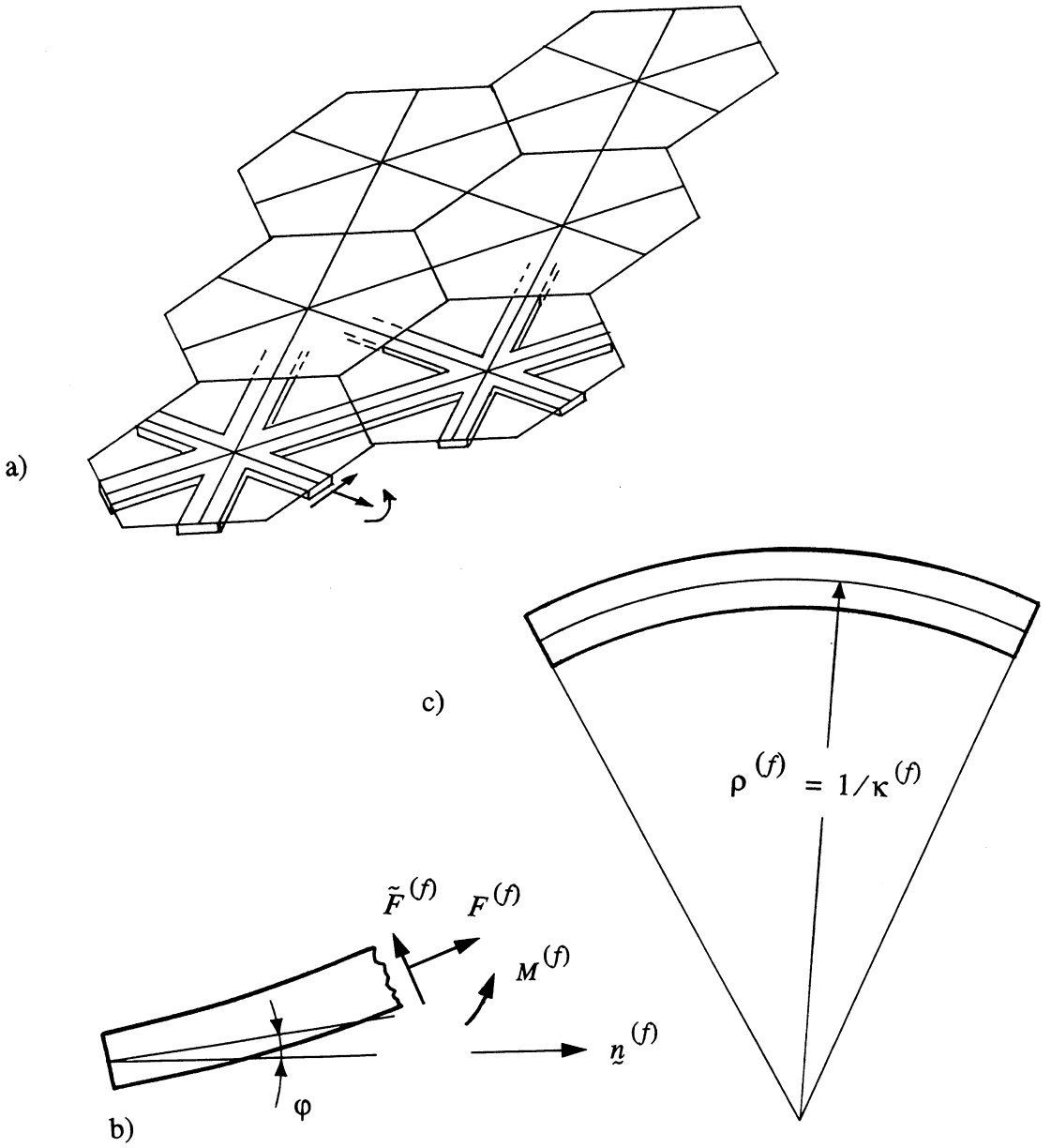

Fig. 2.3a) A perspective view of a triangular lattice of beam-type fibers;
b) internal loads in a fiber; c) curvature of a deformed fiber.

In accordance with the general concepts of Fig. 2.3b), we have to focus on the deformations of a typical beam-fiber, its bending into a curved arch allowing the definition of its curvature, and a cut in a free body diagram specifying the normal force F, the shear force $\tilde{F}$, and the bending moment M. It follows that the force field within the fiber network is now described by fields of force-stresses σ_{kl} and moment-stresses m_k; note the additional presence of moment-stresses due to the beam-type fiber interactions. In a continuum sense, this lattice will be approximated by a micropolar elastic medium discussed in the Appendix [5, 6].

The kinematics of the fiber network are described by three functions

$$u_1(\underset{\sim}{x}) \qquad u_2(\underset{\sim}{x}) \qquad \varphi(\underset{\sim}{x}) \tag{2.16}$$

which coincide with the actual displacements (u_1, u_2) and rotations (φ) at the fiber-fiber intersections. These functions are assumed to be linear, although the torsion-curvature $\bar{\kappa}_i$ now enters the picture in addition to the strain $\bar{\varepsilon}_{ij}$; see Appendix. As before, the overbars denote spatial averages over the unit cell. These two tensors are related to u_1, u_2, and φ by

$$\bar{\varepsilon}_{ij} = u_{j,i} + \varepsilon_{ij}\varphi \qquad \bar{\kappa}_i = \varphi_{,i} \tag{2.17}$$

where ε_{lk} is the 2D counterpart of the permutation tensor.

On the other hand, with reference to Fig. 2.3, we note from the mechanics of beams that the response (force-displacement and moment-rotation) laws of each fiber segment are given as

$$F^{(f)} = E^{(f)}A^{(f)}\gamma^{(f)} \qquad \tilde{F}^{(f)} = \frac{12E^{(f)}I^{(f)}}{s^2}\tilde{\gamma}^{(f)} \qquad M^{(f)} = E^{(f)}I^{(f)}\kappa^{(f)} \tag{2.18}$$

where

$A^{(f)} = t_a w$ is a cross-sectional area of the fiber;

$I^{(f)} = t_a w^3/12$ is a centroidal moment of inertia of the cross-sectional area of the fiber with respect to an axis normal to the plane of the fiber mat;

$E^{(f)}$ = is a fiber Young's modulus (along its axis);

$F^{(f)}$ = is an axial force in the fiber;

$\tilde{F}^{(f)}$ = is a shear force in the fiber;

$M^{(f)}$ = is a bending moment in the fiber;

$\gamma^{(f)}$ is a relative fiber elongation (axial strain);

$\tilde{\gamma}^{(f)}$ is a relative fiber shear deformation (shear strain); and

$\kappa^{(f)}$ is a fiber curvature.

Turning now to the continuum picture, the strain energy of the unit cell is expressed as

$$U_{continuum} = \frac{A}{2}\bar{\gamma}_{ij}C^{eff}_{ijkm}\bar{\gamma}_{km} + \frac{A}{2}\bar{\kappa}_i D^{eff}_{ij}\bar{\kappa}_j \tag{2.19}$$

from which we find

$$C^{eff}_{ijkm} = \sum_{f=1}^{6} n_i^{(f)} n_k^{(f)} (n_j^{(f)} n_m^{(f)} R^{(f)} + n_j^{(f)} n_m^{(f)} \tilde{R}^{(f)}) \qquad D^{eff}_{ij} = \sum_{f=1}^{6} n_i^{(f)} n_j^{(f)} S^{(f)} \tag{2.20}$$

where

$$R^{(f)} = \frac{2E^{(f)}A^{(f)}}{s^{(f)}\sqrt{3}} \qquad \tilde{R}^{(f)} = \frac{24E^{(f)}I^{(f)}}{(s^{(f)})^3\sqrt{3}} \qquad S^{(f)} = \frac{2E^{(f)}I^{(f)}}{s^{(f)}\sqrt{3}} \tag{2.21}$$

Consistent with the assumption of rectangular fiber cross sections ($t_a \times w$), we readily establish that the ratio $\tilde{R}/R$ has a very simple significance in terms of the fiber segment's aspect ratio

$$\frac{\tilde{R}}{R} = \left(\frac{w}{s}\right)^2 \tag{2.22}$$

Now, if we take all the fiber segments to be the same ($R^{(f)} = R$, etc.), we find

$$\begin{gathered} C^{eff}_{1111} = C^{eff}_{2222} = \frac{3}{8}(3R + \tilde{R}) \qquad C^{eff}_{1212} = \frac{3}{8}(R + 3\tilde{R}) \\ C^{eff}_{1122} = C^{eff}_{2211} = \frac{3}{8}(R - \tilde{R}) \qquad C^{eff}_{1221} = C^{eff}_{2112} = \frac{3}{8}(R - \tilde{R}) \\ D^{eff}_{11} = D^{eff}_{22} = \frac{3}{2}S \end{gathered} \tag{2.23}$$

with all the other components of both stiffness tensors being zero. In other words, we have

$$C^{eff}_{ijkm} = \delta_{ij}\delta_{km}\Xi + \delta_{ik}\delta_{jm}\Lambda + \delta_{im}\delta_{jk}\Pi \qquad D^{eff}_{ij} = \delta_{ij}\Gamma \tag{2.24}$$

in which

$$\Xi = \Pi = \frac{3}{8}(R - \tilde{R}) \qquad \Lambda = \frac{3}{8}(R + 3\tilde{R}) \qquad \Gamma = \frac{3}{2}S \tag{2.25}$$

Note that the relation $C_{1212} = \frac{1}{2}(C_{1111} - C_{1122})$ does not hold here, yet the material is isotropic contrary to the conclusion in [16]..

The effective bulk and shear moduli are now identified as

$$K^{eff} = \frac{3}{4}R \qquad \mu^{eff} = \frac{3}{8}(R+\tilde{R}) \tag{2.26}$$

which shows that the presence of angular springs does not affect the dilatational response. Furthermore, it follows that the effective Young's modulus and Poisson's ratio are

$$E^{eff} = 3R\frac{1+\frac{\tilde{R}}{R}}{3+\frac{\tilde{R}}{R}} \qquad \nu^{eff} = \frac{1-\frac{\tilde{R}}{R}}{3+\frac{\tilde{R}}{R}} \tag{2.27}$$

Again, let us note that these reduce to $E^{eff} = R$ and $\nu^{eff} = 1/3$ in the case of fibers carrying axial forces only ($\tilde{R} = 0$). Regarding the Poisson's ratio, we observe that the introduction of beam-type effects (i.e., as $\tilde{R}/R$ increases) has a tendency to reduce it. Furthermore, noting (2.22), the effective Young's modulus (normalized by $E^{(f)}$ and t_a) and the Poisson's ratio may be expressed in terms of the fiber aspect ratio w/s

$$\frac{E^{eff}}{t_a E^{(f)}} = 2\sqrt{3}\frac{w}{s}\frac{1+\left(\frac{w}{s}\right)^2}{3+\left(\frac{w}{s}\right)^2} \qquad \nu^{eff} = \frac{1-\left(\frac{w}{s}\right)^2}{3+\left(\frac{w}{s}\right)^2} \tag{2.28}$$

or, given (2.4), in terms of the porosity

$$\frac{E^{eff}}{t_a E^{(f)}} = 2(1-\sqrt{1-P_f})]\frac{1+\frac{1}{3}(1-\sqrt{1-P_f})^2}{3+\frac{1}{3}(1-\sqrt{1-P_f})^2} \qquad \nu^{eff} = \frac{3-(1-\sqrt{1-P_f})^2}{9+(1-\sqrt{1-P_f})^2} \tag{2.29}$$

Formulas (2.29) have been investigated numerically in Figs. 2.4a) and c). First, we observe that the beam model leads to a gradual increase of E^{eff} as compared to the previous model. This may easily be explained by noting that more energy may be stored in fibers that carry shear and bending forces than in the fibers that carry axial forces only. This effect is accompanied by the Poisson's ratio falling off nonlinearly from 1/3 with P_f increasing. It is gratifying to recall the same result established in [7]: Poisson's ratio tends to decrease with the bonding of the sheet. However, formulas of [7] cannot be plotted in Fig. 2.4 because porosity (i.e., fiber volume fraction) is not present in that derivation.

a)

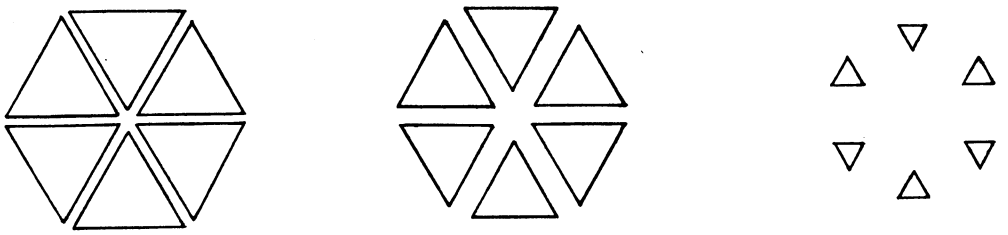

b)

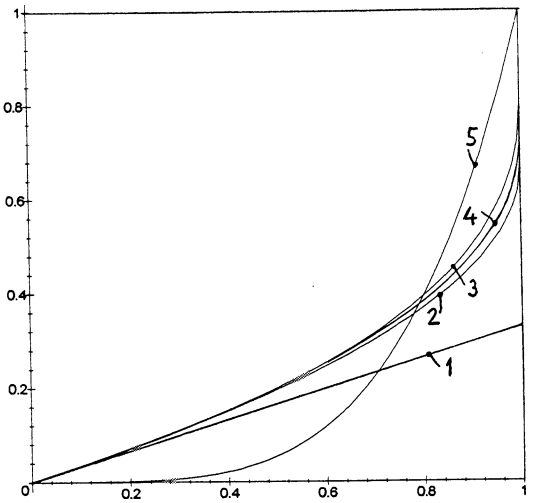

c)

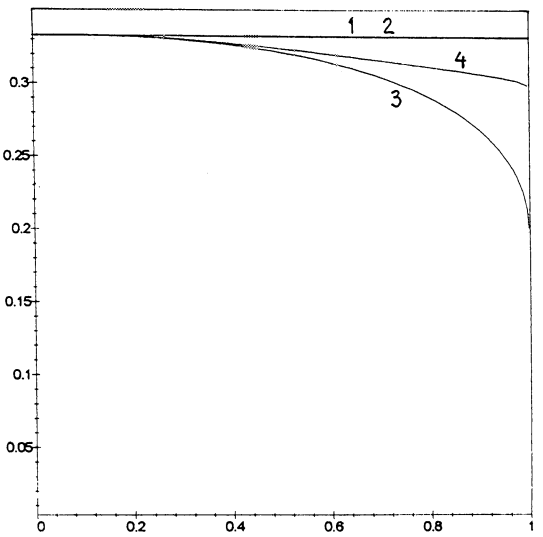

Figure 2.4a) A decrease in pore sizes - from large holes (lattice of slender beams), through a lattice of stubby beams, to a plate perforated with small holes: at P_f = 10%, 50%, and 90%; b) the effective Young's modulus E^{eff}, normalized by the fiber Young's modulus E^f, as a function of the fiber density P_f for: the Cox model (1), the axial-fibers lattice (2), the fiber-beams (Bernoulli-Euler) lattice (3), the fiber-beams (Timoshenko) lattice (4), and the effective medium theory for a perforated plate (5); c) the effective Poisson's ratio ν^f as a function of P_f.

Slender fiber-beams or stubby fiber-beams?

In the foregoing section, we tacitly employed the model of so-called *Bernoulli-Euler* beams for the free fiber segments. It is well known, however, that stubby beams are more adequately described by a so-called *Timoshenko beam* model. The difference between both models consists in admitting the shear effects in the Timoshenko beam. More precisely, if a beam's deflection is described by $w(\underset{\sim}{x})$, a question arises whether the rotation $\theta(\underset{\sim}{x})$ of a planar section, initially orthogonal to the beam's axis, is given by the slope $w'(\underset{\sim}{x})$ ($\equiv dw(\underset{\sim}{x})/(dx)$). An affirmative answer corresponds to a Bernoulli-Euler beam, whereas the situation of $\theta(\underset{\sim}{x})$ being independent of $w'(\underset{\sim}{x})$ is that of a Timoshenko beam.

These considerations will now be made more transparent by a problem of a beam fixed at both of its ends and subjected to a shear displacement at one end, Fig. 2.5. That is, the boundary conditions at the left end are

$$w(0) = 0 \qquad \theta(0) = 0 \qquad w'(0) - \theta(0) = 0 \tag{2.30}$$

while those at the right end are

$$w(s) = \tilde{\gamma}^{(f)} s \qquad \theta(s) = 0 \qquad w'(s) - \theta(s) = 0 \tag{2.31}$$

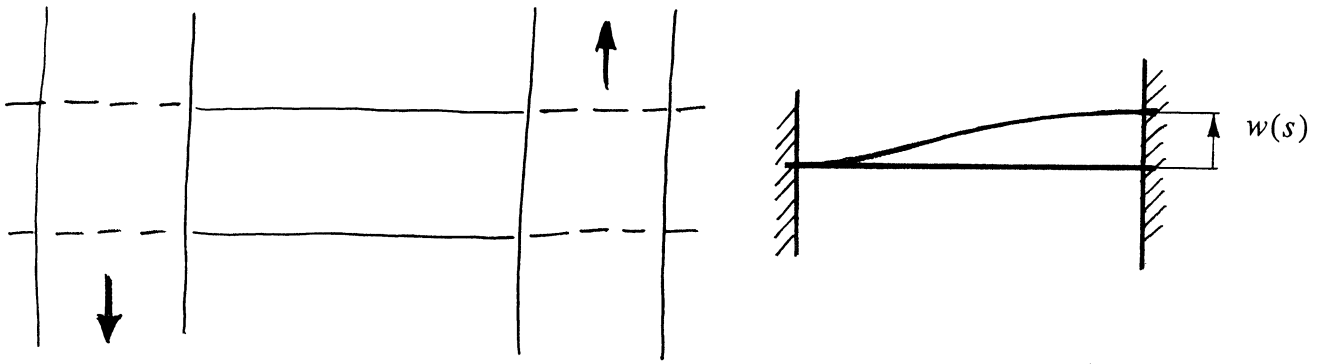

a) b)

Fig. 2.5 Shearing of a fiber-beam fixed ("welded") to its two neighbors (a), and the equivalent mechanical model (b).

It is readily determined from the governing equations

$$EI\theta'' + GA(w' - \theta) = 0 \qquad GA(w'' - \theta') = 0 \tag{2.32}$$

that a following relation holds between the shear force $\tilde{F}^{(f)}$ and the displacement $\tilde{\gamma}^{(f)}s$

$$\tilde{F}^{(f)} = \frac{12E^{(f)}I^{(f)}}{s^2(1+\beta)}\tilde{\gamma}^{(f)} \tag{2.33}$$

where (recall $A^{(f)} = t_a w$ and $I^{(f)} = t_a w^3/12$)

$$\beta = \frac{12EI}{GAs^2} = \frac{E}{G}\left(\frac{w}{s}\right)^2 \tag{2.34}$$

is the dimensionless ratio of bending to shear stiffness. Two limiting cases are noteworthy:

$\beta \to 0$, high shear stiffness and, hence, less deflection owing to shear; the Bernoulli-Euler slender beam is recovered;

$\beta > 1$, low shear stiffness and, hence, deflection owing to shear dominates over that due to the Young's modulus E; this is the general case of the Timoshenko beam.

Let us consider a situation of $E = 9G$, that is typical of many cellulose fibers [15], and three aspect ratios:

$$\begin{aligned} \frac{w}{s} &= 1 \qquad \beta = 9 \\ \frac{w}{s} &= \frac{1}{3} \qquad \beta = 1 \\ \frac{w}{s} &= \frac{1}{9} \qquad \beta = \frac{1}{9} \end{aligned} \tag{2.35}$$

which shows that the shorter the fiber, the more relevant are the shear effects. Observing that (2.33) replaces $(2.18)_2$, we now proceed to derive the effective moduli so that (2.21) is replaced by

$$R^{(f)} = \frac{2E^{(f)}A^{(f)}}{s^{(f)}\sqrt{3}} \qquad \tilde{R}^{(f)} = \frac{24E^{(f)}I^{(f)}}{(s^{(f)})^3\sqrt{3}}\frac{1}{1+\beta} \qquad S^{(f)} = \frac{2E^{(f)}I^{(f)}}{s^{(f)}\sqrt{3}} \tag{2.36}$$

wherein the ratio $\tilde{R}/R$ is

$$\frac{\tilde{R}}{R} = \left(\frac{w}{s}\right)^2\frac{1}{1+\beta} \tag{2.37}$$

Following the same steps as in the previous section, we see that the effective Young's modulus and Poisson's ratio are the same as before

$$E^{eff} = 3R\frac{1+\frac{\tilde{R}}{R}}{3+\frac{\tilde{R}}{R}} \qquad \nu^{eff} = \frac{1-\frac{\tilde{R}}{R}}{3+\frac{\tilde{R}}{R}} \tag{2.38}$$

but expressing them in terms of the fiber aspect ratio and β, we find

$$\frac{E^{eff}}{t_a E^{(f)}} = 2\sqrt{3}\frac{w}{s}\frac{1+\left(\frac{w}{s}\right)^2\frac{1}{1+\beta}}{3+\left(\frac{w}{s}\right)^2\frac{1}{1+\beta}} \qquad \nu^{eff} = \frac{1-\left(\frac{w}{s}\right)^2\frac{1}{1+\beta}}{3+\left(\frac{w}{s}\right)^2\frac{1}{1+\beta}} \tag{2.39}$$

or, given (2.4), in terms of the porosity

$$\frac{E^{eff}}{t_a E^{(f)}} = 2(1-\sqrt{1-P_f})]\frac{1+\frac{1}{3(1+\beta)}(1-\sqrt{1-P_f})^2}{3+\frac{1}{3(1+\beta)}(1-\sqrt{1-P_f})^2}$$

$$\nu^{eff} = \frac{3-(1-\sqrt{1-P_f})^2\frac{3}{1+\beta}}{9+(1-\sqrt{1-P_f})^2\frac{3}{1+\beta}} \tag{2.40}$$

The above are also shown in Fig. 2.4b) and c) for the special case $E = 9G$ of equation (2.35). We see that the consideration of fiber segments as stubby beams has a minor softening effect on E^{eff} relative to the Bernoulli-Euler beam model. This may be explained by noting that the admission of the angle of rotation $\theta(\underset{\sim}{x})$ as an independent degree of freedom amounts to G being finite, rather than infinite, in the Timoshenko beam model. The weak magnitude of this effect, however, is interesting. The Poisson's ratio falls off nonlinearly from 1/3 with P_f increasing in this model just as in the original one. Also here, the admission of finite shear modulus is weak. Summarizing, as the E/G ratio increases (decreases), we go to the axial-fibers (Bernoulli-Euler beam) model.

In-plane elasticity of a perforated plate model

As P_f goes beyond ~60%, the aspect ratio w/s increases so much that one can no longer consider the connections between the lattice nodes to be beams. Given the highly anisotropic nature of fibers and a complex composite structure of fiber systems, a basic question arises: can any simple explicit model be derived for this low porosity range? Probably not, and this problem is reflected

in, for example, a recent paper series [8, 9, 10], which had to culminate in a numerical solution of a somewhat hypothetical equivalent unit cell. Another avenue is offered by brute force solutions of complex fiber systems as done later in Part III. Here, for the sake of completeness of our analysis, we consider the limiting case of a beam model - namely, a perforated plate.

In the limit of $P_f \to 1$, we have a plate with a regular distribution of triangular-shaped pores, Fig. 2.4a). This is a so-called "dilute limit" of a locally isotropic material with holes (in either periodic or disordered arrangements), that has already been solved in [11, 12]. The respective formulas are

$$\frac{E^{eff}}{t_a E^{(f)}} = 1 - \alpha(1 - P_f) \qquad \nu^{eff} = \nu^{(f)} - \alpha(\nu^{(f)} - \nu_0)(1 - P_f) \tag{2.41}$$

The coefficients $\alpha = 4.2019$ and $\nu_0 = 0.2312$ have been computed in the above references, and, in fact, analogous coefficients are also available there for plates with other than triangular holes (squares, pentagons, ...). It is noteworthy that:

i) both formulas are uncoupled from one another;

ii) the formula $(2.41)_1$ gives a correctly expected behavior in Fig. 2.4b) for very high values of P_f, in place of the beam lattice model;

iii) the formula $(2.41)_2$ for ν^{eff} depends on the Poisson's ratio $\nu^{(f)}$ of the plate material, a value which cannot be specified because the fibers are strongly anisotropic; we therefore do not plot ν^{eff} for this model.

One more question remains with reference to Fig. 2.4a): what happens in the range of the P_f values, which are too high for a beam lattice model to hold and too low for the dilute model to be truly dilute? Or, can anything be done to smooth out the transition between the two curves 3 and 5 at P_f around 0.8 ? Let us try here a usual device of micromechanics: an effective medium theory. Following [11, 12], we adopt a so-called 'differential scheme,' which is given by

$$\frac{E^{eff}}{t_a E^{(f)}} = P_f^{\alpha} \qquad \nu^{eff} = P_f^{\alpha}(\nu^{(f)} - \nu_0) + \nu_0 \tag{2.42}$$

For the sake of clarity of Figs. 2.4b) and c), these are not plotted. Summarizing, E^{eff} is modeled by an upper envelope of all the curves in Fig. 2b) - i.e., curves 3 and 5.

Concluding remarks on in-plane elasticity

Summarizing, it is seen from Fig. 2.4 that, as P_f grows, fiber bending tends to increase the effective Young's modulus E^{eff}. In other words, bending effects increase as fibers become wider. On the other hand, in the case of fibers becoming very slender, one can work with segments carrying axial forces only. Thus, beam effects gain in influence as the volume fraction increases, and lead to an increase of the effective Young's modulus relative to the axial forces model. Finally, as the holes in the lattice decrease even further, an effective medium theory, such as [12], results in the Young's modulus of the system being equal to that of the fiber. This case of very low porosity is of academic interest in the case of paper but is presented here for the sake of completeness.

The present model registers one more difference from the Cox model: the effective Poisson's ratio ν^{eff} is not constant but, rather, decreases with changing fiber density. An explanation of these quite different behaviors can be obtained by noting that the Cox model requires:

(i) fibers to span the entire length of the tested area,

(ii) axial forces only to be carried by the fibers,

(iii) a test domain of sufficiently large size to justify an integration over the entire range of the angular distribution.

The first two requirements, along with the assumption of uniform strain, are tantamount to a situation of no interaction between the fibers, so that the Young's modulus of a zero-porosity material equals a third of the fiber's. By contrast, our network model of beam-type fibers naturally forces them to interact via axial, shear, and bending forces under any deformation states. In the zero-porosity limit, the model recovers the Young's modulus of the fiber, whereas in the full porosity limit, the model becomes one of axial force carrying fibers and coincides with the Cox model. In fact, systems of axial force carrying members are characterized by the in-plane Poisson's ratio 1/3 so that we obtain agreement between all the network models at low porosities.

The third requirement of the Cox model is equivalent, with reference to Fig. 3.1 of Part III, to having an infinitely large window (i.e., a test domain). As discussed in the opening section of this paper, this is physically impossible, and thus, a scale-dependent hierarchy of bounds (3.12) applies.

Two more things may be said about the beam network model:

i) Timoshenko beams, although more sophisticated than Bernoulli-Euler beams, remain, in principle, one-dimensional objects - of micropolar type, in fact. Therefore, what they yield is

about as far as one can get with a beam model. A better approach would have to consider beam segments as little plates, i.e., 2D objects.

ii) Properties of the Timoshenko beam can be derived from a micromechanical analysis of fibril bundles.

Plate-bending response

We can apply the same approach as above to the problem of determination of plate-bending response of the single-layer triangular mat of Fig. 2.6 - within the assumptions of a Kirchhoff (thin) plate model. To this end we must consider out-of-plane deformations of a triangular fiber mat, and thus, the kinematics is described by three functions - one out-of-plane displacement and two rotations (with respect to the axes x_1, x_2)

$$u(\underset{\sim}{x}) \qquad v_1(\underset{\sim}{x}) \qquad v_2(\underset{\sim}{x}) \tag{2.43}$$

which coincide with the actual displacement (u) and rotations (v_1, v_2) at the fiiber-fiber intersections. Within each triangular pore, these functions may be assumed to be linear. It follows that the strain and curvature fields are related to u, v_1, v_2 by

$$\kappa_{kl} = v_{l,k} \qquad \gamma_k = u_{,k} + \varepsilon_{kl} v_l \tag{2.44}$$

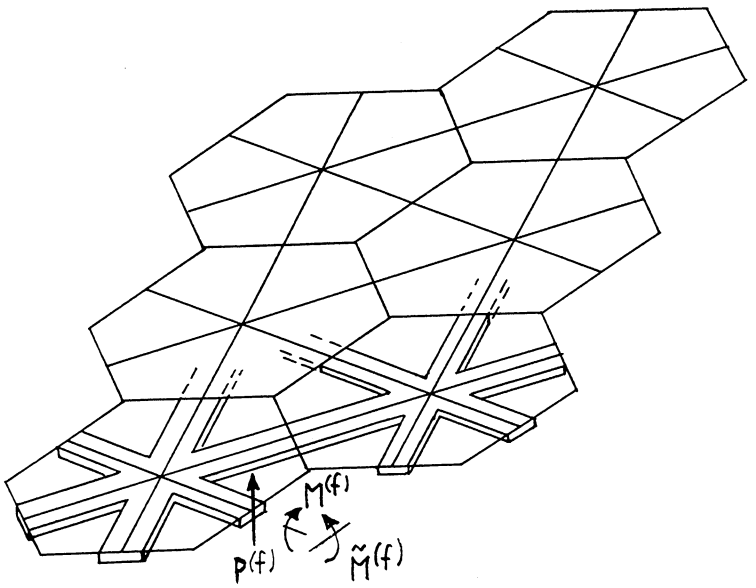

Fig. 2.6 A perspective view of quasi-single-fiber-layer, showing the relevant internal loads in a fiber-beam cross section.

With reference to Fig. 2.5, for a single beam-type fiber, the mechanical (force-displacement and moment-rotation) response laws of each fiber segment are given as

$$\begin{aligned} M^{(f)} &= C^{(f)}\kappa^{(f)} \\ \tilde{M}^{(f)} &= E^{(f)}I^{(f)}\tilde{\kappa}^{(f)} \\ P^{(f)} &= \frac{12E^{(f)}I^{(f)}}{s^{(f)}}\tilde{\gamma}^{(f)} \end{aligned} \tag{2.45}$$

where

$A^{(f)} = t_a w$ is a cross-sectional area of the fiber;

$I^{(f)} = t_a^3 w/12$ is a centroidal moment of inertia of the cross-sectional area of the fiber with respect to an axis normal to the plane of the fiber mat;

$s^{(f)} = 2l^{(f)}$ is the full length of each fiber (same as before);

$C^{(f)}$ is a torsional stiffness of the fiber;

$E^{(f)}$ is Young's modulus of the fiber (same as before);

$M^{(f)}$ = is an in-plane twisting moment in the fiber;

$\tilde{M}^{(f)}$ = is an out-of-plane bending moment in the fiber;

$P^{(f)}$ = is a shear force in the fiber;

$\tilde{\gamma}^{(f)}$ is a fiber shear deformation; and

$\kappa^{(f)}$ is a fiber curvature.

The strain energy of the unit cell is

$$E_{continuum} = \frac{V}{2}\bar{\kappa}_{ij}C^{eff}_{ijkl}\bar{\kappa}_{kl} + \frac{V}{2}\bar{\gamma}_i A^{eff}_{ij}\bar{\gamma}_j \tag{2.46}$$

which is consistent with the Hooke's law

$$m_{kl} = C_{ijkl}\kappa_{kl} \qquad p_k = A_{kl}\gamma_l \tag{2.47}$$

Here m_{kl} is the tensor of moment-stresses, and p_k is the vector of shear tractions.

Proceeding in a fashion analogous to the in-plane problems, we find

where

$$S^{(f)} = \frac{C^{(f)}}{s^{(f)}} \qquad \tilde{S}^{(f)} = \frac{E^{(f)}I^{(f)}}{s^{(f)}} \qquad \widehat{R}^{(f)} = \frac{12E^{(f)}I^{(f)}}{\tilde{s}^{(f)}(s^{(f)})^2} \tag{2.49}$$

$$C_{ijkl}^{eff} = \sum_{f=1}^{6} n_i^{(f)} n_k^{(f)} (n_j^{(f)} n_l^{(f)} S^{(f)} + n_j^{(f)} n_l^{(f)} \tilde{S}^{(f)})$$
$$A_{ij}^{eff} = \sum_{f=1}^{6} n_i^{(f)} n_j^{(f)} R^{(f)} \tag{2.48}$$

In the case of a triangular lattice, we find

$$C_{ijkl} = \delta_{ij}\delta_{kl}\Delta + \delta_{ik}\delta_{jl}Y + \delta_{il}\delta_{jk}\Omega$$
$$A_{ij} = \delta_{ij}B \tag{2.50}$$

in which

$$\Delta = \Omega = \frac{3}{8}(S - \tilde{S}) \qquad Y = \frac{3}{8}(S + 3\tilde{S}) \qquad B = \frac{3}{2}\widehat{R} \tag{2.51}$$

Three constants (S, $\tilde{S}$, $\widehat{R}$) seen here are related to the fiber mat properties as follows

$$S = \frac{2C}{s\sqrt{3}} \qquad \tilde{S} = \frac{2EI}{s\sqrt{3}} \qquad \widehat{R} = \frac{24EI}{s^3\sqrt{3}} \tag{2.52}$$

The same type of derivation may be conducted for a square (rectangular) lattice. The important thing to point out here is that the plate-bending response of paper made of several layers of fibers would not simply be a superposition of the responses calculated above but, rather, a combination of bending and in-plane extension/compression of each of the component layers.

DISCUSSION: PART III
SINGLE-LAYER RANDOM NETWORKS OF FIBER-BEAMS

Is the constitutive response of paper deterministic or statistical?

It is well known that paper possesses a spatially random fiber structure. Indeed, much research effort, dating back to Kallmes & Corte [4], has been and continues to be spent on characterizing the statistics of relevant random geometries, [2] and the references therein. Parallel to these rather purely random geometric investigations there is a line of studies, dating back to Cox [13], on physical and mechanical properties of paper, broadly known as paper physics. The key

feature of almost all of the paper physics developed so far is the deterministic character of the classically derived structure-property relations. This is, essentially, at odds with the above mentioned widely acknowledged random geometry of the fiber structures, and this constitutes the main motivation of present research.

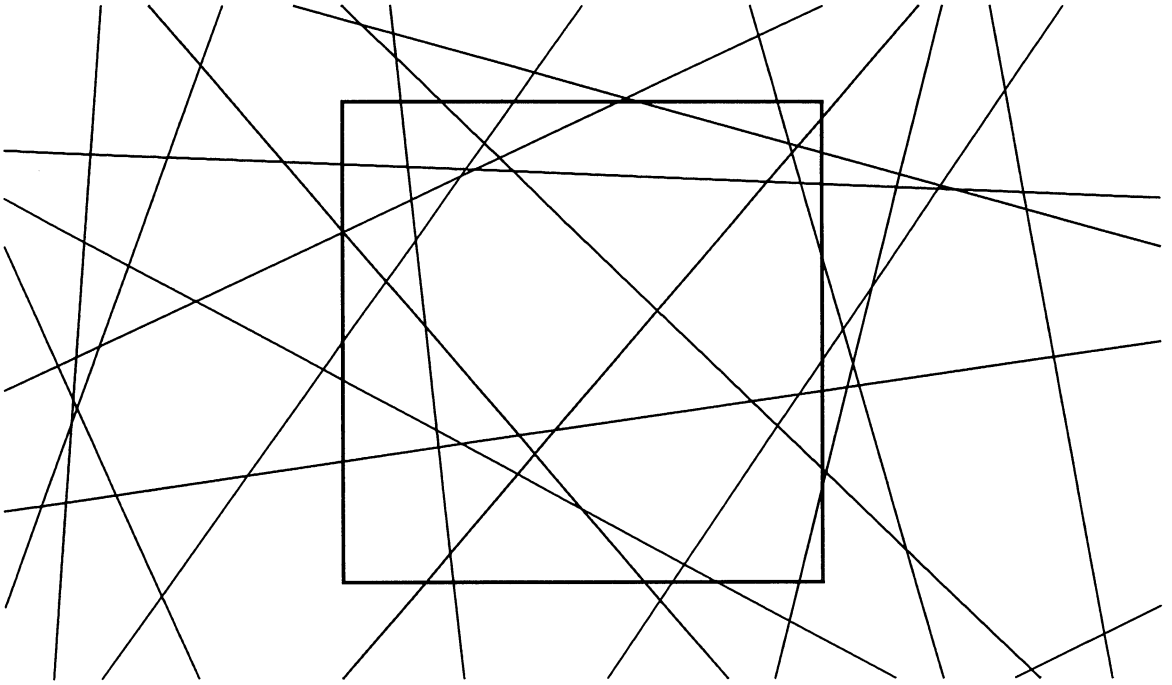

Fig. 3.1 A sample of a random Poisson line field; a window of size $L \times L$ is shown.

In order to clarify this last point, let us consider the geometry of the Cox model [13]. This is, basically, a planar Poisson line field of intensity λ [14], one of whose characteristics is a statistical average free fiber segment length $\langle s \rangle = \pi\lambda$, Fig. 1. Let us consider a window B_δ of size $L \times L$, cut out of the Poisson line field, whereby

$$\delta = L/\langle s \rangle \tag{3.1}$$

is a nondimensional parameter specifying the window size with respect to $\langle s \rangle$. It is immediately observed that on length scales L finite relative to $\langle s \rangle$ there are fluctuations in the local fiber density per unit area ρ. The latter quantity may be defined by

$$P_f = L^{-2} \sum_{l_{(n)} \in B_\delta} |l_{(n)}| w \tag{3.2}$$

where $l_{(n)}$ is a line, of width w, contained in B_δ. Clearly, a finite δ defines a *mesoscale*, whereas an infinite one connotes a *macroscale*.

In order to remove the fluctuations in ρ - equivalent to the fluctuations in the basis weight - one has to consider windows of size $\delta \to \infty$, which is an unwieldy alternative because paper samples of infinite size do not exist. The point is that these fluctuations in the mat's geometric structure, closely related to the flocculation, control the effective physical properties so that the continuum-type constitutive laws must be stochastic in nature and scale-dependent - they become deterministic only in the limit of infinitely large windows, which is the classical continuum limit [5]. Additionally, random streaks in machine direction are often formed on a paper machine, a phenomenon which introduces one more scale of disorder above that of the flocs [6].

This issue leads to a question: How quickly do the fluctuations in local properties tend to zero as a function of increasing δ? In the language of continuum physics, this may be rephrased as follows: what is the approach to a Representative Volume Element (RVE) with δ?

Planar models of random fiber networks

Generation via a random Poisson line process

In order to generate a field of fibers, we proceed in the following steps.

Step 1: In order to generate a field of round disks, we employ a Poisson point process subject to a *sequential inhibition* rule: throw Poisson points on a plane and keep only those which fall no closer than d_{min} to any previous ones. Strictly speaking, the Poisson point process of intensity λ as specified by

$$P\{N(A) = x\} = e^{-\lambda|A|}\frac{\lambda|A|}{x!} \qquad A \subset \boldsymbol{R}^2 \tag{3.3}$$

occurs on the entire $\boldsymbol{R}^2$ plane, and so its numerical simulation must necessarily be done on a compact subset, which actually leads to a binomial point process. Note that the classical "car-parking problem" [14] is a simple sequential inhibition process in 1-D.

Step 2: Generate an angle θ from $[0, \pi]$ according to a probability density

$$f(\theta) = \frac{1}{\pi}(1 + a_1 cos2\theta + a_2 cos4\theta + \ldots + a_n cos2n\theta) \tag{3.4}$$

where θ is the line of inclination of the line to the x-axis. In our simulations, we usually take only

the first term in the cosine series (3.4); in practice, where fitting of experimental data is needed, either more terms need to be included or other types of distributions can be considered, e.g., [15].

Step 3: A line of length l according to a probability density $p(l)$ is generated. Note that, in principle, the subset of $\boldsymbol{R}^2$ on which the binomial process is conducted should be larger than the actual window domain which will be tested for effective moduli because the lines that originated outside the window, up to a distance of $l/2$, should be accounted for.

Conductivity of random networks

Paper is made of networks of finite rather than infinite length fibers. One simple mechanism for generation of such a random fiber network is based on a planar Poisson point process with exclusion (i.e., no two points are closer than a certain minimum distance d_{min}) whereby a line of random length, random inclination, and centered at each point is generated. By varying d_{min} we can change the degree of flocculation in the network as shown in Fig. 3.2, where two networks with and without exclusion, yet of the same fiber density, are shown.

Let us now consider the issue of thermal conductivities of such networks. Assuming linear behavior, we have

$$\vec{q} = \boldsymbol{K} \cdot \nabla T \tag{3.5}$$

where $\vec{q}$ is the heat flux; $\boldsymbol{K}$ is the conductivity; and ∇T is the temperature gradient. This equation suggests that ∇T is controlled. However, by considering a relation inverse to (3) - $\nabla T = \boldsymbol{R} \cdot \vec{q}$ - we would have to take the heat flux as a controllable variable. A question arises: is the resistivity $\boldsymbol{R}$ an inverse of the conductivity $\boldsymbol{K}$? As we shall see below, the answer is no; i.e., the response law is, in general, nonunique.

In accord with the foregoing twofold interpretation of the response law, in order to define the in-plane effective properties, we need to introduce two types of boundary conditions:

a) essential:

$$T = \overline{\nabla T} \cdot \vec{x} \tag{3.6}$$

which yield a conductivity tensor $\boldsymbol{K}_{\delta}^{e}$ ('e' stands for essential boundary conditions), where T is the temperature; $\overline{\nabla T}$ is the spatial average temperature gradient; and $\vec{x}$ is a position vector; and

a)

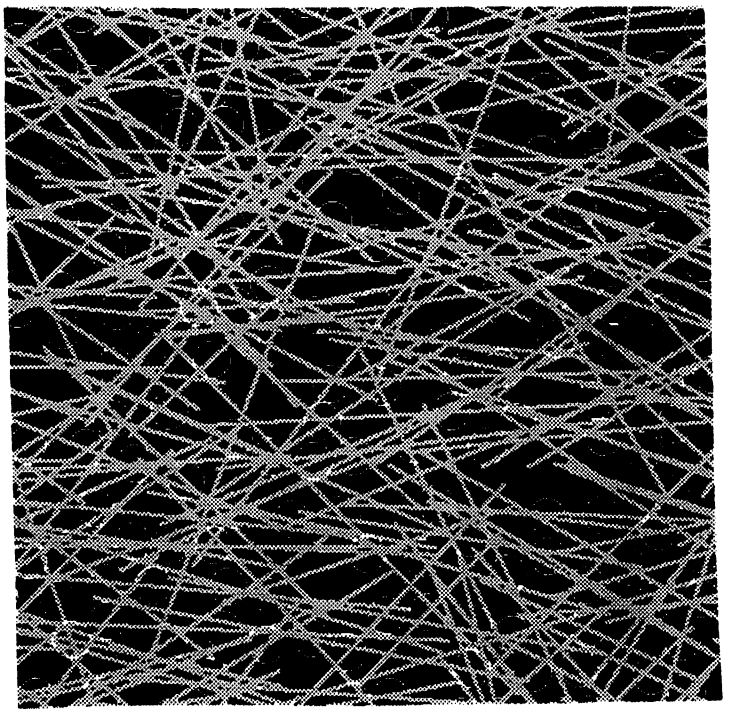

b)

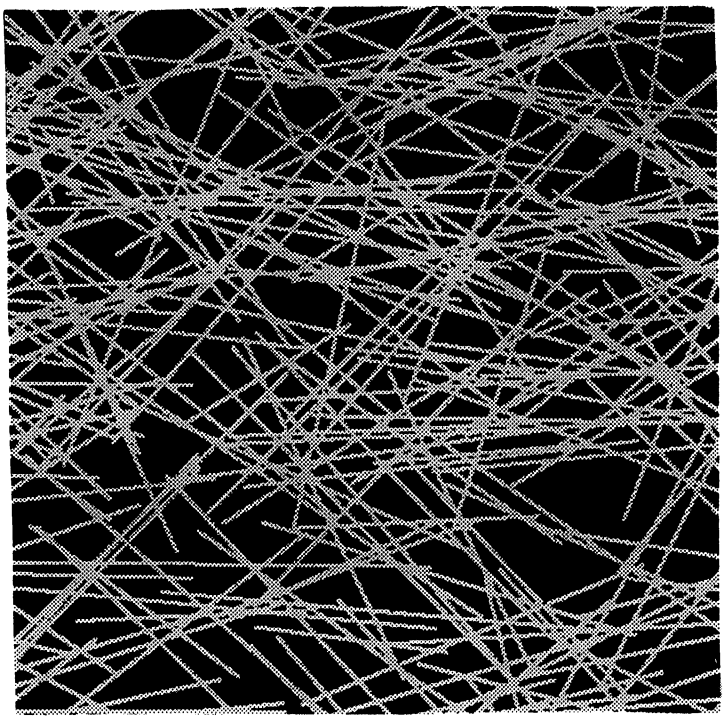

Fig. 3.2a) A realization of a random, anisotropic fiber network, with small disks of radius d_{min} = 0.24 *mm*, indicating the mutual exclusion of Poisson points; $\langle l \rangle$ = 1.2 *mm* and w = 0.03 *mm*.
b) A network of the same fibers generated with no exclusion condition d_{min} = 0. In both cases, fiber angles were sampled from the distribution (3.4) with a_1 = 1 and other a's being zero.

b) natural:

$$\vec{q} \cdot \vec{n} = \bar{\vec{q}} \cdot \vec{n} \tag{3.7}$$

which yield a resistivity tensor $\boldsymbol{R}_\delta^n$ ('n' stands for natural boundary conditions); here $\vec{q}$ is the heat flux, $\bar{\vec{q}}$ is the spatial average heat flux, and $\vec{n}$ is the outer unit normal to the window's boundary. In the above, we employ boldface for a second-rank tensor and an overbar for a spatial average over the window domain.

The essential boundary condition is equivalently known under the name of a Dirichlet, or temperature-controlled one, while the natural boundary condition is also known as a Neumann, or flux-controlled one.

A computer program has been developed to compute effective conductivities and resistivities of random fiber networks such as those shown in Fig. 3.2, for window sizes up to ten times larger than the fiber length. The program was based on the following assumptions:

i) Convection phenomena in pores were disregarded; this was justified by a consideration of the Grashoff number which was estimated to be definitely less than 1000.

ii) Radiation phenomena have a weak contribution to overall conduction compared to the contribution of conduction through the solid fibers - this is especially true for a network viewed as a cellular solid of density much higher than 10% [16]; thus, the radiation was disregarded.

iii) Fiber-fiber bonds present no hindrance to the conductivity so that the entire network could be regarded as a randomly connected two-phase medium comprising fibers of property K^{fiber} and pores of property K^{void}.

Solution of any network, such as those shown in Fig. 3.2, results in an observation that $\boldsymbol{K}_\delta^e$ is, in general, different from $\boldsymbol{K}_\delta^n \equiv (\boldsymbol{R}_\delta^n)^{-1}$. That is, the former one provides an *upper estimate* on the effective thermal conductivity of the given specimen, while the latter represents a *lower estimate*. Now, we have a variability from sample to sample, and from location to location, and so, we should consider the ensemble averages. It follows from the variational principles (e.g., [17]) that the effective macroscopic conductivity tensor $\boldsymbol{K}^{eff}$ is bounded by two tensors $\langle \boldsymbol{K}_\delta^e \rangle$ and $\langle \boldsymbol{R}_\delta^n \rangle^{-1}$. Both ensemble averages, indicated by $\langle\ \rangle$, bound the effective conductivity the more the scale δ approaches its continuum limit $\delta \to \infty$ so that a hierarchy of δ-dependent bounds on $\boldsymbol{K}^{eff}$ can be derived

$$\boldsymbol{K}^R \equiv (\boldsymbol{R}^R)^{-1} \equiv \langle \boldsymbol{R}_1^n \rangle^{-1} \leq \langle \boldsymbol{R}_{\delta'}^n \rangle^{-1} \leq \langle \boldsymbol{R}_{\delta}^n \rangle^{-1} \leq \boldsymbol{K}^{eff} \leq \langle \boldsymbol{K}_{\delta}^e \rangle \leq \langle \boldsymbol{K}_{\delta'}^e \rangle \leq \langle \boldsymbol{K}_1^e \rangle \equiv \boldsymbol{K}^V \qquad \forall \delta' < \delta \tag{3.8}$$

In (3.8), $\boldsymbol{K}^V$ and $\boldsymbol{K}^R$ denote the (elementary) Voigt and Reuss bounds, corresponding to windows at the smallest scale ($\delta = 1$). In other words, the effective response depends on the boundary conditions, and the influence of the latter disappears as the sample becomes infinite.

The order relation employed in (3.8) is to be understood as follows: for two second rank tensors $\boldsymbol{A}$ and $\boldsymbol{B}$, $\boldsymbol{B} \leq \boldsymbol{A}$ means that $\vec{t} \cdot \boldsymbol{B} \cdot \vec{t} \leq \vec{t} \cdot \boldsymbol{A} \cdot \vec{t}$ for any vector $\vec{t} \neq \vec{0}$. In the special case of a microstructure being characterized by an isotropic statistics $\boldsymbol{K}^{eff}$ is isotropic, i.e. $\boldsymbol{K}^{eff} = \boldsymbol{I}K^{eff}$ where $\boldsymbol{I}$ is the identity tensor.

The hierarchy of bounds (3.8) is illustrated on a specific example where the conductivity of the fiber material is on the same order as that of the voids: $K^{fiber} = 5\ K^{void}$. The resulting bounds are shown as functions of δ in Fig. 3.3a) below. The δ employed here is redefined from the one introduced in (3.1) in terms of the mean fiber length $\langle l \rangle$, namely

$$\delta = L/\langle l \rangle \tag{3.9}$$

Besides the asymptotic convergence of both bounds to $\boldsymbol{K}^{eff}$ with δ increasing, the other important thing noticeable from Fig. 3.3 is the anisotropy in the structure due to the assumption of the angular distribution function. Although, as mentioned in the legend of Fig. 3.2, the latter was assumed in a very simple form $f(\theta) = (1 + \cos 2\theta)/\pi$, in principle, any other type of distribution can easily be considered.

It is noteworthy that the medium's response is closer to the estimates $\langle K_{11}^e \rangle$ and $\langle K_{22}^e \rangle$, resulting from the temperature-controlled boundary conditions (4) than to $\langle R_{11}^n \rangle$ and $\langle R_{22}^n \rangle$, resulting from the heat flux-controlled boundary conditions (5). This is especially pronounced in the situations of very low or negligible conductivities of the voids, which are shown in Fig. 3.4. This suggests that, effectively and approximately, paper may be considered to be a plate with holes in which fibers tend to assure a uniform temperature gradient (or strain in case of elasticity) as opposed to a material reinforced with stiff inclusions where the heat flux distribution (or stress in case of elasticity) is nearly uniform. However, with high mismatch (1000 : 1) of fiber and void conductivities, such as studied in Fig. 3.4, (i) the uniform temperature gradient is worse, and (ii) the approach to a homogeneous, deterministic continuum is very slow.

a)

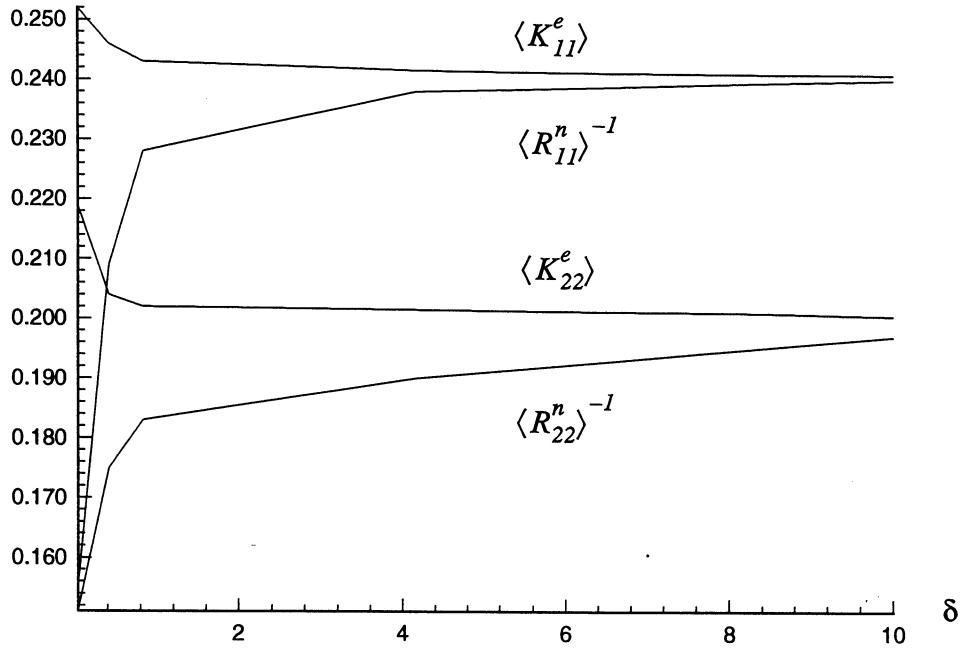

b)

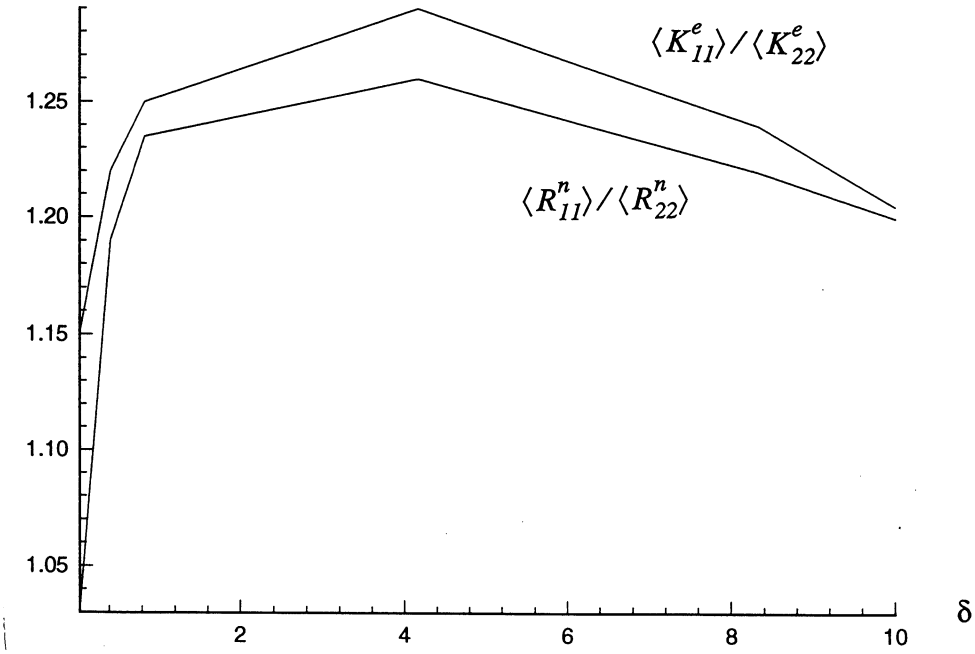

Fig. 3.3a) Hierarchies of bounds, normalized by $K^{fiber} = 1.0$, for the fiber systems of Fig. 3.2a) showing convergence of $\langle K^e_{11} \rangle$ to $\langle R^n_{11} \rangle^{-1}$ and $\langle K^e_{22} \rangle$ to $\langle R^n_{22} \rangle^{-1}$ with increasing δ; $K^{void} = 0.2$. b) Dependence of anisotropies $\langle K^e_{11} \rangle / \langle K^e_{22} \rangle$ and $\langle R^n_{11} \rangle / \langle R^n_{22} \rangle$ on the mesoscale $\delta = L / \langle l \rangle$.

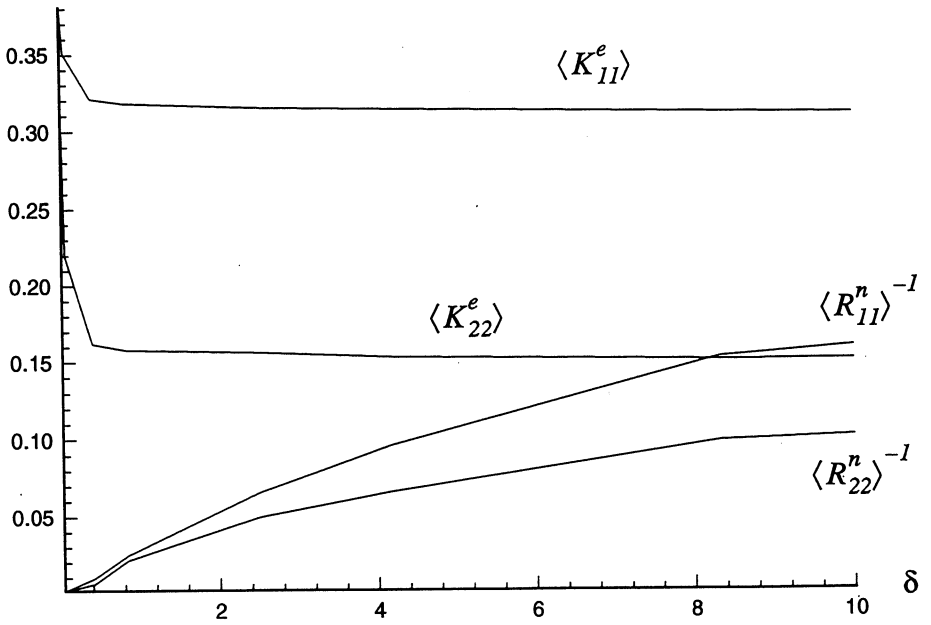

a)

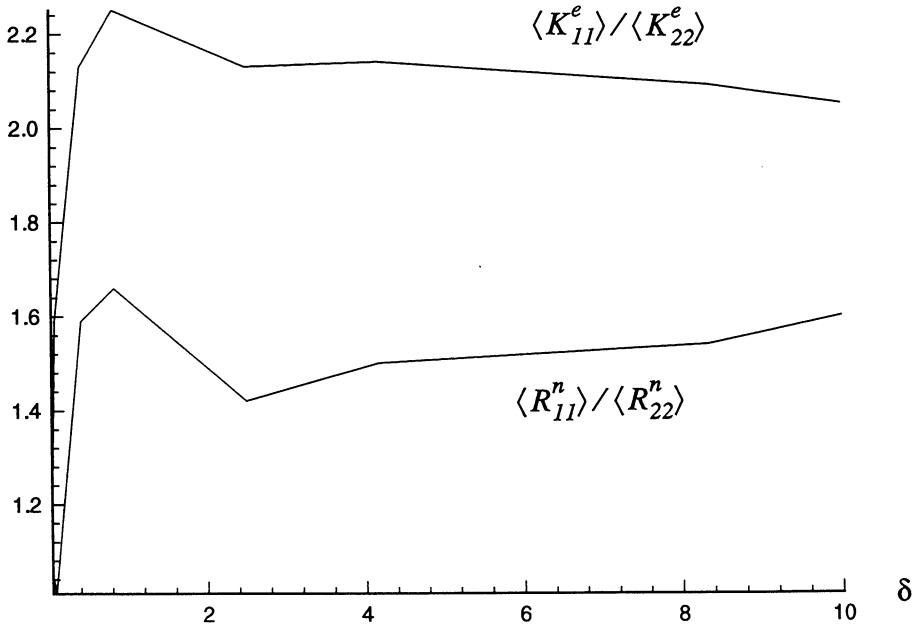

b)

Fig. 3.4a) Hierarchies of bounds, normalized by $K^{fiber} = 1.0$, for the fiber systems of Fig. 3.2a) showing convergence of $\langle K^e_{11}\rangle$ to $\langle R^n_{11}\rangle^{-1}$ and $\langle K^e_{22}\rangle$ to $\langle R^n_{22}\rangle^{-1}$ with increasing δ; $K^{void} = 10^{-3}$. b) Dependence of anisotropies $\langle K^e_{11}\rangle/\langle K^e_{22}\rangle$ and $\langle R^n_{11}\rangle/\langle R^n_{22}\rangle$ on the mesoscale $\delta = L/\langle l\rangle$.

Elasticity of random networks

The scale dependence of effective thermal conductivity discussed in Part I forms the basis for analyzing the analogous effects in mechanical response problems. In fact, in the linear elastic response range of paper, the same type of hierarchy of bounds holds with respect to the effective stiffness tensor $\boldsymbol{C}^{eff}$ as (3.8) of Part I with respect to $\boldsymbol{K}^{eff}$, namely [18]

$$\boldsymbol{C}^R \equiv (\boldsymbol{S}^R)^{-1} \equiv \langle \boldsymbol{S}_1^n \rangle^{-1} \leq \langle \boldsymbol{S}_{\delta'}^n \rangle^{-1} \leq \langle \boldsymbol{S}_{\delta}^n \rangle^{-1} \leq \boldsymbol{C}^{eff} \leq \langle \boldsymbol{C}_{\delta}^e \rangle \leq \langle \boldsymbol{C}_{\delta'}^e \rangle \leq \langle \boldsymbol{C}_1^e \rangle \equiv \boldsymbol{C}^V \qquad \forall \delta' < \delta \tag{3.12}$$

Here $\boldsymbol{C}^e$ and $\boldsymbol{S}^n$ stand for the stiffness and compliance tensors obtained under essential ($u_i = \overline{\varepsilon_{ij}} \cdot x_j$) and natural ($t_i = \overline{\sigma_{ji}} \cdot n_j$) boundary conditions, respectively, whereby $\overline{\varepsilon_{ij}}$ and $\overline{\sigma_{ji}}$ are mean strain and stress.

The actual determination of the effective mechanical response of any sample depends on the choice of a model of a single fiber and fiber-fiber interactions. As discussed in Part II, there are basically two choices: (i) fibers carrying axial forces, or (ii) fibers carrying axial, shear, and bending forces. Note that choice (i) implies perfect (frictionless) joints at the fiber-fiber contacts, while the second choice requires welded-type joints. The latter is a more realistic model preventing these contacts from being sheared under rotations, and it was already pointed out in Part III that the choice of any such fiber network model is closely related to the type of a continuum approximation: either classical or micropolar.

Guided by the periodic lattice study in Part II, we see that the random fiber network should be simulated by a system of beam-type finite elements. The resulting values will show statistical scatter, nonuniqueness, and dependence of the response law on the window size. A paradigm of scale dependence of effective moduli of random spring networks, albeit of a different (that is, Delaunay-Voronoi) geometry and carrying axial forces only, has been reported in [19, 20]. As discussed earlier, a state of uniform strain, rather than uniform stress, is a good approximation of the actual one in a plate with holes. Thus, relatively small networks under kinematic boundary conditions can be used to estimate the large-scale effective elastic moduli.

In Fig. 3.6, we give results for effective moduli of a random fiber network of geometry shown in Fig. 3.2b), which is made of beam-type fiber elements that are perfectly bonded ("welded") at all the fiber-fiber bonds. The latter ensures that the hydrogen bonding at fiber contacts is realisti-

cally being modeled. In order to make comparisons to [21], the same fiber parameters were taken here: fiber length $l^f = 1\ mm$, cross-sectional area $A = 2.5 \cdot 10^{-10} m^2$, the moment of inertia $I = 2 \cdot 10^{-21} m^4$, the axial modulus $E^f = 35\text{GPa}$, the axial Poisson's ratio $\nu_a = 0.1$, and the transverse Poisson's ratio $\nu_t = 0.04$.

With these parameters, two cases have been investigated: an isotropic and anisotropic fiber distribution. In the second case, (with $a_1 = 1$ and other a's being zero in (3.4)), four moduli were obtained: E_x, E_y, ν_{xy}, ν_{yx}; these were then averaged as follows

$$E^{eff} = \langle \frac{E_x + E_y}{2} \rangle \qquad \nu^{eff} = \langle \frac{\nu_{xy} + \nu_{yx}}{2} \rangle \tag{3.13}$$

to get the effective modulus E^{eff} and Poisson's ratio ν^{eff}. In fact, everything was done as a function of the fiber volume fraction P^f in a window of size $L = 1.2\ mm$. Five cases of P^f were tried, in each of which several networks were generated in a Monte Carlo sense and solved. For each network, the program carried out three tasks:

i) generation of a specific number of fibers according to three steps outlined earlier;

ii) determination of connectivities between all the beams - accounting for every fiber-fiber intersection;

iii) solution of the resulting planar fiber-beam network problem.

Fibers have multiple connections, and, as their number F in the window grows, the number of degrees of freedom $3N$ associated with all the mutual nodes (fiber-fiber intersections) increases approximately as $\sim F^{2.5}$, see Fig. 3.5. Consequently, the second task above becomes even more computationally challenging and time-consuming than the mechanics solution itself (!).

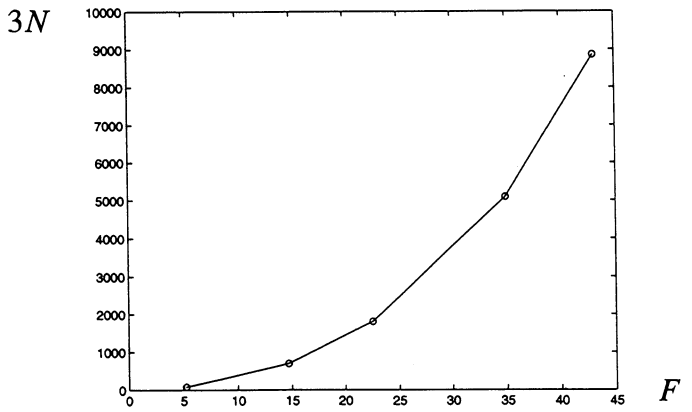

Fig. 3.5 Number of a network's degrees of freedom as a function of the number of fibers.

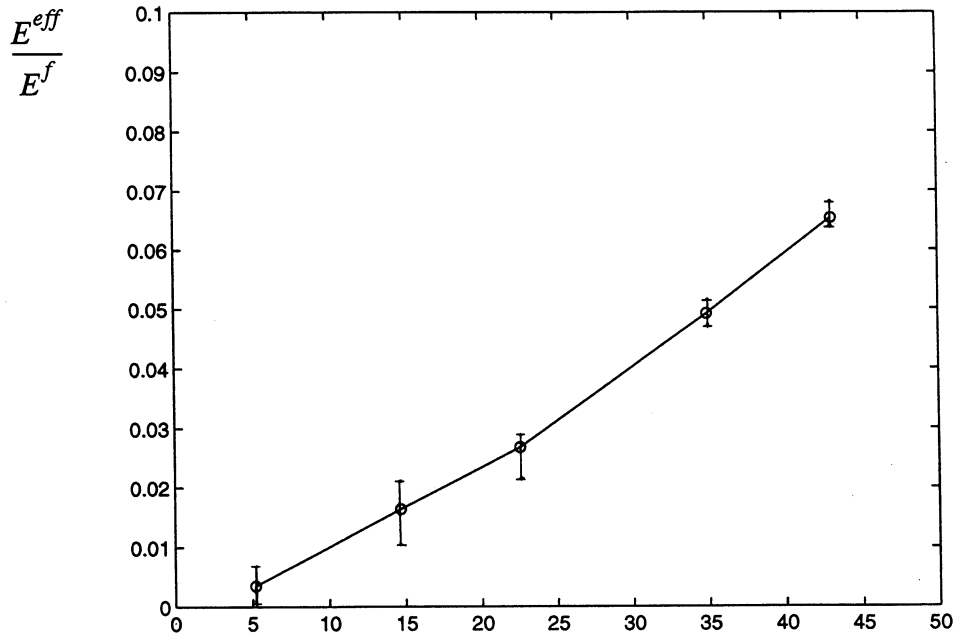

a)

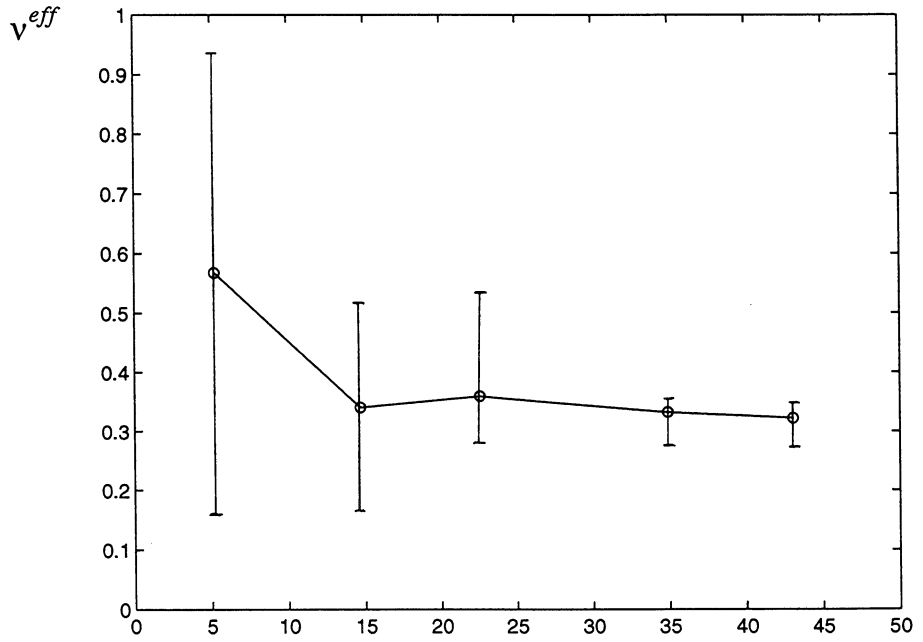

b)

Fig. 3.7 The average Young's modulus (a) and Poisson's ratio (b) of a random, anisotropic network versus the fiber volume fraction in a test window; error bars show the range of variability.

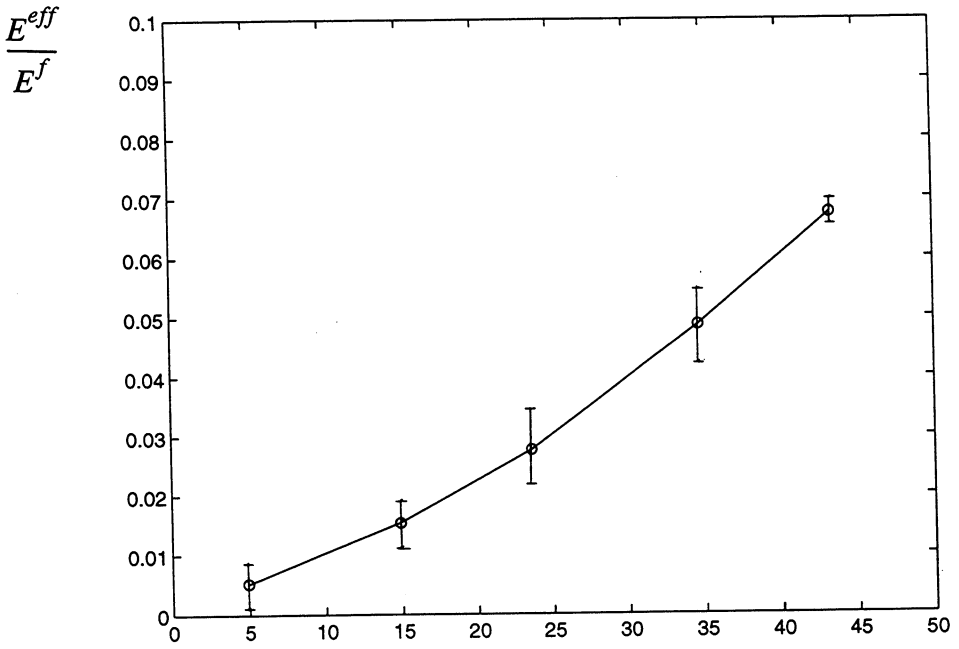

a)

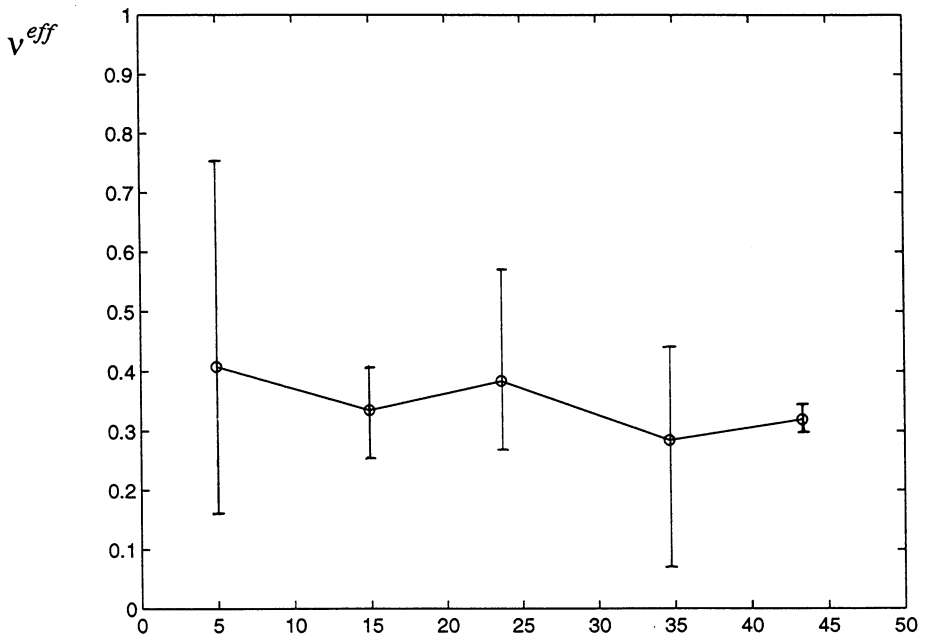

b)

Fig. 3.6 The average Young's modulus (a) and Poisson's ratio (b) of a random, isotropic network versus the fiber volume fraction in a test window; error bars show the range of variability.

The cases of isotropic and anisotropic angular distribution of fibers are shown in Figs. 3.6 and 3.7, respectively. It is seen from Figs. 3.6a) and 3.7a) that a nearly linear dependence of E^{eff}, normalized by the fiber modulus E^f displays a convex dependence on P^f - this is in accord with Fig. 2.4b). The Poisson's ratio ν^{eff} fluctuates strongly around 0.3 and begins to stabilize with increasing fiber volume fraction; larger networks have to be run on a computer to determine its behavior at much higher densities. On one hand, guided by Fig. 2.4c), we will expect a lowering of ν^{eff} with P^f increasing, whereas studies on central force networks [19, 20] tell us that the spatial disorder is known to increase the effective Poisson's ratio. This and related issues are presently under study.

Elastodynamics of random networks: eigenfrequencies as a function of geometric disorder

The discrepancy in measurements of static and dynamic elastic moduli of paper is well known. Basic considerations suggest that this may be due to two causes:

i) Rheology of a cellulosic fiber network.

ii) Presence of a random, rather than periodic, fiber network geometry.

At this stage, we have a setting to quantitatively investigate the latter of these. Thus, the static model of a disordered network of interacting fiber-beams

$$\{f\} = [K]\{q\} \tag{3.12}$$

just needs to be generalized to a dynamic situation: elastodynamics of a multi-degree-of-freedom system

$$\{f\} = [K]\{q\} + [M]\{\ddot{q}\} \tag{3.13}$$

In the above, we have

$\{f\}$ = vector of generalized forces;

$\{q\}$ = vector of $3N$ generalized coordinates (displacements and rotations of all N nodes);

$[K]$ = stiffness matrix; and

$[M]$ = inertia matrix.

Now, by considering a harmonic motion,

$$q_i = A_i \sin(\omega t + \varphi) \tag{3.14}$$

we arrive at

$$\{0\} = [K - M\omega^2]\{A\} \tag{3.15}$$

The determinant of a characteristic equation of (3.15) will result in $3N$ eigenfrequencies. A shift of the lowest of these with respect to the lowest eigenfrequencies of the unperturbed, periodic system will give an indication of the effect of spatial disorder on harmonic wave propagation: the poorer the formation of paper, the stronger the effects. Now, the lowest eigenfrequencies correspond to the longest in-plane waves that can be modeled by the $L \times L$ window of the fiber network. In fact, λ (in-plane wavelength) of typical ultrasound applications is on the order of several fiber lengths, which we can just model with our windows comprising several hundred fibers.

Finally, it appears that the introduction of fiber viscoelasticity into the model (3.13) should be possible so as to make an additional connection with existing microphysically-based rheological models [23].

DISCUSSION: PART IV
STRENGTH AND FRACTURE OF PAPER

The computer program of networks of fiber-beams described in the previous section is the basis for an ongoing development of a program for simulation of paper fracture, where two failure modes would be present: fiber segment failure and fiber-fiber debonding. In order to verify this model, tensile displacement and strength tests on small (2 *mm* x 2 *mm*) very thin paper specimens of Kozo fibers are being set up in a load cell under an optical microscope equipped with video recording equipment. Such experiments, in concert with the computer model, will also permit a determination of microscale strength properties, e.g., fiber-fiber bond strength. This idea has its roots in a recent study carried out on a very thin polycrystalline aluminum foil [24], where thanks to the practically two-dimensional nature of the system, cracks could be observed very well in the laboratory, and parameters of the computer model could be calibrated so as to obtain the same crack pattern. Thus, an otherwise inaccessible grain boundary strength criterion could be inferred. Spring-networks have recently become a powerful tool in studies of fracture of composites, see, e.g., [25] for a modern update.

Additionally, two-meter-wide grips (Fig. 4.1) are being developed for strength tests to allow statistical size/scale effects on very large paper specimens. Thus, our experiments are going to

allow an investigation of paper specimens over a very wide (!) range of parameter space: from 2 *mm* to 2 *m* with a consideration of CD-profile as well as MD-profile effects. The strength tests are going to be carried out on Instron and MTS machines, the second one of which will allow strain-rate-dependent, rather than quasi-static, investigations. In effect, the new tensile tester will be very much closer (!) to the actual mill-scale than is typically being used.

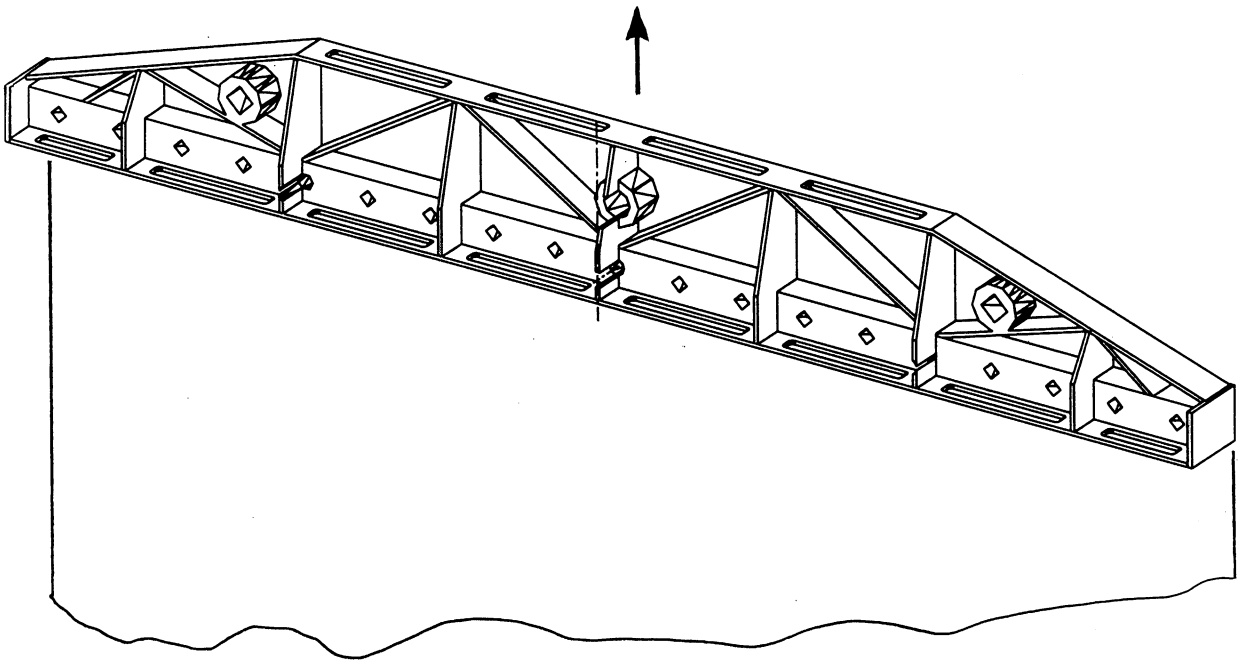

Fig. 4.1 One set of two-meter-wide grips for tensile strength tests.

DISCUSSION: PART V

CONCLUSIONS AND FUTURE GOALS

This report continues the study of the adaptation of spring networks to the modeling mechanics of paper, that was first reported in [1]. We started with the simplest, periodic geometries that permitted an explicit derivation of effective properties as a function of the fiber volume fraction (equivalent to porosity) based on the unit cell concept. Following are the main observations:

i) Triangular networks with axial interactions result in the Young's modulus, which is progessively stiffer than the Cox model with increasing fiber volume fraction, and the Poisson's ratio,

which is the same, i.e., 1/3.

ii) Presence of the bending fiber action (after the Bernoulli-Euler model) in addition to the axial one has the effect of increasing the Young's modulus and of decreasing the Poisson's ratio down from 1/3 with respect to the axial fibers model. A more realistic beam model (of Timoshenko), accounting for shear effects in fibers, results in a minor softening of the original beam model.

iii) In the case of high fiber density (from 50 to 100%), the beam lattice model could be replaced by a perforated plate model, which gives the theoretically correct, although physically unattainable, limiting behavior of the Young's modulus. This model is introduced here for the sake of completeness of the study. However, it is more desirable to extend, in the future, a composite laminate model of Schulgasser and Page [7] so as to inlcude the porosity.

iv) Given the orthotropic character of paper sheets, lattice models can easily be generalized to anisotropy, both in 2D and in 3D (also modeling the multilayered paper structure). However, closed-form solutions can only be obtained under the approximate assumption of uniform strain.

v) The beam lattice models - axial lattice models being a special case - can be generalized, via a computer simulation, to deal with random geometries of fiber arrangements, shapes, sizes, and physical properties. This is the basis for an ongoing study of elasticity, strength, and transport phenomena in most realistic models of paper. However, no close-form formulas can be derived, and this is where the periodic models may serve as a guidance, while various types of microstructural disorder can be investigated quantitatively.

vi) Once fully developed, these computer models can be run to assess the statistical size/scale effects of fiber network properties and their dependencies on a wide range of microstructural paramters such as the degree of flocculation, types of fibers used, fiber-fiber bond strength, etc.

vii) Tensile strength tests of very small paper specimens in a load-cell under a microscope are being conducted to verify the performance of the computer model.

viii) An experimental setup is being prepared to investigate the statistical size/scale effects in tensile strength of paper to more closely approximate real loads on a paper web in paper-mill conditions than heretofore possible.

REFERENCES

1. Ostoja-Starzewski, M., PAC Report (1996).

2. Bristow, J.A. and Kolseth, P., *Paper: Structure and Properties*, Marcel Dekker, New York, 1986.

3. Deng, M. and Dodson, C.T.J., *Paper: An Engineered Stochastic Structure*, TAPPI Press, Atlanta (1994).

4. Kallmes, O.J. and Corte, H., "The structure of paper - I. The statistical geometry of an ideal two dimensional fiber network," *Tappi J.* 43: 737-752 (1960).

5. Wozniak, C., *Surface Lattice Structures* (in Polish), Polish Sci. Publ., Warsaw (1970).

6. Ostoja-Starzewski, M., Sheng, P.Y., and Alzebdeh, K., "Spring network models in elasticity and fracture of composites and polycrystals," *Comput. Mater. Sci.*, Vol. 7 (1&2), pp. 82-93 (1996).

7. Schulgasser, K. and Page, D., "The influence of transverse fibre properties on the in-plane elastic behaviour of paper," *Composites Sci. Tech.* 32: 279-292 (1988).

8. Lu, W., Carlsson, L.A., and Andersson, Y., "Micro-model of paper. Part I: Bounds on elastic properties," *Tappi J.* 78(12): 155-164 (1995).

9. Lu, W. and Carlsson, L.A., "Micro-model of paper. Part II: Statistical analysis of the paper structure," *Tappi J.* 79(1): 155-210 (1996).

10. Lu, W. and Carlsson, L.A., "Micro-model of paper. Part III: Mosaic model," *Tappi J.* 79(2): 197-205 (1996).

11. Jasiuk, I., Chen, J., and Thorpe, M.F., "Elastic moduli of two dimensional materials with polygonal holes," *Appl. Mech. Rev.* 47(1, Part 2): S18-S28 (1994).

12. Jasiuk, I., "Polygonal cavities vis-à-vis rigid inclusions: Effective elastic moduli of materials with polygonal inclusions," *Intl. J. Solids Struct.* 32: 407-422 (1995).

13. Cox, H.L., "The elasticity and strength of paper and other fibrous materials," *Brit. J. Appl. Phys.* Vol. 3, pp. 72-79, (1952).

14. Stoyan, A. Kendall, W.S. and Mecke, J., *Stochastic Geometry and Its Applications*, J. Wiley & Sons, Chichester, (1980).

15. Mark, R.E. and Murakami, K., *Handbook of Physical and Mechanical Testing of Paper and Paperboard*, Marcel Dekker, New York (1983).

16. Gibson, L.J. and Ashby, M.F., *Cellular Solids*, Pergamon Press (1988).

17. Ostoja-Starzewski, M. and Schulte, J., "Bounding of effective thermal conductivities of multiscale materials by essential and natural boundary conditions," *Phys. Rev. B*, Vol. 54, pp. 278-285, (1996).

18. Huet, C ., "Application of variational concepts to size effects in elastic heterogeneous bodies," *J. Mech. Phys. Solids*, Vol. 38, pp. 813-841 (1990).

19. Ostoja-Starzewski, M. and Wang, C., "Linear elasticity of planar Delaunay networks: Random field characterization of effective moduli," *Acta Mech.* 80: 61-80 (1989).

20. Ostoja-Starzewski, M. and Wang, C., "Linear elasticity of planar Delaunay networks. II: Voigt and Reuss bounds, and modification for centroids," *Acta Mech.* 84: 47-61 (1990).

21. Jangmalm, A. and Östlund, S., "Modelling of curled fibers in two-dimensional networks," *Nordic Pulp Pap. Res. J.* 3: 156-161 (1995).

22. Batten, G.L. Jr., "Unification of phenomenological, structural, and hydrogen-bonded theories of paper, using percolation concepts," *Nordic Pulp Paper Res. J.*, Spec. Issue, pp. 8-14 (1987).

23. Nissan, A.H. and Batten, G.L. Jr., "The differences between sonically and mechanically determined elastic moduli of paper," *Mat. Res. Soc. Proc.*, Vol. 197, pp. 163-172 (1990).

24. Grah, M., Alzebdeh, K., Sheng, P.Y., Vaudin, M.D., Bowman, K.J. and Ostoja-Starzewski, M., "Brittle intergranular failure in 2D microstructures: Experiments and computer simulations," *Acta Materialia*, Vol. 44(10), pp. 4003-4018, 1996.

25. Krajcinovic, D., *Damage Mechanics*, Elsevier/North-Holland (1996).

26. Thorpe, M.F. and Jasiuk, I., "New results in the theory of elasticity for two-dimensional composites," *Proc. Roy. Soc. Lond.,* Vol. A438, pp. 531-544 (1992).

27. Nowacki, W., *Theory of asymmetric elasticity*, Pergamon Press/Polish Sci. Publ., Oxford/ Warsaw (1986).

28. Ostoja-Starzewski, M. and Jasiuk, I., "Stress invariance in planar Cosserat elasticity," *Proc. Roy. Soc. Lond.*, Vol. A451, pp. 453-470 (1995).

APPENDIX: TWO-DIMENSIONAL (PLANAR) VERSUS THREE-DIMENSIONAL ELASTICITY

Classical elasticity

Measurement of the z-direction strain in tensile tests of paper sheets is a challenge, e.g., [2, 15]. Noting such experimental constraints as well as the 2D character of a generic fiber mat model, it is more convenient to work with a so-called planar rather than the conventional *3D elasticity.* This

section is thus devoted to a brief exposition of the basic concepts of a *planar elasticity* (or *2D elasticity*) in x_1-x_2 and its relation to the 3D elasticity.

We begin by noting that the constitutive relations for a linear elastic isotropic 3D material are

$$\varepsilon_{11} = \frac{1}{E_{3D}}[\sigma_{11} - \nu_{3D}(\sigma_{22} + \sigma_{33})] \qquad \varepsilon_{12} = \frac{1+\nu_{3D}}{E_{3D}}\sigma_{12} \tag{A.1}$$

together with cyclic permutations $1 \rightarrow 2 \rightarrow 3$, whereby E_{3D} and ν_{3D} stand for the conventional 3D Young's modulus and Poisson's ratio. On the other hand, in 2D elasticity, there is no x_3 direction so that we have

$$\varepsilon_{11} = \frac{1}{E}[\sigma_{11} - \nu\sigma_{22}] \qquad \varepsilon_{12} = \frac{1+\nu}{E}\sigma_{12} \tag{A.2}$$

with cyclic permutation $1 \rightarrow 2$. In (A.2), E and ν stand for the 2D (or planar) Young's modulus and Poisson's ratio. Applying the concept of bulk and shear moduli to the above relations, we readily find that the *planar bulk and shear moduli* are

$$K = \frac{E}{2(1-\nu)} \qquad \mu = \frac{E}{2(1+\nu)} \tag{A.3}$$

Furthermore, the planar Young's modulus, E, and Poisson's ratio, ν, are connected to these by

$$\frac{4}{E} = \frac{1}{K} + \frac{1}{\mu} \qquad \nu = \frac{K-\mu}{K+\mu} \tag{A.4}$$

It is important to note here that ν is seen to range from -1 through +1, in contradistinction to ν_{3D}, which is bounded by $-1 \le \nu_{3D} \le 0.5$. For positive values of ν and ν_{3D}, we have the following relationships

$$E = \frac{E_{3D}}{1-\nu_{3D}^2} \qquad \nu = \frac{\nu_{3D}}{1-\nu_{3D}} \tag{A.5}$$

We refer to [26] for a detailed discussion of relationships among this planar, the well-known plane stress, the well-known plane strain, and the 3D isotropic elasticity.

Micropolar elasticity

It will be shown below that the presence of beam-type interactions in a fiber network necessitates a consideration of an additional degree of freedom besides two in-plane dispalcements,

namely the rotation φ about an axis normal to the plane of the sheet. The force transmission now occurs not only through the surface force traction, but also through the surface moment traction. This leads to a so-called *micropolar elasticity* model, and the corresponding constitutive law is of the following form

$$\varepsilon_{11} = \frac{A+S}{4}(\sigma_{11}+\sigma_{22}) - \frac{S}{2}\sigma_{22} \qquad \varepsilon_{12} = \frac{S}{4}(\sigma_{12}+\sigma_{21}) + \frac{P}{4}(\sigma_{12}-\sigma_{21}) \qquad 1 \to 2$$
$$\kappa_1 = M\mu_1 \qquad 1 \to 2 \tag{A.6}$$

with cyclic permutations as shown. In the above, we use κ's to denote torsion-curvatures, while ε_{ij}'s are now asymmetric strains and σ_{ij}'s asymmetric stresses. Also, in (A.6), we introduced four planar compliances

$$A = \frac{1}{K} = \frac{1}{\lambda+\mu} \qquad S = \frac{1}{\mu} \qquad P = \frac{1}{\alpha} \qquad M = \frac{1}{\gamma+\varepsilon} \tag{A.7}$$

Observe that $(A.7)_1$ defines a planar bulk compliance K, different from the 3D one, and $(A.7)_2$ a planar shear compliance S, which is the same as the 3D shear compliance. It is noteworthy that the planar Young's modulus and Poisson's ratio are given through (A.4) as before; see [27] for a complete exposition of the 3D micropolar theory and [28] for a planar setting. Results of the latter reference, together with the formulas of Part II of this report, form the basis for a future investigation of optimal paper microstructures.

FUNDAMENTALS OF REFINING AND FIBER PROPERTIES

STATUS REPORT

FOR

PROJECT F024

John Waterhouse
Hiroki Nanko

March 26, 1997

Institute of Paper Science and Technology
500 10th Street, N.W.
Atlanta, Georgia 30318

TECHNICAL PROGRAM REVIEW

Project Title:	Fundamentals of Refining and Fiber Properties
Project Code:	PROPTY
Project Number:	F0024
Division:	Engineering and Paper Materials Division
Project Staff:	John F. Waterhouse, Hiroki Nanko, Helena Rislaaki
Project Budget:	$100,053

OBJECTIVE

To better understand and characterize changes in fiber structure produced by refining, especially as they related to paper machine runnability and paper properties.

SUMMARY

1. Visited Crane and Company, Dalton, MA; Beloit Jones, Dalton, MA; and Mead Corporation, Chillicothe, Ohio to present a seminar on refining, obtain feedback, on proposed refining project, and staying in touch with member companies.

2. Conducted a literature and patent search in the area of refining.

3. Developing a plan and goals for continuing research in refining.

4. Working together with Dr. Hiroki Nanko to establish methods for determining selected changes in fiber structure due to refining.

5. A Project NewsBrief is being developed dealing with items relevant to the project as a means of communicating with members of the Paper Physics Committee. The NewsBrief will occur at fairly regular intervals.

6. Presenting a paper Whither Refining? to the 1997 International Refining Conference, Fiuggi, Italy, March 18-20, 1997.

VALUE TO INDUSTRY

1. Better use and savings in raw materials.

2. Energy reduction associated with refining and water removal.

3. Improved papermachine productivity.

4. Better tools for the characterization of pulps with respect to refining.

5. Improved understanding and control of the refining process.

PROJECT GOALS

Precise goals and tasks are still in the process of being developed, however, the following goal should be seen as a first attempt to meet this need.

To produce and characterize specific changes in fiber structure and measure their impact on water removal and paper properties.

According to Page (4), there are nine changes associated with refining. It is proposed that initially we limit our attention to only three of these changes namely **internal changes, external changes, and fines generation.**

Tasks

1. Select and characterize pulp types to be used, e.g., chemical pulps in the yield range of 40 to 70%

2. Develop methods to selectively produce the above changes in fiber structure.

3. Determine the energy consumed with each of the above changes.

4. Measure the changes (wet and dry state) associated with each change.

5. Measure properties as they might relate to machine runnability and paper performance.

Program Structure

Establishment of Fundamentals -> Applied Research -> Technology Transfer

The research program is primarily formulated (in consultation with, and the support of member companies) to meet industry needs and should be driven by the following considerations.

A. Current state of knowledge (IPST + Industry), i.e., how much of our present knowledge, specifically in the area of refining, is being used and why isn't more being utilized?

B. New experimental/theoretical program is designed to address NEEDS not met by A above.

INTRODUCTION

Refining or beating (terms used interchangeably) is defined as the changes in fiber structure of a pulp necessary to maximize its paper making potential. We understand the term paper making potential to mean achieving the right balance between critical paper properties and paper machine runnability within certain economic restraints.

The purpose of the literature review which follows is to briefly examine what progress has been made in the area of refining and characterization of changes in fiber structure brought about by such treatment over approximately the last twenty years, and to highlight those areas worthy of further attention. These findings, together with input from the Paper Physics Committee and Refining Subcommittee, will determine the content and future direction of the research plan associated with this project.

LITERATURE REVIEW

The literature on refining is quite extensive (1), however, there have been several notable reviews (2)-(7) during the last twenty years. Furthermore, refining has been the subject of a number of conferences organized by the Institute of Paper Chemistry and PIRA (Paper Industry Research Association, Leatherhead, UK) (8)-(11).

	← wet state →	← dry state →
RAW MATERIALS ⇒	**REFINING ⇒ PAPER MAKING⇒**	**PAPER PROPERTIES**
virgin, recycled fibers	changes in fiber water removal	surface & bulk
non-wood fibers	structure	
genetically modified fibers		

The general relationship between raw materials, refining, papermaking, and the properties one is trying to produce is shown in the above diagram. We note that both refining and

papermaking involve wet state variables, while paper properties are mainly in the dry state.

According to the review by Page (4) there are 9 types of fiber structural change as given below:

Fiber Structural Changes Produced by Refining

1. Cutting or shortening of the fiber
2. **Fines production**
3. **External Changes in Fiber Structure**
4. **Internal Changes in Fiber Structure**
5. Curling the fiber or curl removal
6. Inducing microcompressions or removing them
7. Dissolving or leaching out colloidal material.
8. Redistribution of hemicellulose from the interior to the exterior of the cell wall
9. Surface abrasion at the molecular level to produce a more gelatinous surface

The above changes in fiber structure are mainly produced by mechanical stresses imparted to the fiber by some type, or combination of refiners. The extent to which changes are brought about will depend on a number of factors, i.e., type of fiber, pulp consistency, pH, presence of counter-ions, temperature, etc.

The type of treatment that a fiber needs will very much depend on the desired end use performance of the paper being made. In other words there is no one desirable treatment to fit all paper making and paper property requirements.

In a production refining situation, once the desirable changes in pulp properties have been identified, the aim is to produce them with the minimum amount of fluctuation, even though the characteristics of the incoming pulp may be varying. Minimizing energy consumption and down time (say due to plate wear) are also highly desirable. Changing refining action, so as to alter the relative balance of the above 9 refining effects is, in most cases, not an easy matter. Currently, the disk refiner is the most commonly used production refiner. In addition to the factors mentioned previously, plate design, energy input, and sizing of the refining system are the main factors controlling refining action. Continuous measurement of the changes in fiber structure are still rudimentary, i.e., freeness or drainage changes.

To better understand [and optimize] the relationship between changes in fiber properties, the paper making process, and paper properties, some form of modeling is highly desirable. One of the goals of paper physics research is to determine these relationships,.

Significant reviews of the refining literature were carried out by Attack in 1977 (2), Ebling in 1980 (3), Page in 1989(4), and Hietanen and Ebling in 1990 (5). Attack stated that during the period of his review (20 years) that refining of chemical pulps was reasonably well understood, but there was still a need to better understand the refining of high yield pulps. Ebling (3) and later Hietanen and Ebling (5) both carried out an extensive review of the refining literature. They concluded, and this may be over simplified, that one of the central problems of refining to be addressed is the break down of flocs so that fibers can be more readily treated.

Page's review (4) concludes with seven goals for future beating research which are summarized below.

Page's Goals for Future Beating Research

1. **More precise physicochemical description of the structure of the cell wall matrix.**

2. **Rapid measurement of fiber length, coarseness, cell wall thickness, and fibril angle.**

3. **Better characterization of raw materials and pulps.**

4. **Rapid measurement of beating effects, i.e., fibrillation, cell wall cracks, microcompressions, kinks, and curl.**

5. **Multivariate analysis of beating.**

6. **Improved images of beating zone especially to capture individual fiber movement.**

7. **Mechanistic theory of beating action in terms of the stresses the fibers experience, and their response to those stresses.**

During the past seven years progress has been made towards addressing these goals, particularly items 2 (fiber length), 4 (kinks and curl), 5. (multivariate analysis), and 7. (mechanistic beating theory) which we will now briefly review.

2. (measurement of fiber length, coarseness)

Instrumentation is now available for the fairly rapid measurement of fiber length distribution and coarseness (12)(13).

4. (measurement of kinks and curl)

The Fiber Quality Analyzer appears to be a fairly rapid method for the measurement of fiber kinks and curl (13).

5. (Multivariate Analysis MVA)

Factor analysis has been used by Howard, Poole, and Page (14) to examine a variety of laboratory beating processes, i.e., Aylesford Beater, Banning-Seybold Beater, PFI Mill, Lampen Ball Mill, Valley Beater, and a Noble & Wood Beater involving 9 different pulps and the measurement of 9 pulp and paper variables.

The data set was used by the above authors to determine the number of FACTORS or independent variables involved. The factors are mathematically derived, and through logical reasoning their underlying meaning can be deduced. It was found in using the data for all pulps that 3 Factors accounted for 94% of the total variance. The three factors were identified from the dependent variables involved to be 1. ***bonding, 2. fiber length and fines, and 3. microcompressions.*** For example Factor 1, accounting for 49.6% of the common variance, had a strong positive correlation with burst, breaking length, fold, and a strong negative correlation with scattering coefficient hence ***bonding*** was identified as the most likely candidate for Factor 1. It should be emphasized that none of these variables (or related variables) were measured, or part of the original data set on which the MVA analysis was performed. Furthermore, it is not known to what extent more fundamental factors, e.g., internal fibrillation, or external fibrillation, that ***bonding*** might be related.

The authors in their discussion recommend that an experiment be designed which would include a much wider range of treatments and measured variables. Once factors have been identified variables termed "marker variables" e.g., fiber strength, fiber saturation point, fines content, fiber length, and curl index, would be measured.

Although the above factor identification seems reasonable there could be alternative interpretations. Perhaps what is impressive is that just 3 factors were identified out of a possible total of 9, although factor 2 did involve both fiber length and fines. Interestingly, the beating effects identified in Page's review (4) total 9.

7. (Mechanistic Beating Theory)

The more recent research of Kerekes and co-workers (7)(15)(16)(21)-(25) has attempted in a systematic way to address in part Page's 7th recommendation. Central to this work is the C-Factor concept in which the specific energy of refining **E** is decomposed into the number of impacts a fiber receives in the refining zone **N**, and the intensity of those impacts **I.**

$$E = N \times I$$

and if **P** is the net power input, **F** is the fiber mass flow then ***C (or C-Factor) is defined as the capacity of the refiner to inflict impacts*** and we have:

$$N = C/F \text{ and } I = P/C$$

I refers to some form of cyclic deformation imposed on the fiber by bar crossings.

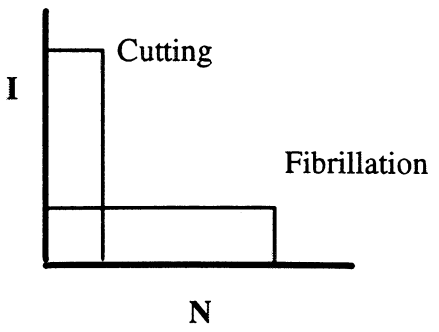

We see from the above diagram (as given by Kerekes) that the same amount of energy can be imparted to the fibers in many different ways. At one extreme we have a small number of impacts at high intensity which leads to cutting, and at the other extreme a large number of impacts of high intensity which leads to fibrillation.

Kerekes (15) has attempted to rigorously derive C-Factor, and the key issue is associated with the number of impacts a fiber is likely to receive as it pass through the refiner.

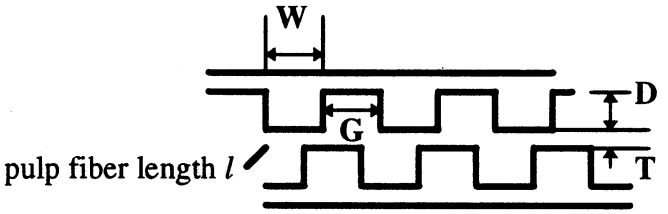

Now N^* is the number of impacts a fiber receives and M is the mass of the fiber and the rate of impacts is dN^*/dt and is proportional to the product $n_1 x\ n_2 x\ \omega$ where n_1, n_2, and ω are respectively the number of bars on the rotor, stator, and the angular velocity of the rotor with respect to the stator. The correct estimate of the **proportionality factor** is, according to Kerekes, a crucial assumption of the analysis, and is estimated according to the probability of fiber contact with the leading edge of the bar, which is given by $l/(l + D + T)$.

Several cases involving fiber length and bar geometry were considered by Kerekes. Now the number of impacts per unit time on a fiber are given by:

$$dN^*/dt = [l/(l + D + T)] \times [l/2\pi r] \times [n_1 n_2 \omega]$$

Case 1: $(D + T) << l$ i.e.bar depth and clearance are small compared with fiber length,

Case 2: $(D + T) << l$ and $l = (W + G)$, i.e., only one impact at a time on a fiber from the bar of the opposing plate - $dN^*/dt = n_2\omega$]

Case 3: $(D + T) >> l$ i..e., bar depth and clearance large compared with fiber length - $dN^*/dt = l^2 n_1 n_2 \omega/2\pi r (D + T)$

C-Factor analysis is perhaps the most rigorous and comprehensive theory developed to date, and in essence builds on the theories or models of Brecht (17), Danforth (18), Rihs (19), and Lumianen (20). It has been applied to a variety of refiner geometry's including disk, conical, and the PFI mill.

The C-factor is ultimately a function of plate geometry (bar width, depth, length, angle, and edge geometry), speed, consistency, fiber length, and coarseness.

The structure of the fiber is modified by a fatigue process, i.e., the average number of impacts the fiber receives in the refiner N, with a certainly level of intensity I as already stated. Cutting and fibrillation are treatments identified at the extremes of the treatment envelope. What other effects, as discussed earlier, are present, and what happens between these extremes has yet to be identified.

Refining action is concerned with how to efficiently and effectively impart changes to the fiber to improve its papermaking and product quality characteristics. If for the moment we limit our discussion to bar type refiners, e.g., disk, conical, a variety of mechanical stresses are applied to the fiber either directly or indirectly. These stresses include: shear, compressive, tensile, friction, and ploughing. By direct we mean the individual fibers would be receiving one or more of these stresses, whereas indirect would mean that the floc would be subjected to one or more of these stresses. It is also possible that fibers may be specifically oriented, as in a network to receive fiber treatment.

It is perhaps surprising when we consider the size of the softwood fiber, 2 to 3 mm length, 50 μm in width, that the moving elements of most refiners or beaters are large by comparison, i.e., 10 to 20 mm bar width. However, disk refiners do not in general act on individual fibers, but rather on fiber flocs which are very prevalent in the consistency range associated with refining, i.e., 3 to 7%. It is through these flocs, which are subjected to the above stresses, that the individual fibers receive their treatment. Kerekes's group is also involved in the prediction and measurement of stresses that are applied to fiber flocs (21)-(25).

Steenberg's refining concepts involving grinding and ore milling (26)-(28) also appear to be relevant to disk refining. In Figure1we see how the gap or clearance in a refiner varies with the time the material is being treated. In the control situation A the gap will decrease with time, however, if either long fiber B or fines C are added the gap will respectively increase or decrease. In case C presumably the decrease in gap would be equivalent to some point on curve A at the same total equivalent fines content? In case D polyethylene oxide is added which dramatically decreases the gap. This behavior might be interpreted as a change in the rheology of the stock, i.e., its effective viscosity; and/or as Steenberg argues, be related to the condition of the stock, i.e., does it ooze or consolidate as shown in Figure 1 In an oozing flow regime it would be difficult to refine the fibers, while in the consolidation flow regime the flocked fibers would be treated at a consistency higher than that going into the refiner. Interestingly, Steenberg (28) shows that a roughened surface, e.g. grooves, is necessary to promote the consolidation phase.

Experimental Refiners

Disk refining the main means of fiber treatment in the paper industry is a complex process. Whether there will be a paradigm shift to a completely different method of refining remains to be seen. In the meantime there has been a significant effort to improve the disk refiner, at least as is indicated by the patent literature. How much

control in terms of refining action, and concomitantly changes in fiber structure we can ultimately exercise remains to be determined.

A number of novel attempts have been made to refine fibers, some of which have been designed to produce a specific refining action or change in fiber structure. These as we shall see include viscometric-rheological type devices, ultrasonic methods, abrasive and porous devices. Specialized production equipment has also been developed to produce more specific changes in fiber structure, including high consistency devices such as the Chemifiner (29) and Frotapulper (30) to produce kinked , curled, and microcompressed fibers. At the other extreme homogenizers (31) have used to produce microfirillated cellulose (essentially fines).

A selection of these devices are shown in Figures 2, 3, 4, 6, 7, 8. The "Shear Refiner" (32) shown in Figure 2 was designed to measure the rheology associated with refining in a shear field, the energy consumed, and treatment of enough pulp to make handsheets and evaluate the refining action. One critical question was whether turbulent flow was necessary for effective refining. As Figure 2 illustrates the flow in the annulus of the shear refiner was laminar, furthermore, the energy consumption was considerably greater than a disk refiner at the same level of slowness. In retrospect one reason for this might be due to the use of a fixed gap, i.e., constant clearance in the annulus. Strength properties were developed, but the performance was not equal to that of the Valley beater (32).

The roll refiner Figure 3 was developed by Hartman (33) as a means to produce internal fibrillation in the fiber structure. In addition he also sought to determine the added influence of fines, and external fibrillation. The roll refiner was quite successful at producing internal fibrillation as evidenced by transmission electron photomicrographs of treated fibers. Roll refined pulp showed no drop in freeness, although there was an increase in water retention value WRV. When compared with valley beating the roll refining of fibers resulted in handsheets with lower tensile strength when compared at constant apparent density. A 16%

fines addition at two levels of Roll Refining resulted in a strength improvement almost equal to that produced by the valley beater.

External fibrillation was produced in an abrasion refiner developed by Higgins (33) a schematic of which is shown in Figure 4. Hartman found that roll refining followed by abrasion refining resulted in only an increase in density without a concomitant increase in strength. It is possible that drying effects and pulp type (sulfite) were responsible for the lack of strength improvement.

An interesting finding in Hartman's thesis (34) was a comparison of the energy consumption of roll refining and disk refining as shown in Figure 5. It is seen that roll refining reaches a strength plateau around 40 kwh/t (1.24 HPD/T) while disk refining continues to improve strength beyond roll refining, consuming around 400 kwh/t (12.4) HPD/T. It is speculated that internal fibrillation for the roll refiner is close to being over 90% homogeneous, whereas the disk refiner, which was producing a variety of effects, e.g., internal fibrillation, fines production etc., was much less homogeneous.

Biasca"s thesis (35) was focussed on internal changes in fiber structure and he developed a bending refiner, shown in Figure 6 as a means to flex fibers. He also repeated some of the roll refining experiments of Hartmann.

Biasca found that refining action in the bending refiner was in some ways different to that produced by the roll refiner. For example out-of-plane modulus was significantly increased with the bending refiner over other methods of refining. However, the roll refiner gave a better performance than the bending refiner with respect to in-plane elastic properties.

What methods produce changes in the external structure of the fiber, i.e., external fibrillation? We have already mention the abrasion refiner developed by Higgins (33). Interestingly, if both surfaces of the apparatus shown in Figure 4 are smooth no significant refining action takes place, i.e., the shear stresses are not affectively transmitted to the fiber

suspension. Grit size was found to play an important role. However, the pulps were dried prior to refining for the purpose of consistency control, since only small amounts of fiber were processed, and therefore the extent to which the findings can be generalized is limited.

Cumpston (36) used abraisive grit to generate gelatinized fiber surfaces by fiber-particle interaction. The use of abrasive surfaces and abrasive particles have also appeared in the patent literature. Presumably fiber-fiber interaction will also result in external fibrillation. It is likely that methods to promote external fibrillation will also result in fines generation. The relative importance of external fibrillation in the refining of chemical pulps has not yet been established in the opinion of this reviewer.

Secondary fines generated by refining, i.e., material passing through a 200 mesh screen, can be generated by a variety of methods. At one extreme is the production of microfibrillated cellulose from softwood fibers using an homogenizer (31), as shown in Figure 7. There has recently been a flurry of activity in understanding the behavior of fines, particularly in the area of recycling (37)-(39).

As demonstrated by Hartman (33) and other researchers (37)-(39), fines can have a significant impact on many paper properties. The down side is that drainage and water removal are adversely affected. Drying generally has a negative impact on fines contribution to a number of paper properties (38).

Disk refining is currently central to real world papermaking as mentioned earlier. It is therefore not surprising that considerable effort has been expended to better understand this process, and has been the subject of earlier reviews. More recently Kerekes and his coworkers have further contributed to our understanding of this process (7)(21)-(25). One focus of their research is to predict and measure the stresses involved in refining. How these stresses alter the structure of the fiber and the extent to which they can be controlled has yet to be determined. Nevertheless, their results to date are quite impressive and represent a step forward in refining research.

Silvy and his colleagues in ongoing research are viewing the refiner as a viscometer (40)-(42) in a manner reminiscent of the earlier work of Steenberg (43) and Waterhouse (32). A schematic of their refiner-viscometer is shown in Figure 8. Their findings indicate that pulp behaves as a shear thinning fluid, i.e., that as refining progresses effective viscosity decreases as shear rate increases, and fiber length decreases. The optimum properties are produced at constant load and with minimum energy consumption. In the consistency range of 2.5 to 5.0% effective viscosity is correlated with consistency, WRV, SR (schopper reigler, shear rate, and geometry).

Homogeneity of Refining

One of the major differences between laboratory refining and production refining is the homogeneity of treatment. Hietenan (6) in Appendix II of her thesis examines this problem and as others have concluded finds that flocs can pass through the refiner and be untreated.

The Refining Characteristics of Different Pulp Types

It is well recognized that species, pulp type and bleaching process, and the relative amounts of thick and thin walled fibers can affect refining. Work in progress on genetic modifications, changes in pulping and bleaching, and enzyme use are all likely to impact refining. The viscoelastic-plastic behavior of wood and wood fibers is considered to be particularly important in mechanical pulping and the refining of mechanical pulps in regard to fiber separation, changes in fiber structure, and energy consumption (44)-(46).

Cellulose may be viewed as a semicrystalline material consisting of crystalline (ordered) and amorphous (less ordered) regions. Hemicellulose and the disordered regions of the cellulose chain contribute to the amorphous content and are important with respect to their association with water. Lignin when present is another amorphous polymer.

Page (47) has suggested that differences in the beatability and refining action of kraft and sulfite pulps is due to differences in their viscoelastic behavior. As shown in Table 1 beating time increases as one progresses from an acid sulfite to a kraft pulp, and is attributed by Page to an increase in the amorphous content of the pulp.

Table1 Beating Time (Valley Beater) to 45° SR for a 50% Yield Spruce Pulp (47).

PULP TYPE	BEATING TIME MINS.
Acid Sulfite	23
Bisulfite	25
Bisulfite-carbonate	51
Kraft	85

The differences in beating time shown in Table 1 may well be attributable to differences in their viscoelastic behavior. However, this may not be the fundamental reason and this issue requires further attention if a pulps response to refining is to be better understood.

With regard to pulp characterization it may be useful, in addition to monitoring the characteristics mention above, i.e., species etc., to measure the % crystallinity as proposed by Salmen ( ). He defined it as measured by x-ray diffraction as follows:

$$\%\ crystallinity = \frac{\text{int}egrated\ \text{int}ensity\ of\ crystalline\ peaks}{\text{int}egrated\ \text{int}ensity\ of\ both\ crystalline\ \&\ amorphous\ peaks}$$

Papermaking Behavior - Water Removal

A stated in the objective we are particularly concerned with the impact of refining on paper machine runnability and paper properties. Water removal is central to machine runnability and productivity affecting drainage, wet pressing, and drying.

Prediction of a refined pulp's drainage characteristics is potentially the most problematic, since wet end chemistry, retention, forming fabrics, and table activity can make predictions made on the thick stock seem irrelevant. Nevertheless, we will focus on changes in drainage behavior occurring after refining, and hopefully they can be successfully integrated into models of drainage on the papermachine.

Rapid measures of drainage include CSF, SR, and Williams Slowness. Many regard these measurements as being useless, in spite of the efforts to better understand them (49),(50). More fundamental measurements of drainage include filtration resistance, and its resolution into specific surface area and volume when mat compressibility behavior has been determined (51).

How the various changes in fiber structure impact these various drainage measurements is imperfectly understood. We have seen at one extreme that internal changes in fiber structure can occur with no impact on CSF, while at the other extreme fines because of their large surface area can dominate CSF and other drainage measurements.

Once the web structure has been established water removal and web consolidation in the wet press is the next important papermaking step to be considered. Both intra and inter fiber water removal occur in the press section. Laivins and Scallan (52) have proposed that fiber saturation point (determined by the solute exclusion) be used as a measure of water removal in the press section. Stratton found that whereas hydrodynamic specific surface area did not correlate with water removal in the wet press, hydrodynamic specific volume did.

However, in processes such as impulse drying, measurement of hydrodynamic specific surface of the web after pressing is an important parameter in relatingto, and avoiding web delamination.

Impact of Refining on Paper Properties

Basic paper properties fall into three categories namely structure, bulk, and surface properties, examples of which are given below.

* **STRUCTURE** - Apparent density, R.B.A., and formation
* **BULK** - Elastic properties, strength, permeability, and optical properties.
* **SURFACE** - Roughness, strength, pore structure.

A number of models have been established for predicting both elastic and strength properties (53)-(55), however, their relationship to changes in fiber structure produced by refining is still imperfectly understood. Nevertheless, the models do provide a good basis for understanding the effects of refining.

Patent Literature 1976-1996

Patent literature has a variety of functions in addition to protection of intellectual property rights. It is a valuable source of information not readily available in textbooks or papers, as well as providing some sense of activity and areas of focus in a given field. Of course not everyone reveals their creativity in patents. The majority of patents document improvements in a concept e.g. tape recorders, golf ball retrievers, disk refiners; and yet the improvements and the claims which are their true basis, should not be obvious to one skilled in the art. In refining we will see that patent activity has been most productive in the field of disk refining. Like an automobile disk refiners are better engineered today, but without any radical change in concept, e.g., vacuum tube to transistor.

This is not an exhaustive patent search but hopefully we have not missed significant ones. We have also been very selective in our area of interest with the focus being on new or

radical concepts in refining or refining action. In addition we have gained a limited perspective of international activity in the field of refining.

The patent search strategy found that the total number of patents in the time period is 1650, and was reduced to just over 1000 by discarding areas which were not of immediate interest. From a general inspection of the abstracts associated with the selected patents further sub-categories of refining activity have been defined as shown in Table 2.

Table 2 Categories of Patent Activity in Refining

Refining Action
Uniformity of Refining
Plate or Tackle Design
Energy Reduction
Refiner Control
Plate Materials
Novel concepts of Refining
Additives
Plate clearance control
High consistency refining
Abrasive materials
Steam flow
Inlet flow uniformity
Fractionation
Acoustic and ultrasonic wave generation
Other.....

Worldwide patent activity in the above categories is shown in Figure 9. A surge of activity is noted in 1980 and again in 1988. Could another surge of activity be on the horizon after the low in 1996? Patent activity over the time period is further broken down into the major contributors USA, Russia and USSR, Japan, Germany, France, and Canada, and the total contributions are shown in Figures 10 and 11 respectively. We see that the most active countries have been the USA and Canada. Surprisingly, Russia and the USSR have been the most productive.

In the time and space available it is not possible to review all of the patents, however, we have tried to select those patents that are most directly concerned with refining action mainly in the area of chemical pulp refining.

[*Please note that this section is incomplete]

The Future of Refining

One can envisage two extremes, at one extreme is a radical new concept of refining, and at the other no refining is required at all! The latter may be brought about by genetic engineering, enzyme and chemical treatments, and better blending of raw materials. The latter option may simplify the papermaking process and even save energy. Efforts to improve refining will probably continue from both ends of the spectrum in order to satisfy current and future needs.

AREAS FOR FUTURE RESEARCH AND PULP CHARACTERIZATION

Awareness of the literature, personal experience and knowledge, input from stakeholders, colleagues, and future needs forums, are possible sources from which to formulate future areas of research in refining and related fiber characterization. Perhaps the needs are best stated as questions to be answered, examples of which are given below.

1. How readily (energy, refining strategy,...) do pulps (softwoods, hardwoods, yield, pulp type, ...) respond to refining treatment to produce desirable changes in fiber structure?

2. What types and levels of cyclic stresses are required to produce certain types of changes in fiber structure?

3. How does the refining treatment of floc structures compare with the treatment of individual fibers?

4. Why is the refining process so inefficient?

5. What role, if any, does local water movement, e.g., local floc dewatering, play in the refining process.

6. Are there effective separation or fractionation strategies, e.g., fiber treatment, earlywood and latewood separation, which might improve energy utilization and control of the refining process.

7. Of what importance is homogeneity of refining treatment and how can it be measured and controlled?

8. What are the minimum number of direct (or indirect) measurements necessary to characterize refining and ensure the correct balance between paper machine productivity and paper product properties?

9. What are the consequences of refining for furnishes involving recycled fiber?

10. What is needed to more accurately control refining action in a refiner?

LITERATURE CITED

1. IPC Bibliographic Series: Beating 1953, 1962, 1970; Refining 1953, 1962, 1970; beating and Refining 1982.

2. Attack, D. "Advances in beating and refining" in Fiber Water Interactions in Papermaking trans. of the symposium held at Oxford, UK Sept. 1977 Vol. 1 261-295.

3. Ebling, K. "A critical review of current theories for the refining of chemical pulps" International Conference Fundamental Concepts of Refining IPC September 16-18, 1980.

4. Page, D.H. "The beating of chemical pulps - the action and the effects" in Trans. of the FRS, Cambridge, UK 1989.

5. Hietanen, S. and Ebling, K. "Fundamental aspects of the refining process" Paperi Ja Puu (1990).

6. Hietanen, S. "The role of fiber flocculation in chemical pulp refining" Doctor of Technology Dissertation, Helsinki, Finland, 1991.

7. Martinez, M. "The energy expended on pulp fibres during low consistency refining" Ph.D. Thesis The University of British Columbia, March 1995.

8. International Conference Fundamental Concepts of Refining IPC September 16-18, 1980.

9. Second International Refining Conference PIRA Birmingham, UK Dec. 1986.

10. Third International Refining Conference PIRA/IPST Atlanta, USA March 19-22, 1995.

11. Fourth International Refining Conference PIRA, Italy, March 1997.

12. Kajaani FS-100, and FS-200

13. Fiber Quality Analyzer, Optest.

14. Howard, R.C. Poole, R. and Page, D.H. "Factor analysis applied to the results of a laboratory beating investigation" JPPSc. 20(5):J137-J141 (1994).

15. Kerekes, R.J. "Characterization of pulp refiners by a C-factor" Nordic Pulp and Paper Res. J. No.1(5):3-8, (1990).

16. Kerekes, R.J., Clara, M., Dharni, S. and Martinez, D.M. "Applications of the C-Factor to characterize pulp refiners" JPPSc. 19(3):J125-J130 (1993).

17. Brecht, W. "A method for the comparitative evaluation of bar-equipped beating devices" Tappi 50(8):40A-44A, (1967).

18. Danforth, D.W. Southern Pulp and Paper Manufacture 32(7):52-53 (1969).

19. Rihs, J. "How good are current disc refiner models to predict refining intensity or relative fiber strength?" invited seminar presentation to the Institute of Paper Chemistry, Appleton, WI Nov. 30, 1984.

20. Lumianen, J. "Specific surface load theory" in Conference Proceedings Third International Refining Conference PIRA/IPST Atlanta, USA March 19-22, 1995.

21. Martinez, D.M. and Kerekes, R.J. "Forces on fibers in low-consistency refining" Tappi J. 77(12):119-123 (1994).

23. Kerekes, R.J. Ouellet, D. and Martinez, D,M. "New Perspectives on Refining Intensity" in Conference Proceedings Third International Refining Conference PIRA/IPST Atlanta, USA March 19-22, 1995.

24. Martinez, D.M., Batchelor, W.J., Kerekes, R.J. and Ouellet, D. "Forces on fibers in low-consistency refining: normal force" JPPSc. 23(1):J11-J18, (1997).

25. Batchelor, W.J., Martinez, D.M., Kerekes, R.J. and Ouellet, D. "Forces on fibers in low-consistency refining: shear force" JPPSc. 23(1):J40-J45, (1997).

26. Steenberg, B. "Beating and refining - a new approach" Das Papier 10A October (1979).

27. Steenberg, B. "Oozing and consolidation in fibre/water systems under compression" Paper Technology and Industry, 20: 282-285 (1979).

28. Steenberg, B. "Wet milling: a model based on hydrodynamics and particulate media mechanics" Poweder Tech. 37: 289-297 (1984).

29. Harbron, D.L. Jr. Marsh, P.G. "New kinks in refining with the Chemifiner." Paper Trade Journal 151(28): 42-48 July 10, (1967).

30. Brauns, O. "The frotapulper in modern papermaking" Svensk Papperstidning 75(3):81-87 Feb. 15 (1972).

31. Turbak, A.F. "Microfibrillated Cellulose - a new composition of commercial significance" Tappi 1984 Nonwovens Symposium Notes 115-123.

32. Waterhouse, J.F. "Refining by shear" Tappi 53(10):1890-1894, (1970).

33. Hartman, R.R. "Mechanical treatment of pulp fibers for paper property development" Trans. 8th Fundamental Res. Symp. Oxford, UK September 1985. Vol. 1 413-442.

34. Hartman, R.R. "Mechanical treatment of pulp fibers for paper property development" Ph.D. dissertation IPC, Appleton, WI 1984.

35. Biasca, J. "Oriented fiber refining - application of individual modes of mechanical action to single pulp fibers" Ph.D. dissertation IPC, Appleton, WI 1989.

36. Cumpston, E.H. "The development of the idar stock refining process" Tappi 38(6): 353-359 (1955).

37. Retulainen, E. Moss, P. and Nieminen, K. "Effect of fines on the properties of fiber networks" in Vol. 1 Transactions of the Fundamental Research Symposium held at Oxford: September 1993, Edited C.F. Baker, publishers PIRA International, Leatherhead, Surrey, UK.

38. Waterhouse, J.F. and Omori, K. "The effect of recycling on the fines contribution to selected paper properties" in Vol. 2 Transactions of the Fundamental Research Symposium held at Oxford: September 1993, Edited C.F. Baker, publishers PIRA International, Leatherhead, Surrey, UK.

39. Laivins, G.V. and Scallan, A.M. "The influence of drying and beating on the swelling of fines" JPPSc. 22(5): J178-J183 (1996).

40. Radoslavova, D., Silvy, J. and Roux, J.C. "The beating of pulp considered as a hydrodynamic process" in Conference Proceedings Third International Refining Conference PIRA/IPST Atlanta, USA March 19-22, 1995.

41. Radoslavova, D., Silvy, J. and Roux, J.C. "The concept of apparent viscosity of pulp for beating analysis and the development of the paper properties" in Tappi 1996 Papermakers Conference Proceedings 195-206.

42. Silvy, J. 1996 International Progress in Paper Physics - a seminar, Stockholm, Sweden June, 1996.

43. Steenberg, B. and Johansson, B. Svensk Papperstid 61 (18B): 696 (1958).

44. Salmen, L. "The effect of the frequency of a mechanical deformation on the fatigue of wood" JPPSc. 13(1): J23-J28, (1987).

45. Ostberg, G. and Salmen, L. "Effects of fibrillation of wood fibers on their interaction with water" Nordic Pulp and Paper Research J. 1 23-26, (1991).

46. Damani, R. and Powell, R.L. "Viscoelastic characterization of medium consistency pulp suspensions" in of AIChE Proceedings 1991 Forest Products Symposium 135-140.

47. Page, D.H. "The origin of the differences between sulphite and kraft pulps" JPPSc. March TR 15-TR20 (1983).

48. Salmen, L. "Moisture-dependent thermal softening of paper, evaluated by its elastic modulus" Tappi J. 63(6):117-120, (1980).

49. El-Hosseiny, F. and Yan, J.F. "Analysis of Canadian Standard Freeness Part 1 theoretical considerations; Part 2 practical implications" Pulp Paper Can 81(6) T113-T118 (1980).

50. Swodzinski, P.C. and Doshi, M.R. "Mathematical models of Canadian Standard Freeness (CSF) and Scopper-Riegler Freeness (SR) IPC(now IPST) Tech. Paper Series No. 172, May 1986.

51. Ingmansson, W.L. and Andrews, B.D."The effects of beating on filtration resistance and its components specific surface and specific volume" Tappi 42(1): 29-35, (1959).

52. Laivins, G.V. and Scallan, A.M. "Removal of water from pulps by pressing Part 1:Inter- and intra-wall water" Tappi J. 77(3):125-131 (1994).

53. Baum, G.A. Subfracture Mechanical Properties of Paper in Vol. 1 Products of Papermaking Trans. Tenth Fundamental Research Symposium held at Oxford September 1993 Edited by C.F. Baker Published by Pira International, UK.

54. Niskanen, K. "Strength and fracture of paper" in Vol. 2 Products of Papermaking Trans. Tenth Fundamental Research Symposium held at Oxford September 1993 Edited by C.F. Baker Published by Pira International, UK.

55. Waterhouse, J.F. "Ultimate strength of paper" in Design Criteria for Paper Performance (Editors: Kolseth, P., Fellers, C. and Salmen, L.) STFI Meddelande A969, August 1987.

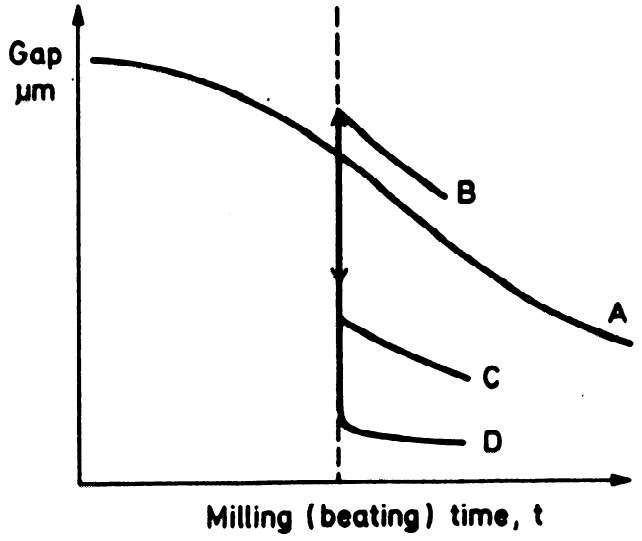

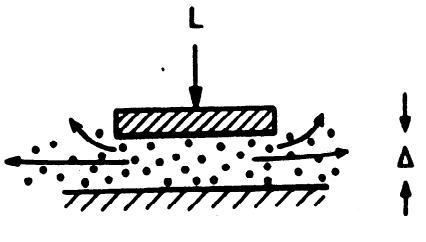

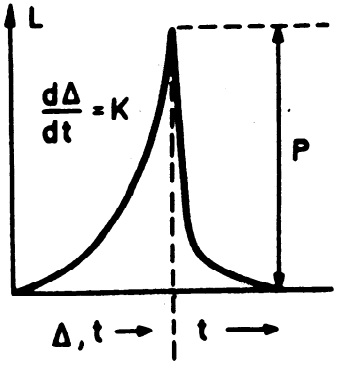

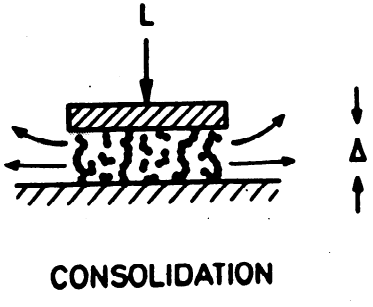

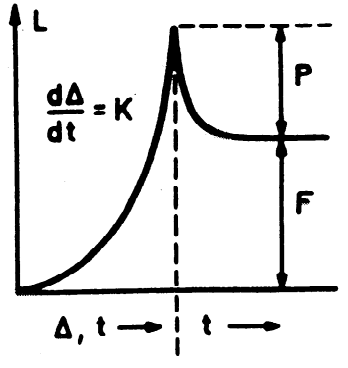

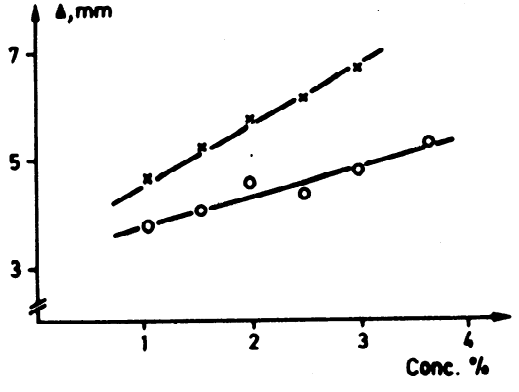

Figure 1 Steenberg's Refining Concepts (26)-(29).

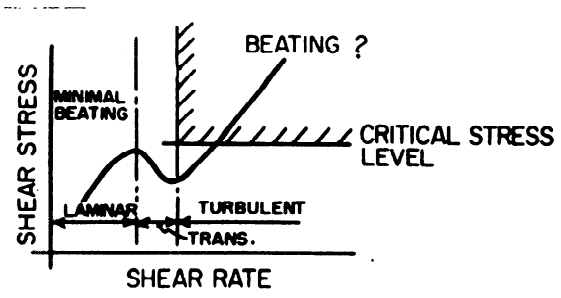

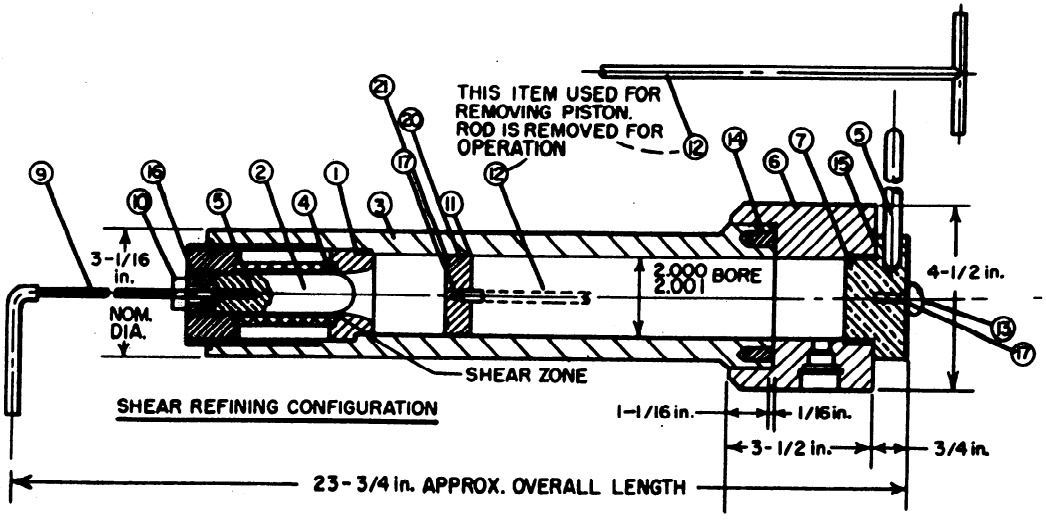

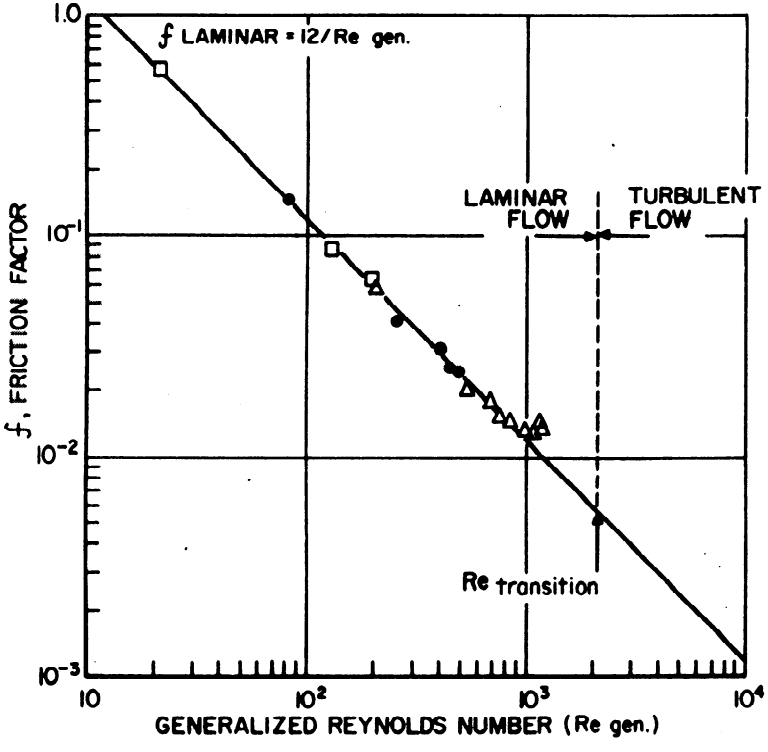

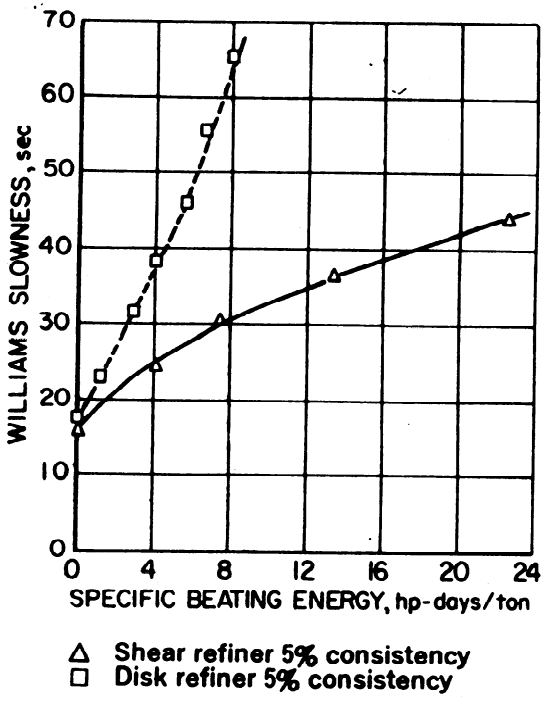

Figure 2. "Shear Refiner" taken from Waterhouse (32).

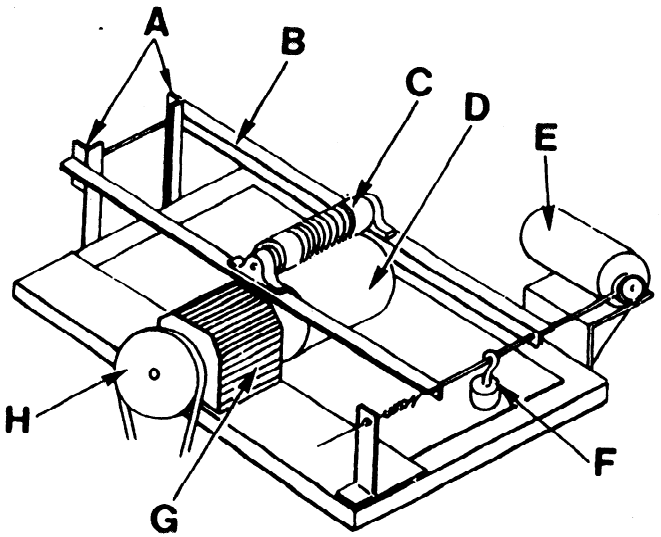

Fig 1—Schematic of roll refiner

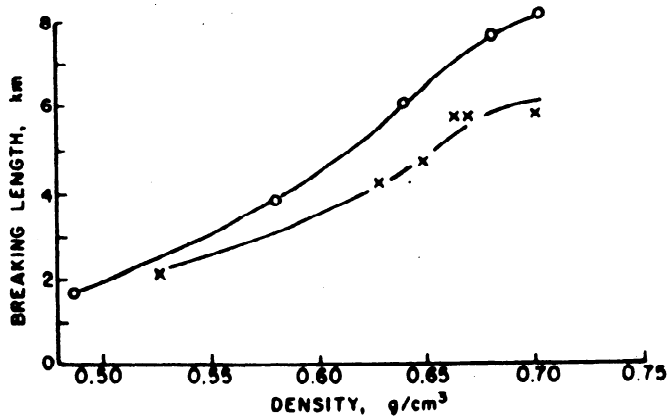

Fig 3—Breaking length vs density
x = roll refined, o = Valley beaten

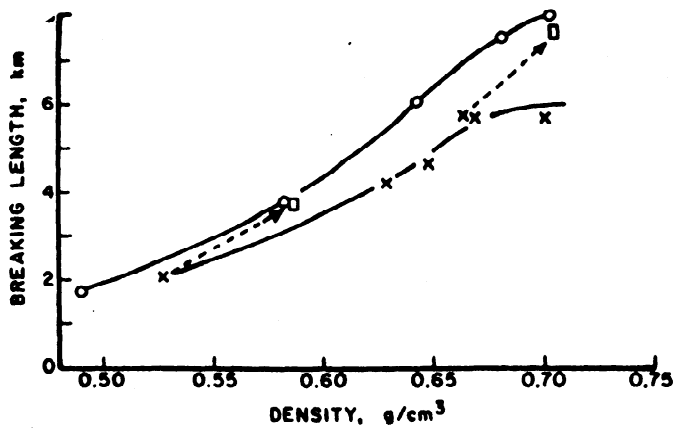

—Breaking length vs density
x = roll refined, o = Valley beaten, □ = fines addition

Figure 3. Roll Refiner taken from Hartman (33).

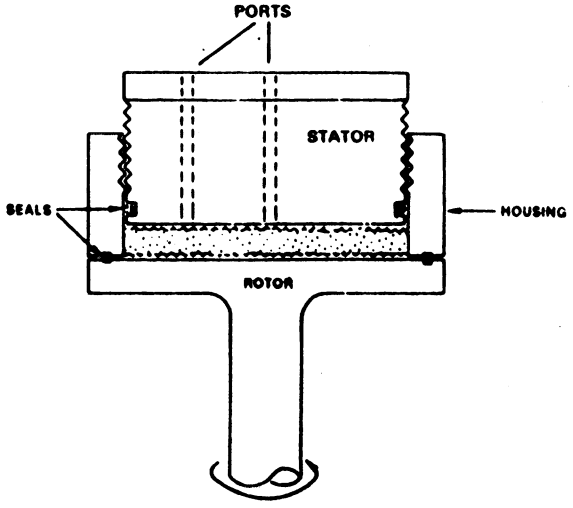

Fig 2—Schematic of abrasion refiner

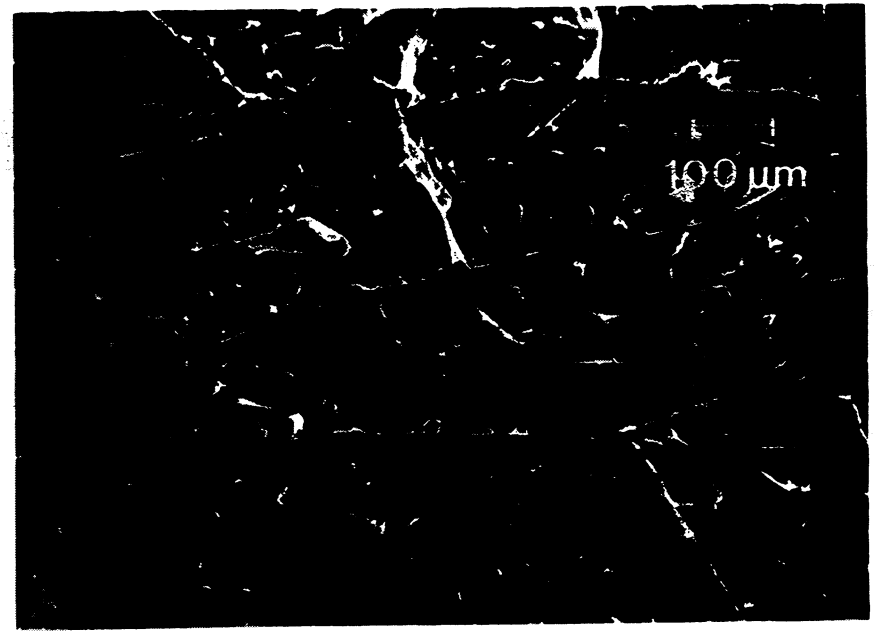

Figure 4. Abrasion Refiner taken from Hartman (33).

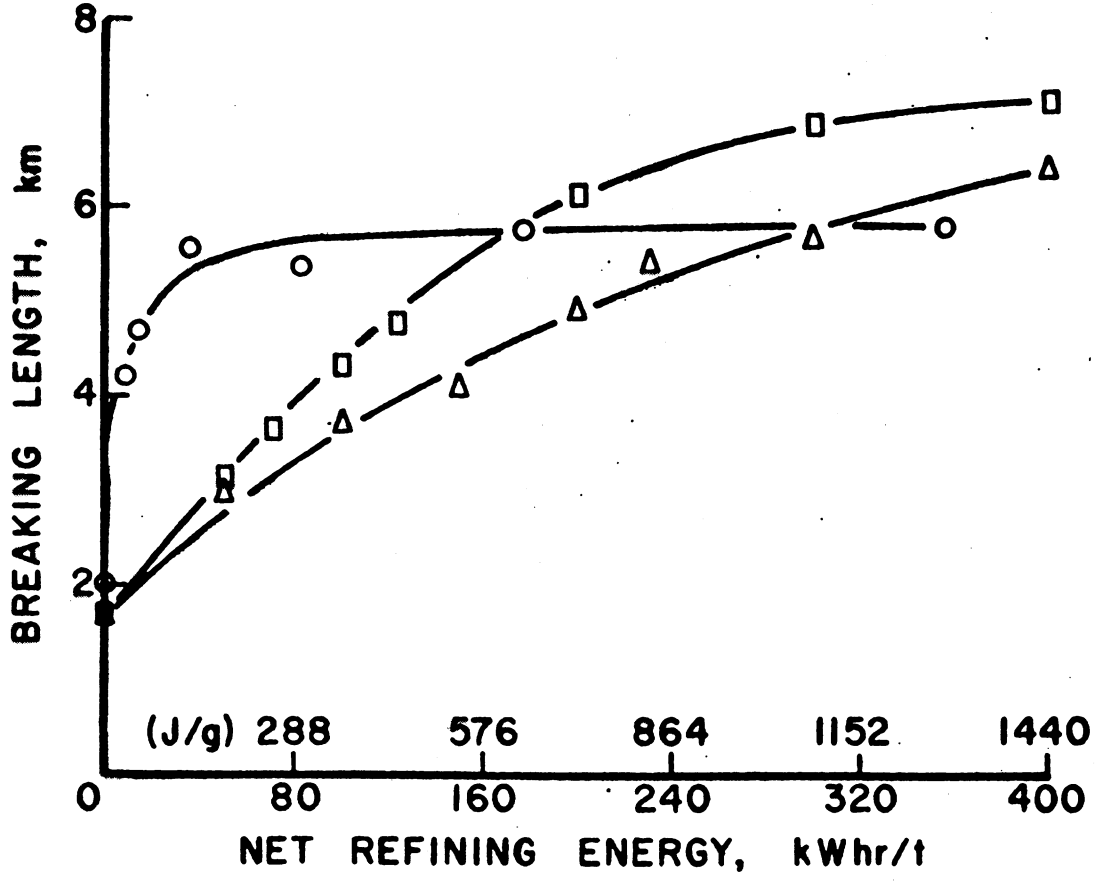

Figure 5. Refining Energy Roll versus Disk Refiner taken from Hartman (34).

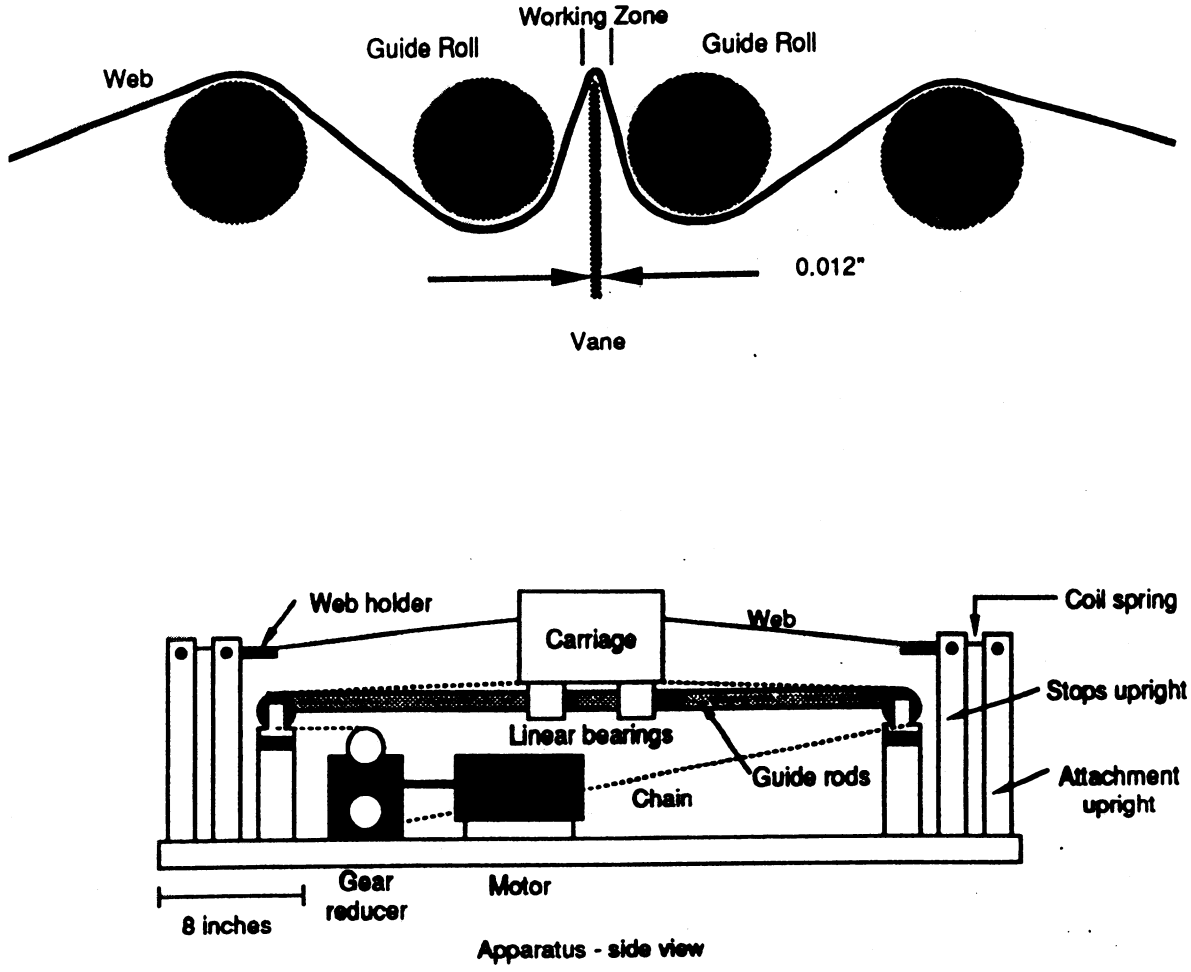

Figure 6. Bending Refining taken from Biasca (35).

* **APV GAULIN HOMOGENIZER**

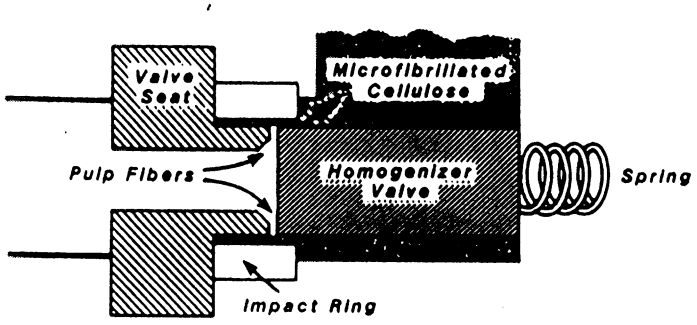

FIG. 1. Schematic representation of homogenizer action.

FIGURE 2 SEM OF STARTING PULP C (1000X)

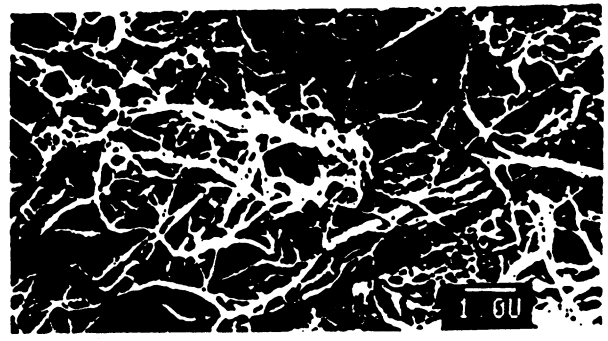

FIGURE 3
SEM OF MICROFIBRILLATED PULP C (10000X)

* **SPECIFIC ENERGY = 1.0707 X 10^{-4} P/C HPD/TON**

where P is stagnation pressure (8,000 psi max.) and C is consistency or solids fraction.

Example: P=8,000 psi, C=5%; Specific Energy = 17 HPD/T

Figure 7. Homogenizer taken from (31).

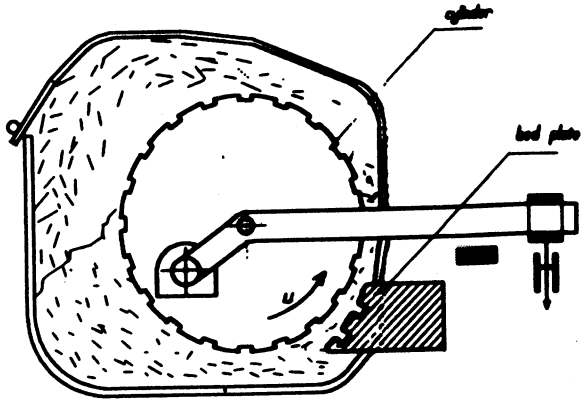

Figure 8 Refiner-Viscometer taken from (41).

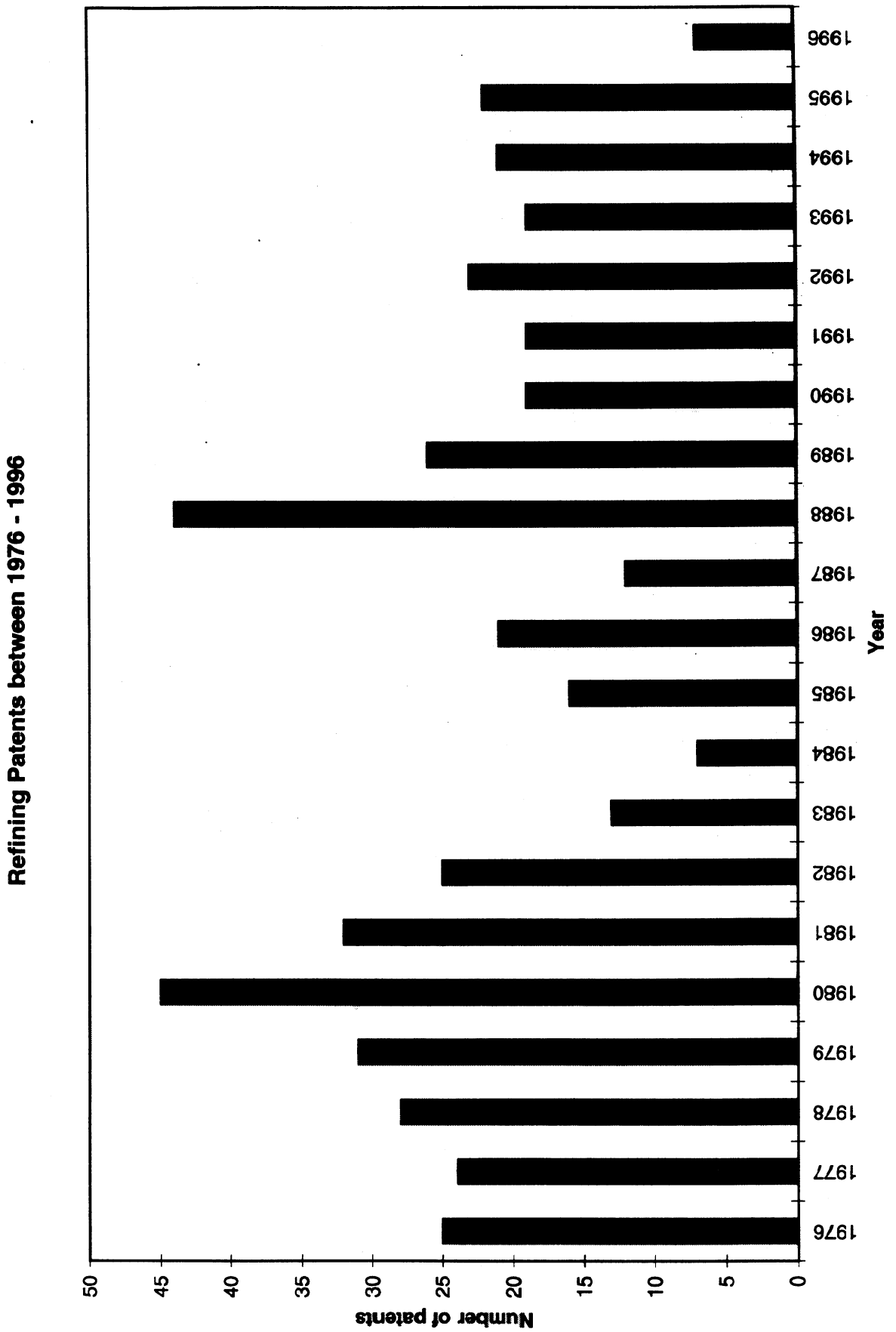

Figure 9. Selected Patent Activity Worldwide between 1976-1996.

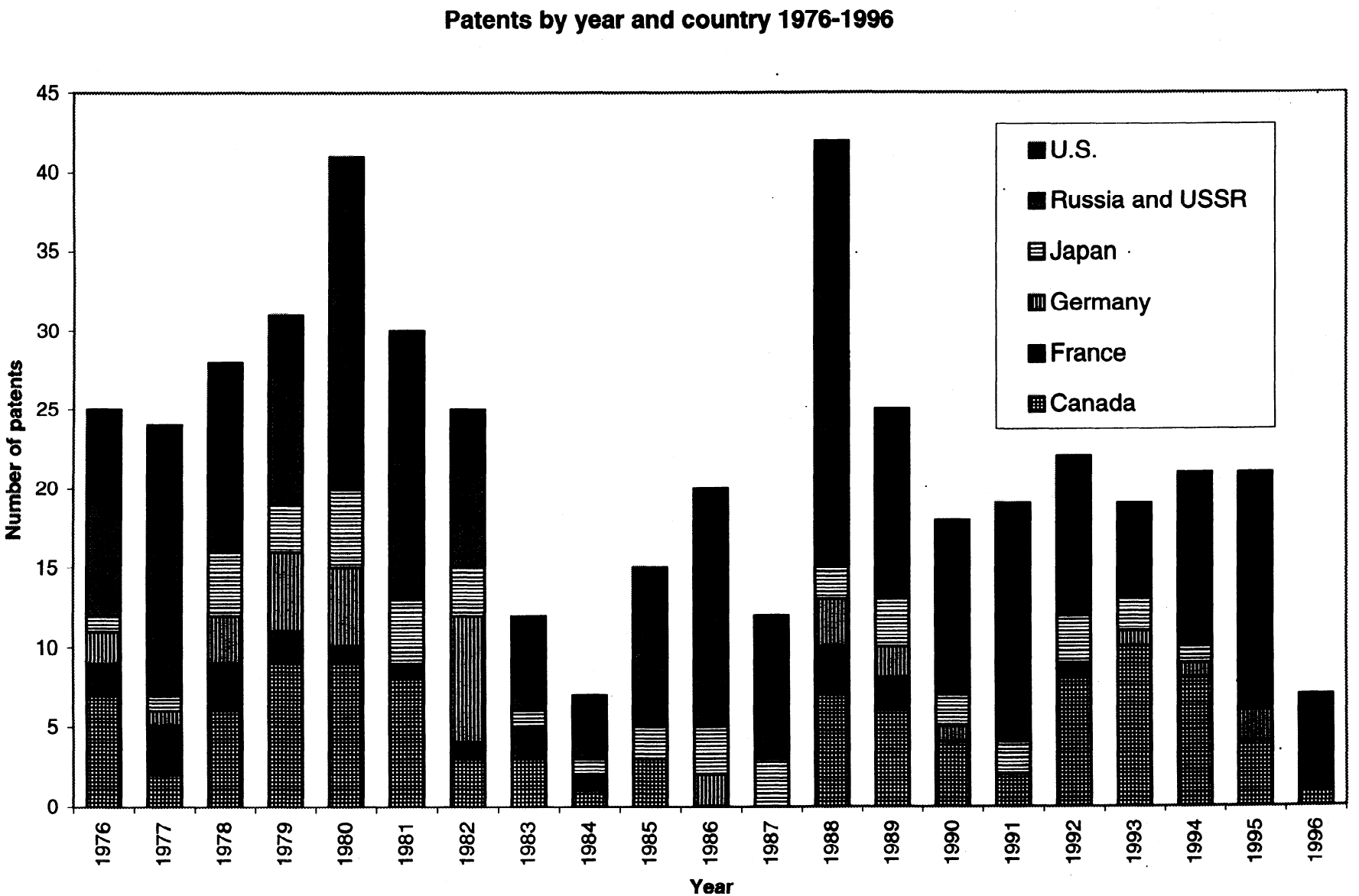

Figure 10 Selected Patent Activity by Country between 1976-1996

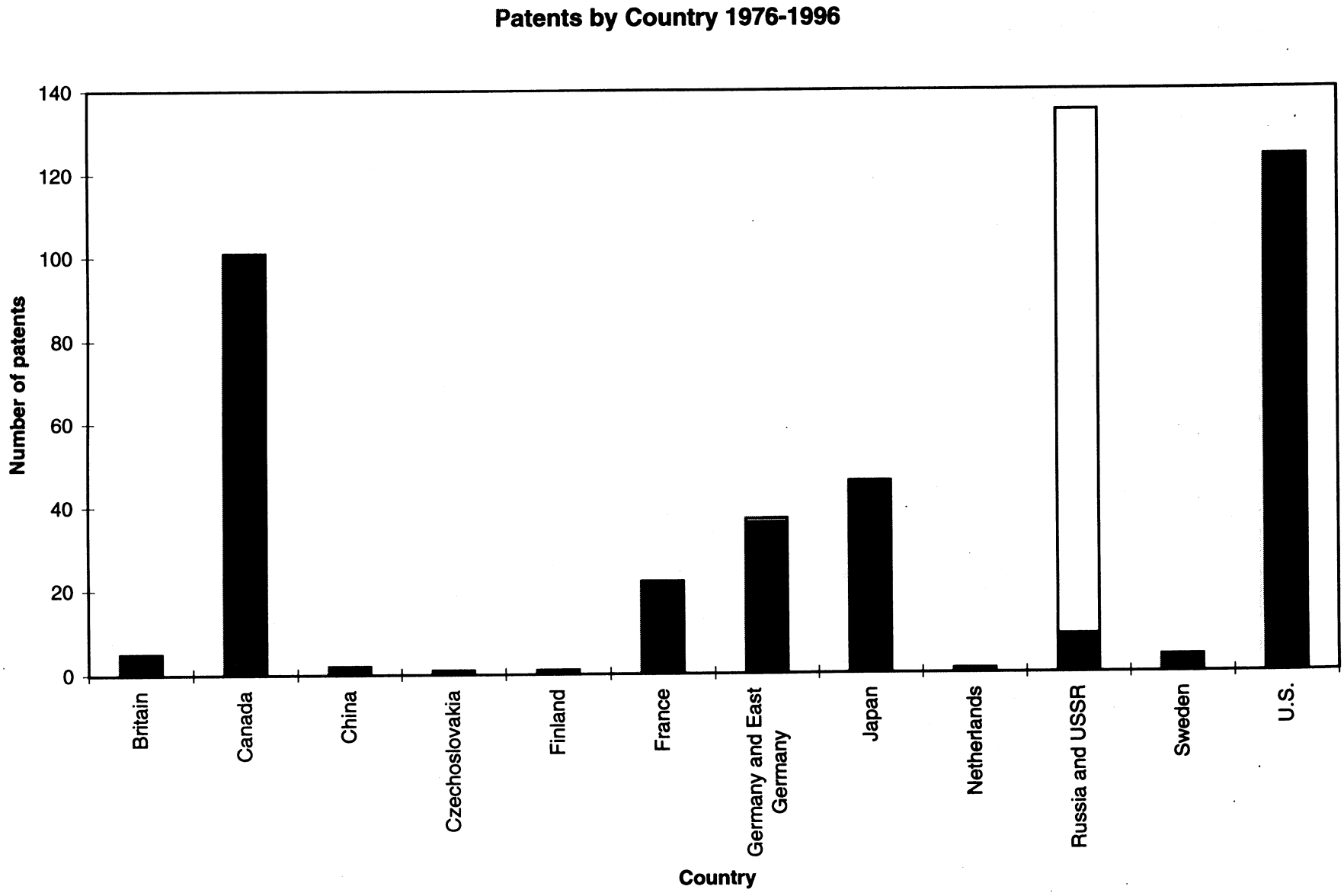

Figure 11 Total Selected Patent by Country between 1976-1996

ON-LINE MEASUREMENT OF PAPER PROPERTIES

STATUS REPORT

FOR

PROJECT F007

Maclin Hall
Ted Jackson
Andy Brown

March 26, 1997

Institute of Paper Science and Technology
500 10th Street, N.W.
Atlanta, Georgia 30318

TECHNICAL PROGRAM REVIEW

Project Title: ON-LINE MEASUREMENT OF PAPER PROPERTIES
Project Code: ONLIN
Project Number: F007
Division: Engineering and Paper Materials
Project Staff: Mac Hall, Ted Jackson, Andy Brown
Project Budget: $128,574

OBJECTIVE

This project is focused on the fundamentals of paper stiffness measurement and the relationships of ZD and in-plane stiffnesses to on-machine process parameters. It supplements the project to develop commercially viable sensors and instrumentation capable of measuring the velocity of ultrasound in the in-plane and thickness directions of the paper web as it is being made on the paper machine.

SUMMARY

In-plane and thickness-direction (ZD) ultrasonic velocity measurements and basis weight measurements are made at cross-direction (CD) intervals as small as 1 millimeter on CD strips in the laboratory. These measurements are repeatable and show large short-range variations in the properties of typical machine-made paper samples. Evaluation of the potential relationships of the measured short-range variations in CD strip properties to the nonuniformities, streaks, and "dry-line fingers" observed on the forming table (Aidun, 1996) continues.

Various measurement and correlation techniques have been examined to determine relationships between the ultrasonic velocity measurements and compressive strength measurements [Ring Crush (RC) and short-span compression (STFI)]. Ultrasonic elastic stiffness measurements vs. CD Ring Crush demonstrated a correlation of R=0.90 for CD linerboard samples. The correlation was improved only slightly when the ZD data was included. Fairly large variations in ZD measurement are observed. However, the in-plane values are nearly an order of magnitude greater than the ZD values and are dominant in the calculations. It appears that for a CD strip,

reasonably good relationships with Ring Crush can be obtained using only the in-plane ultrasonic velocity measurements.

The sensitivity of ZD and in-plane ultrasonic measurements to wet pressing and calendering for some samples made on a pilot machine was evaluated. It is apparent that the ZD measurements are significantly more sensitive to these process changes than are the in-plane measurements. This suggests that on-machine ZD measurements may also be more sensitive to certain process changes.

GOALS

Establish procedure to deal with the large short-range variations in basis weight and fiber orientation when relating STFI and Ring Crush to in-plane and ZD ultrasonic velocity measurements.

Determine whether dry line variations coincide with in-plane and ZD ultrasonic velocity variations observed in CD strips.

Determine relationships between in-plane and ZD ultrasonic velocity measurements and compressive strength measurements (Ring Crush and STFI) for samples that include deliberate process changes, e.g., refining, wet pressing, wet straining, and calendering. Determine the sensitivity of the correlation to the ZD data.

DISCUSSION OF MEASUREMENTS

Review

In a study reported by William Whitsitt in 1985 (Whitsitt, 1985), the following regression equation was developed using liner samples of several weights from various sources:

$$\textbf{CD Ring Crush} = a\,E_Y t^{0.75}\,E_z t^{0.25} + b E_X t^{0.75}\,E_Z t^{0.25} + c \qquad (1)$$

Using the same stiffness functions and the CD data taken at 2-inch intervals on a CD strip of 180g.m^2, we determined the regression equation and obtained an R = 0.815. Whitsitt suggested smoothing the data somewhat in view of the short-range variability. Each point was averaged with its adjacent neighbors (average of 3) and the resulting regression equation gave an R = 0.903.

The CD data was also examined using correlation based upon linear combinations of the extensional stiffnesses:

$$\mathbf{E_Yt = (V_{CD})^2 * BW;\ E_Xt = (V_{MD})^2 * BW;\ E_Zt = (V_{ZD})^2 * BW}$$

Again averaging each point with its adjacent neighbors (average of 3) and the regression equation gave an R essentially the same as that obtained using Equation 1. The correlation is improved only slightly when the ZD data is included. Fairly large variations in ZD measurement are observed; however, the in-plane values are nearly an order of magnitude greater than the ZD values and are dominant in the calculations. It appears that for a CD strip, reasonable good relationships with Ring Crush can be obtained using only the in-plane ultrasonic velocity measurements.

ZD ultrasonic velocities are expected to respond in particular to refining, consistency, wet pressing, wet straining, and calendering. None of these parameters should vary within a particular CD strip. It is anticipated that ZD measurements may be more sensitive than the in-plane ultrasonic measurements to these process parameters.

High Resolution Measurements

In-plane and thickness-direction (ZD) ultrasonic velocity measurements and high resolution basis weight measurements show large short-range variations in the properties of typical machine-made paper. In-plane measurements can be made on cross-direction (CD) strips at intervals as small as 1 millimeter.

The transit time and velocity of ultrasound in the thickness direction (ZD) are measured by mounting CD strips spliced as part of a 12-meter belt on the IPST web handling system. Using

transducers mounted in fluid-filled wheels, the transit time of ultrasound through the thickness of the paper can be determined 50 times a second. This provides a reading at 5-millimeter intervals for a sample moving at 15 meters per minute.

Hardware and software have been developed to collect measurement data at a high sampling rate directly from the sensors in an AccuRay® 1190™ System with the Smart Platform™ 1200 that is installed on the IPST web handling system. For a web moving at approximately 15 meters per minute, the basis weight sampling rate may be sufficient to provide readings at web increments less than 1 millimeter.

High Resolution in-Plane Ultrasonic Measurements

In-plane measurements on CD strips made at 5- or 10- cm intervals have been presented previously. However, with the interest in short-range variations of cross-machine properties, the possibility of making higher resolution in-plane measurements was examined. Direct measurement of the CD longitudinal velocity would require a transducer spacing of several centimeters, thus limiting the resolutions of short-range variations. However, if one uses the relationship (Baum, et al., 1981)

$$(V_{SH})^2 = 0.387\,(V_{MD})(V_{CD}), \qquad (2)$$

it is only necessary to measure the MD longitudinal velocity (V_{MD}) and the shear velocity (V_{SH}) to determine a value for the CD longitudinal velocity (V_{CD}). Because the shear velocity (V_{SH}) is the same whether measured in CD or MD, both the longitudinal velocity and the shear velocity are measured in the MD, and the CD longitudinal velocity is calculated using the above relationship,

$$V_{CD} = 2.58\,(V_{SH})^2/V_{MD}. \qquad (3)$$

The IPST robot for in-plane measurements can be programmed to align the transducer pair in the MD and increment the position of the transducers in steps as small as 1 millimeter along the CD of a CD strip. Figure 1 presents MD specific stiffness data for a segment of a CD strip determined by measuring the MD longitudinal velocity at 1-millimeter intervals by this procedure.

The application of Equation 3 is presented in Figure 2. MD longitudinal velocity and MD shear velocity were measured at 2-millimeter intervals along an entire CD strip of 80 g/m^2 kraft. The CD longitudinal velocity was calculated using Equation 3. Data are presented in Figure 2 for a 1-meter segment of this CD strip. The MD longitudinal velocity measurements at 2-millimeter intervals along the CD strip were repeated. These data are also plotted in Figure 2 to demonstrate the repeatability of the MD velocity measurements.

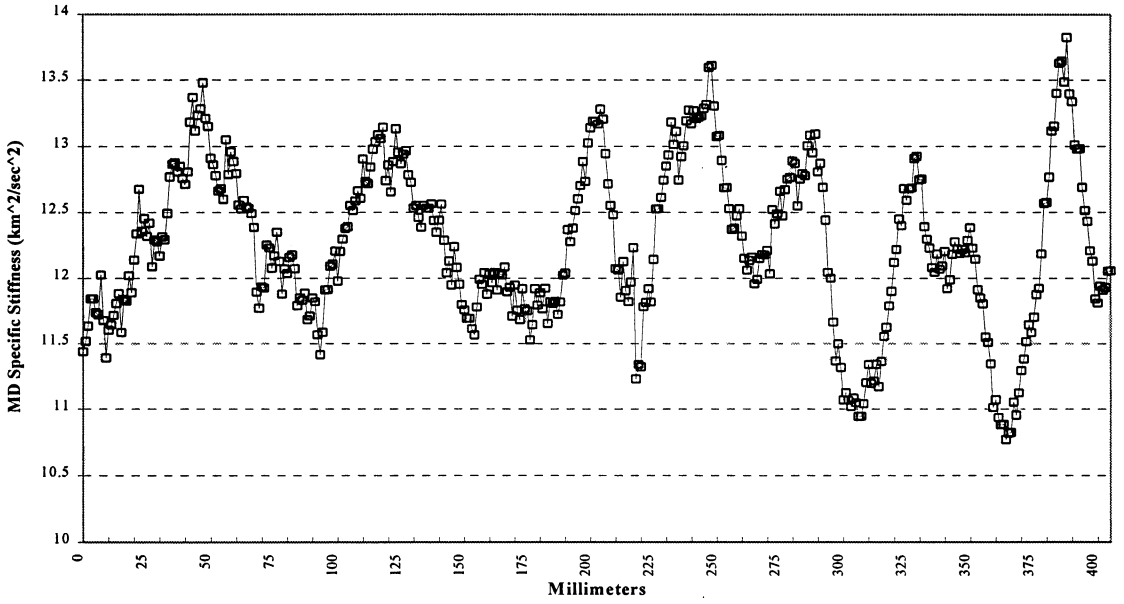

Figure 1. MD Specific Stiffness at 1-millimeter CD intervals on a 40-cm segment of a 80 g/m^2 kraft CD strip.

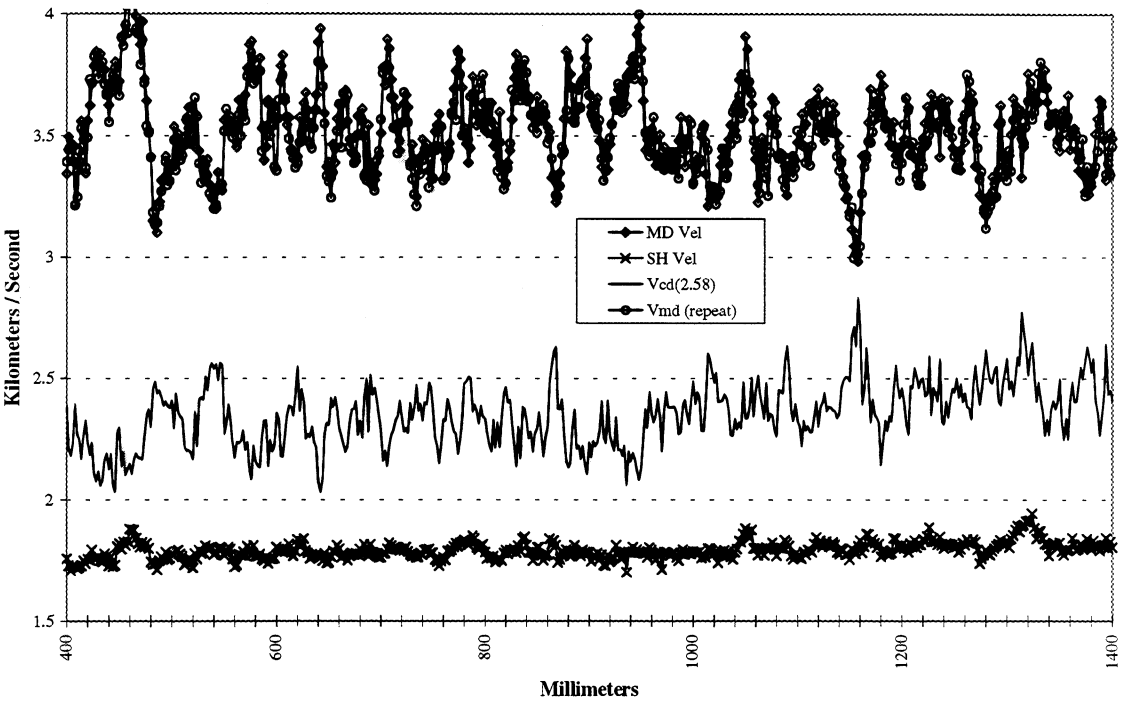

Figure 2. MD longitudinal velocity, MD shear velocity, and calculated CD longitudinal velocity at 2-millimeter CD intervals on a 1-meter segment of a 80 g/m^2 kraft CD strip.

High Resolution ZD Ultrasonic Measurements

The transit time and velocity of ultrasound in the thickness direction (ZD) are measured by mounting CD strips on the IPST web handling system. Using transducers mounted in fluid-filled wheels, the transit time of ultrasound through the thickness of the paper can be determined. Figure 3 shows the ZD ultrasonic transit time for a CD strip of 205 g/m^2 liner. The 6.6-meter CD strip was spliced with other paper to make a continuous loop 12 meters in length. The transit time was recorded 50 times a second. With the web moving at 15 meters per minute (25 cm/second), a reading is obtained every 5 millimeters. Figure 3 presents data recorded in this way for two passes of the CD strip. The time scale in nanoseconds for Pass #1 (the upper plot) is on the left, and the time scale for Pass #2 (the lower plot) is on the right. The plots are offset to enable one to visually judge the repeatability.

To further demonstrate the repeatability of the measurements, Figure 4 presents the comparison of Pass #1 and Pass #2 for a 24-cm section of the CD strip using the segment of the data ending at the 100-cm mark of Figure 3.

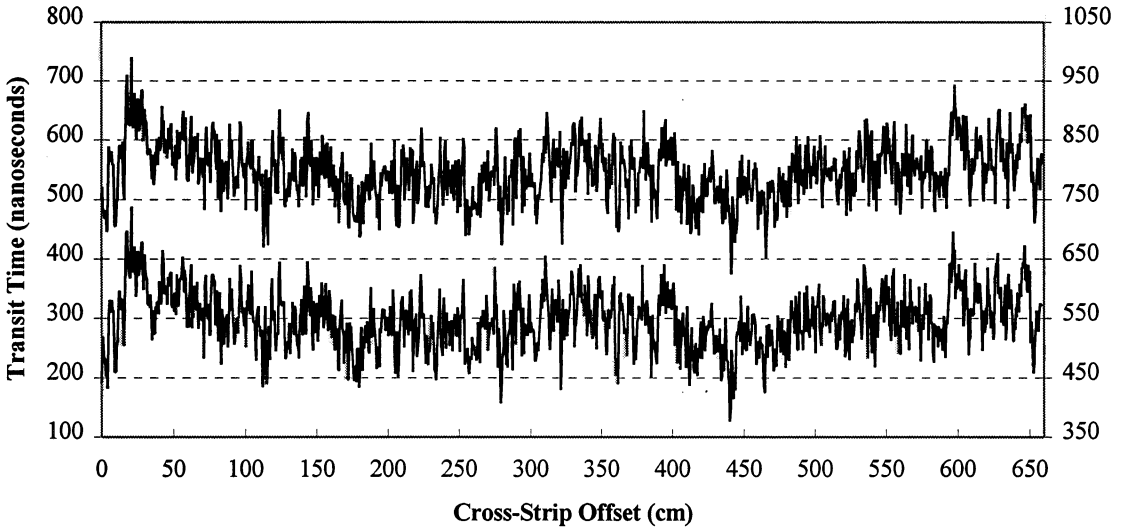

Figure 3. ZD ultrasonic transit time for a CD strip of 205 g/m^2 liner. The time scale for Pass #1 (the upper plot) is on the left, and the time scale for Pass #2 (the lower plot) is on the right. The plots are offset for visual comparison.

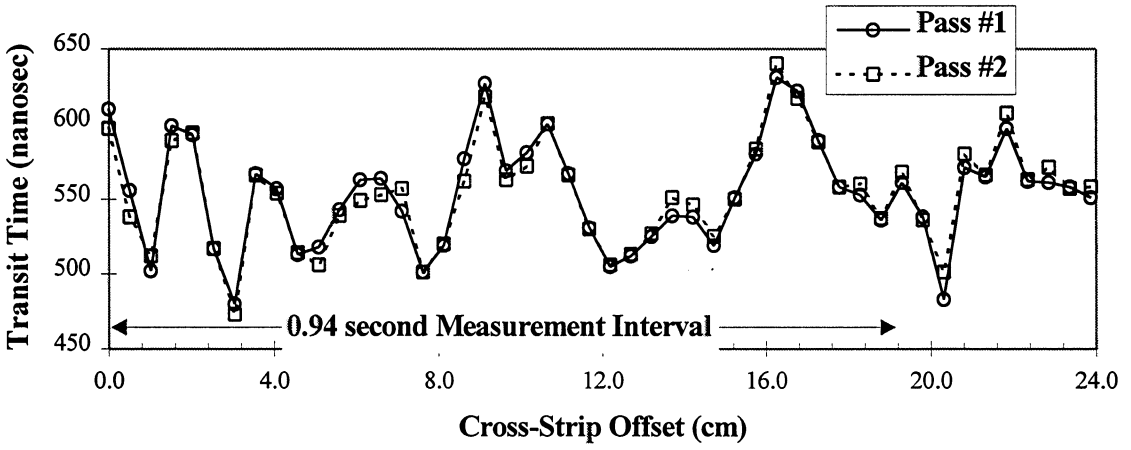

Figure 4. ZD ultrasonic transit time measurements over a 24-cm section of a 205 g/m^2 liner CD strip. Comparison of two passes to illustrate repeatability.

High Resolution Basis Weight Measurement

Hardware and software have been developed to collect measurement data at a high sampling rate directly from the sensors in the AccuRay® 1190™ System with a Smart Platform™ 1200 that is installed on the IPST web handling system. CD strips or smaller samples may be spliced as part of a 12-meter belt on the web handler for high resolution measurement. For a web moving at approximately 15 meters per minute, the basis weight sampling rate may be sufficient to provide readings at web increments less than 1 millimeter. As an example, Figure 5 presents basis weight data for a 60-cm section of a CD strip at a resolution of 13 points/cm.

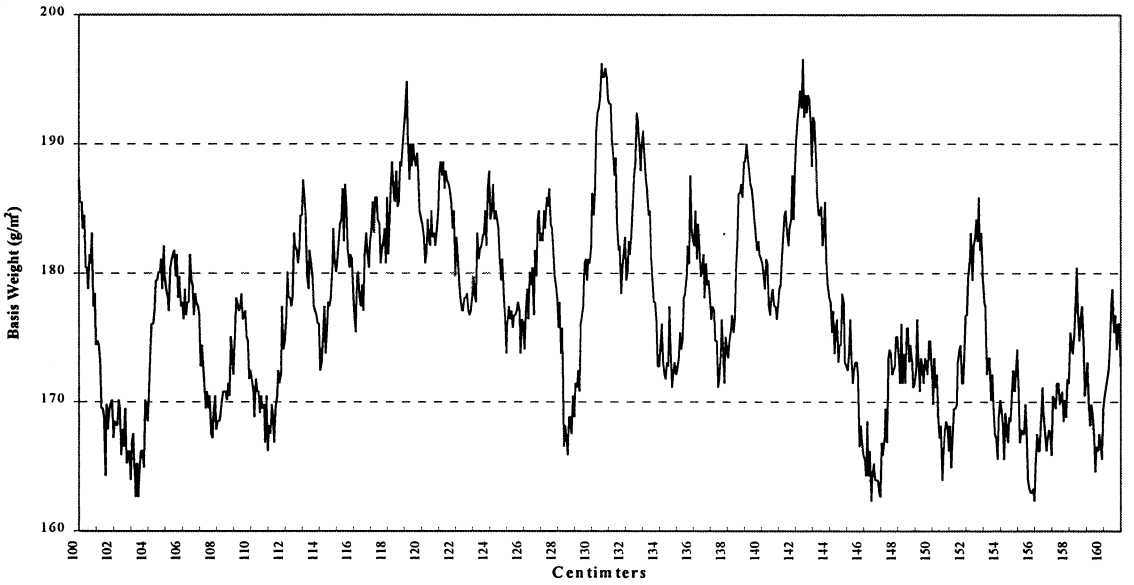

Figure 5. Basis weight of 60-cm section of a CD strip at a resolution of 13 points/cm.

Effects of Wet Pressing and Calendering

The ZD wheels mounted on the test stand in the laboratory were used to collect data for each of the four paper rolls prepared from the pilot machine runs at Herty on March 28 & 29, 1996. The transit time of the ZD ultrasonic signal through the paper was determined with the ZD wheels and the grammage (basis weight) and caliper were measured with the ABB sensors.

The effect of wet pressing and calendering on ZD properties are of particular interest. The four combinations of these conditions for each of the three basis weights are collected in the plots

included at the end of this report. One plot shows the effects on caliper and ZD velocity (=caliper/transit time) and the other plot shows the effects on acoustic impedance, Z (=grammage/transit time). Each point on the plots represents the average of 1000 measurements. The -\+ symbols indicate whether the wet pressing \ calendering were high or low for the associated data.

The following table presents the process conditions and an average of the measured values for each process condition presented in the attached plots. In addition to the measured values of grammage, caliper, and ZD transit time, the ZD velocity (=caliper/transit time) and the acoustic impedance, Z (=grammage/transit time) are presented in the table. The table also includes the CD velocity and the MD velocity measured on cut samples with the IPST robot.

BW	CSF	Wet Press	Calender	Caliper	ZD time	Gram mage	Imped ance	ZD Vel	CD Vel	MD Vel
lb/1000	mliter	pli	pli	microns	micro sec	g/m^2	BW/t	km/sec	km/sec	km/sec
26	452	-- = 150	-- = 0	239.0	0.462	130.4	282.1	0.517	2.291	3.305
26	452	--	+ = 600	204.8	0.533	129.5	243.1	0.385	2.368	3.373
26	452	+= 300	--	228.0	0.389	130.6	336.0	0.587	2.321	3.338
26	452	+	+	196.6	0.478	129.8	271.7	0.412	2.332	3.303
32	452	--	--	284.5	0.537	162.9	303.6	0.530	2.373	3.323
32	452	--	+	236.4	0.635	159.4	251.2	0.373	2.298	3.209
32	452	+	--	264.9	0.447	158.1	354.0	0.593	2.406	3.358
32	452	+	+	230.6	0.576	165.6	287.3	0.400	2.271	3.262
42	462	--	--	383.9	0.944	208.9	221.3	0.407	2.247	3.057
42	462	--	+	301.3	0.933	204.8	219.4	0.324	2.089	2.840
42	462	+	--	351.8	0.676	199.4	295.0	0.523	2.243	2.946
42	462	+	+	294.0	0.803	201.5	250.9	0.368	2.125	2.831

In order to evaluate the sensitivity of the ZD and in-plane ultrasonic measurements to wet pressing and calendering, the ultrasonic velocities were squared and these specific stiffnesses were then normalized. These data are presented in a plot at the end of this report together with an indication of the high and low conditions of wet pressing and calendering. It is apparent that the ZD measurements are significantly more sensitive to these process changes than are the in-plane measurements.

Strips several feet long and 7 inches wide were cut from each of the 31 sections of the four rolls prepared at Herty. In-plane and ZD ultrasonic velocities were recorded for each of these strips. Samples punched from these strips were weighed for determining basis weight and then used to determine Ring Crush and STFI. CD and MD Ring Crush and CD and MD STFI have been determined for each of the 31 sections. The correlation relationships reviewed previously were applied to this data. Again the relationships of the ultrasonic data with Ring Crush and STFI were only slightly improved when the ZD data was included.

Another project at IPST has prepared several hundred samples on the Formette and then impulse dried them under various conditions. In-plane and ZD ultrasonic velocities have been recorded for each of these samples. As part of the project the samples are weighed for determining basis weight and then cut appropriately to determine CD and MD Ring Crush, and CD and MD STFI. The evaluation of various combinations of the ultrasonic velocity measurements with the measured data is incomplete.

TOWARD COMMERCIALIZATION

Background

The variations of the elastic stiffnesses of paper with refining, fiber orientation, wet pressing pressure, wet straining (draws), and drying restraints have been studied and reported (Baum et al., 1984; Habeger and Baum, 1986). These studies have demonstrated that elastic stiffnesses are sensitive to changes in furnish and to changes in various process parameters. Measurement on the paper machine of the elastic stiffnesses in both the in-plane and thickness directions along with the basis weight, moisture, and caliper of the web should provide a means to continuously monitor product quality and to control the paper manufacturing process. This will enable more effective use of raw materials and minimize waste of energy while producing products with improved uniformity and performance.

The instrumentation should be applicable to most grades of paper, but will be particularly beneficial to the heavier weight grades, packaging paper and paperboard, because "strength" properties are of

primary importance for these products. Energy waste is avoided by minimizing the amount of substandard production which must be repulped and remanufactured. Further energy savings result from optimum utilization of energy intensive processes, such as refining and drying (Lantz and Chase, 1988), and from efficiency improvement in subsequent converting processes as a result of product uniformity.

It requires the equivalent of approximately 30 million Btu/ton to produce pulp and then paper from wood. Refining and papermaking or repulping and remanufacture require about 13.5 million Btu/ton. The electrical usage for repulping and paper machine operation is approximately 520 kWh per ton. With approximately 10,500 Btu required to produce one kWh of electrical energy, the electrical usage is equivalent to about 5.5 million Btu/ton. In addition, steam usage by the paper machine for drying is approximately 8 million Btu/ton. Thus, a 1000-ton/day machine producing 350,000 ton/year uses 4.725 trillion Btu/year. For each 1% of production that is substandard and reprocessed at 13.5 million Btu/ton, the 1000-ton/day machine wastes 47.25 billion Btu/year. Substandard production may be as high as 5 percent. Assuming this technology will reduce substandard production by 2% (e.g., to 3% rather than 5%), the energy saving would be 94.5 billion Btu/year or $378,000 (@ $4/million Btu) annually for the 1000-ton/day machine..

Refining requires approximately 200 kWh/ton or 2.1 million Btu/ton (1 kWh = 10,500 Btu). For a 1000-ton/day machine, the annual energy usage for refining is approximately 70.0 million kWh or 735 billion Btu. Assuming the optimization of refining could reduce the energy required by 10%, this would be equivalent to a savings of 73.5 billion Btu or $294,000 annually.

By decreasing refining, the web produced dewaters more readily, requiring less steam for drying. The steam required for drying is equivalent to approximately 8 million Btu/ton, or 2.8 trillion Btu/year for a 1000-ton/day machine. If the moisture of the paper entering the dryer is reduced by 1.0%, the dryer steam required would be reduced by about 3%. This would save an additional 84 billion Btu/year or $336,000 annually.

Summary for a 1000-ton/day paper machine:

Annual Energy Use = 4.725 trillion Btu = $18,900,000 @ $4/million Btu

Reprocessing savings:

*	Electricity	38.5 billion Btu	
*	Steam	56.0 billion Btu	
	Total reprocessing savings	94.5 billion Btu	= $378,000

Refining savings:

*	Electricity	73.5 billion Btu	= $294,000

Drying savings:

*	Steam	84.0 billion Btu	= $336,000

Total potential savings for 1000-ton/day machine:

*	Electricity	112.0 billion Btu	= $448,000
*	Steam	140.0 billion Btu	= $560,000
		@ $4/million Btu	= $1,008,000
	Total savings/year	252 billion Btu/year	= 5.3%

Additional benefits of the technology are difficult to quantify. The ability to control to stiffness targets not only minimizes energy waste, but also provides the potential environmental benefit of using fewer trees. The specified "strength" for some products would be achieved with less pulp, and more recycled fiber would be used. The paper manufacturer would be able to monitor the effect of recycled fiber utilization on product quality and thus could use higher percentages of recycled fiber with confidence that the product remains within specifications.

Minimizing the need to repulp and remanufacture reduces water utilization and provides consequential benefits to the environment. An additional waste that is difficult to quantify is the "waste" of fiber quality that occurs each time the fibers are dried and rewet. This type of waste is avoided by making quality paper the first time through the paper machine.

Commercialization Status

The Institute has a Cooperative Agreement with the U.S. Department of Energy's Office of Industrial Technologies (DOE-OIT) for a development and demonstration project to commercialize on-line ultrasonic velocity sensors. The initial target for this application is linerboard. The project includes the implementation of two pilot-scale prototypes and a full-scale production system with the ability to measure both in-plane and out-of-plane (ZD) ultrasonic velocity.

The ultimate objective is to provide real-time data for improved control of the papermaking process. Extensive on-machine testing and performance demonstration is anticipated as a requirement to gain acceptance by the paper industry.

IPST is prime contractor with cost-share participation by ABB Industrial Systems Inc., Columbus, Ohio, the Herty Foundation, Savannah, Georgia, and the Georgia-Pacific Cedar Springs Mill. We are in the third year of the proposed 4-year development and testing program.

An AccuRay® 1190™ System with a Smart Platform™ 1200 has been installed on the web handling system in the laboratory at IPST. A similar system is being installed on a pilot machine at the Herty Foundation. A similar system has been shipped to the Georgia-Pacific Cedar Springs Mill and will be installed on their paper machine #1 which produces linerboard. The sensor carriage on the scanner contains state-of-the-art basis weight, moisture, temperature, and caliper sensors. The in-plane and ZD ultrasonic velocity sensors will be added after system startup.

REFERENCES

Aidun, C.K., "A Fundamental Opportunity to Improve Paper Forming" *Tappi J.* 79 (6): 55(1996).

Baum, G.A., Brennan, D.C., and Habeger, C.C., "Orthotropic Elastic Constants of Paper," *Tappi J.* 64 (8):97(1981).

Baum, G.A., Pers, K., Shepard, D.R., and Ave'Lallemant, T.R., "Wet Straining of Paper," *Tappi J.* 67 (5):100(1984).

Habeger, C.C., and Baum, G.A., "On-line Measurement of Paper Mechanical Properties," *Tappi J.* 69 (6): 106(1986).

Lantz, K.G., and Chase, L.M., "On-line Measurement and Control of Strength Properties," *Tappi J.* 71 (2): 75(1988).

Whitsitt, W.J., "Relationships Between Elastic Properties and End-Use Performance," Project 2695-23, Report One, A Progress Report to the Fourdrinier Kraft Board Group of the API (January 30, 1985).

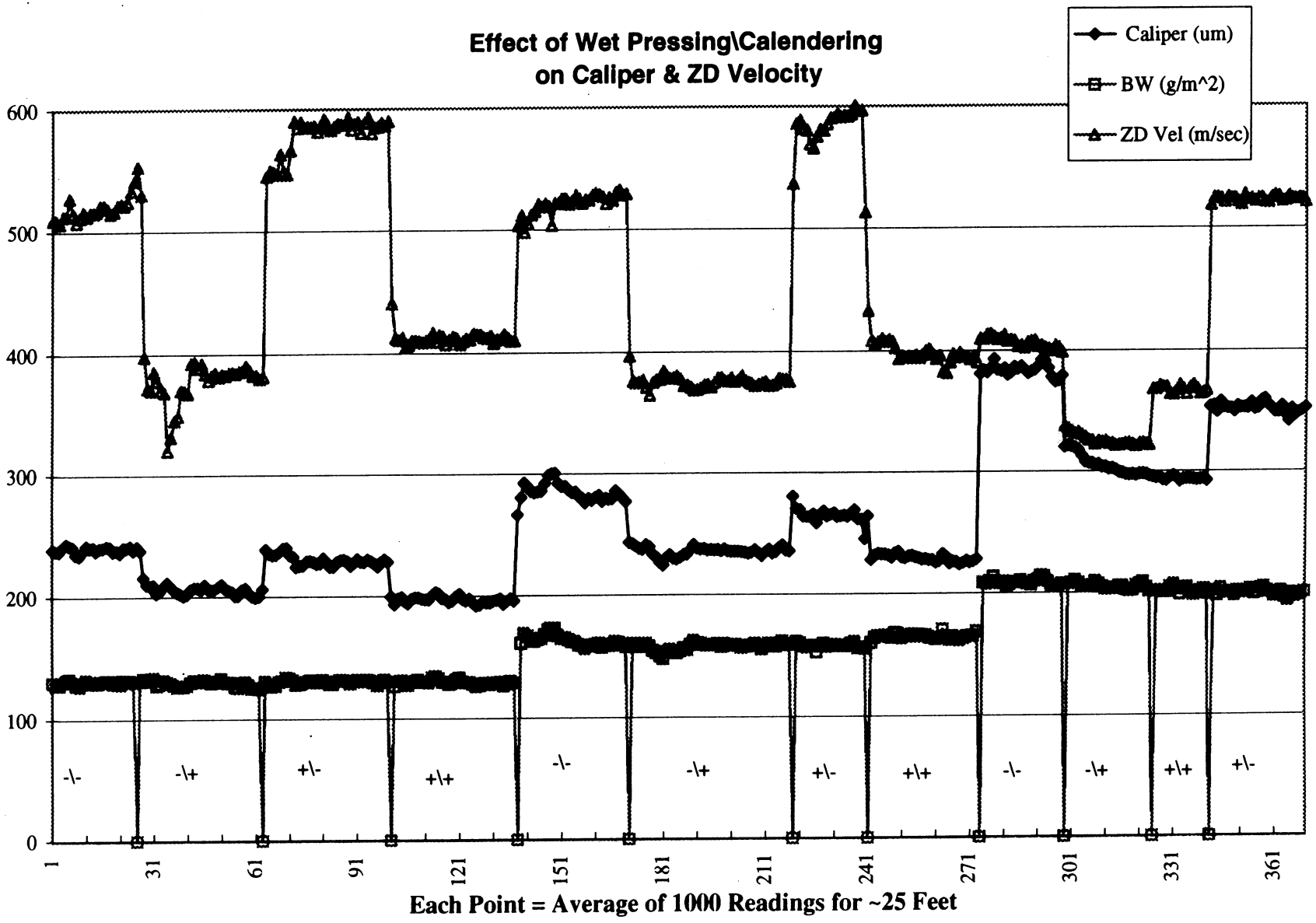
Effect of Wet Pressing\Calendering
on Caliper & ZD Velocity
Caliper (um)
BW (g/m^2)
ZD Vel (m/sec)
600
500
400
300
200
100
0
-\-
-\+
+\-
+\+
-\-
-\+
+\-
+\+
-\-
-\+
+\+
+\-
1
31
61
91
121
151
181
211
241
271
301
331
361
Each Point = Average of 1000 Readings for ~25 Feet

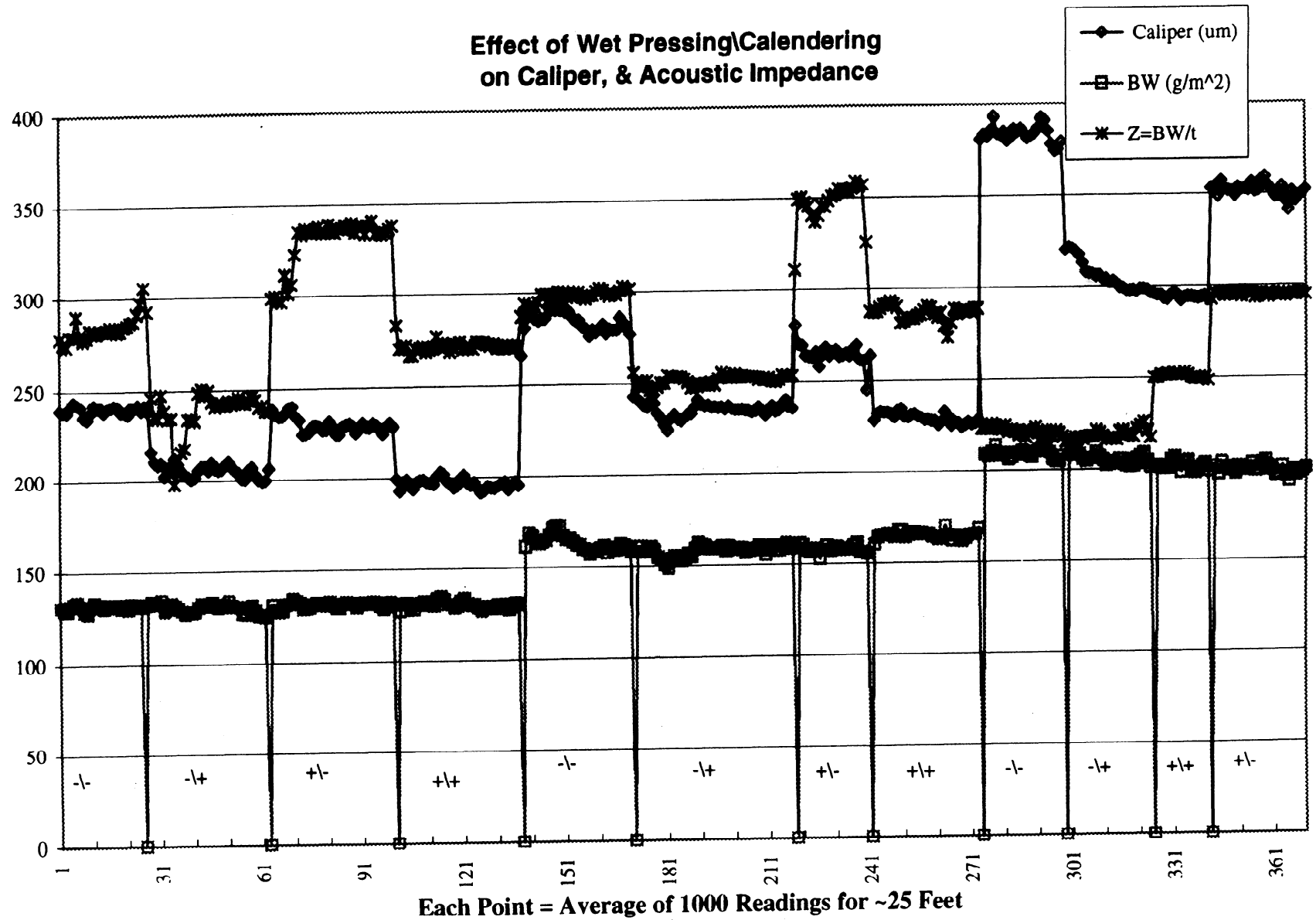
Effect of Wet Pressing\Calendering
on Caliper, & Acoustic Impedance
Caliper (um)
BW (g/m^2)
Z=BW/t
400
350
300
250
200
150
100
50
0
-\-
-\+
+\-
+\+
-\-
-\+
+\-
+\+
-\-
-\+
+\+
+\-
1
31
61
91
121
151
181
211
241
271
301
331
361
Each Point = Average of 1000 Readings for ~25 Feet

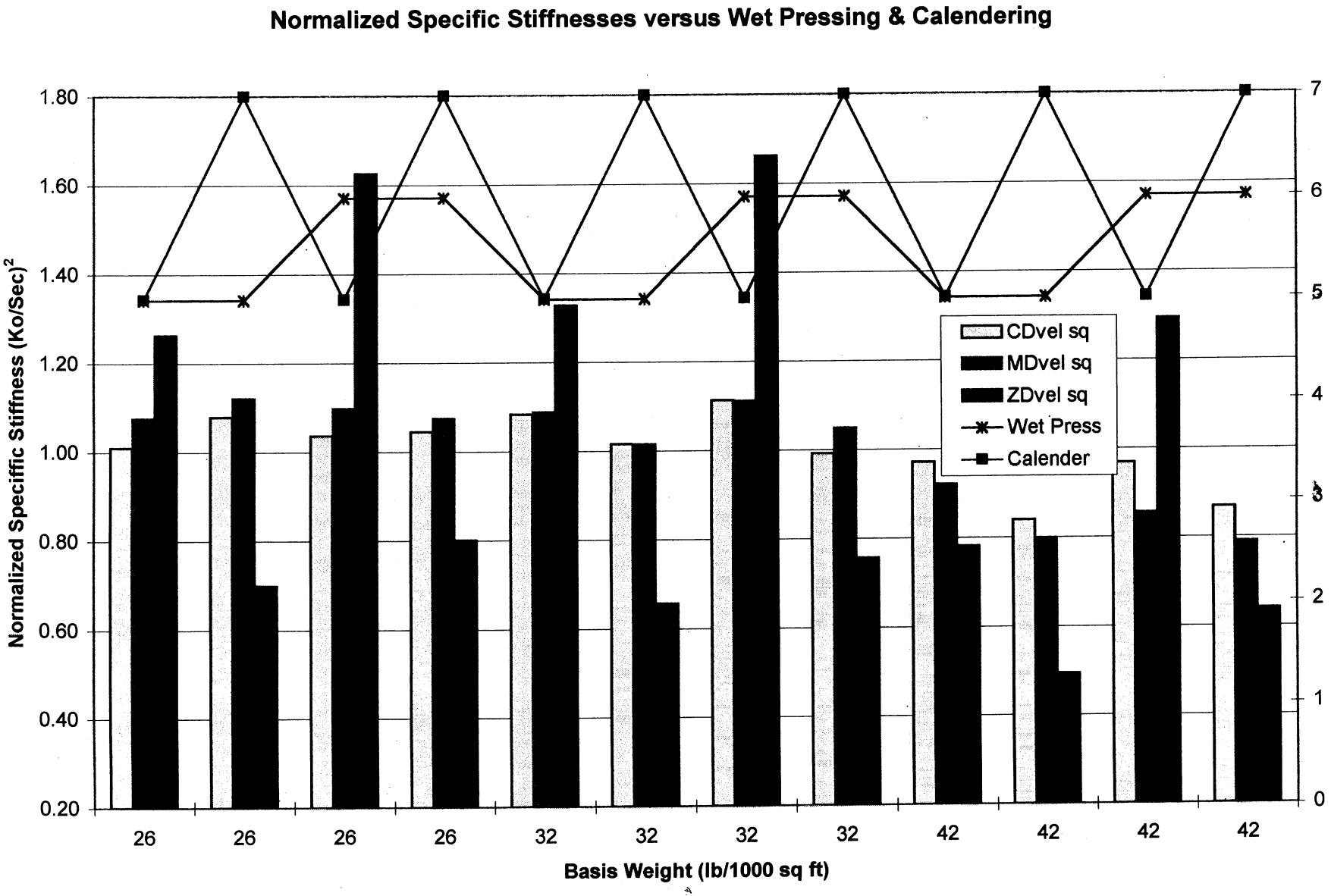
Normalized Specific Stiffnesses versus Wet Pressing & Calendering
Normalized Specific Stiffness (Ko/Sec)²
1.80
1.60
1.40
1.20
1.00
0.80
0.60
0.40
0.20
7
6
5
4
3
2
1
0
CDvel sq
MDvel sq
ZDvel sq
Wet Press
Calender
26
26
26
26
32
32
32
32
42
42
42
42
Basis Weight (lb/1000 sq ft)